ΠΟΛΥΤΕΧΝΕΙΟ ΚΡΗΤΗΣ
ΣΧΟΛΗ ΗΛΕΚΤΡΟΝΙΚΩΝ ΜΗΧΑΝΙΚΩΝ
ΚΑΙ ΜΗΧΑΝΙΚΩΝ ΥΠΟΛΟΓΙΣΤΩΝ
ΤΟΜΕΑΣ ΤΗΛΕΠΙΚΟΙΝΩΝΙΩΝ

Analysis of Magnetoencephalographic signals from children with Reading Difficulties using realistic Head Modeling and Machine Learning

Diploma Thesis
in Electrical and Computer Engineering

by
Maria Aikaterini Dourida

July 8, 2024

Committee Members: Professor Zervakis Michail, School of Electrical and Computer Engineering

Professor Liavas Athanasios, School of Electrical and Computer Engineering
Professor Christopoulos Dionysios, School of Electrical and Computer Engineering

Acknowledgments

I would like to thank my supervisor Prof. Zervakis Michail for his guidance and support. I would also like to thank the thesis committee, Prof. Liavas Athanasios, and Prof. Christopoulos Dionysios.

Special thanks to Dr. Antonakakis Marios for his valuable insights. He provided the data used in this study and offered his help and support throughout this thesis. His guidance was crucial to the completion of this study.

Περίληψη

Οι Δυσκολίες στην Ανάγνωση είναι ο πιο συνηθισμένος τύπος μαθησιακής δυσκολίας, οι οποίες εμφανίζονται συχνά σε νεαρή ηλικία. Τα συμπτώματα που παρουσιάζονται αφορούν ελλείψεις στην κατανόηση και ανάγνωση κειμένων, στην αποκωδικοποίηση των λέξεων, στην ορθογραφία και στη φωνολογία. Η Μαγνητοεγκεφαλογραφία (MEG) είναι μια νευροεικονική τεχνική που απαθανατίζει τη δραστηριότητα του εγκεφάλου με ακρίβεια χιλιοστών του δευτερολέπτου. Η ανάλυση των πηγών των καταγεγραμμένων σημάτων MEG μπορεί να παρέχει μια ακριβή εκτίμηση της υποκείμενης δραστηριότητας του εγκεφάλου, χωρίς να επηρεάζεται από τις επιδράσεις της αγωγιμότητας μεταξύ των ιστών. Έτσι δημιουργείται μια κατάλληλη βάση για τη μελέτη των μοτίβων της λειτουργικής συνδεσιμότητας του εγκεφάλου. Σε αυτή τη διπλωματική, μέσα από την ανάλυση των, καταγεγραμμένων σε κατάσταση ηρεμίας, σημάτων MEG από 40 παιδιά υγιή (NI) και 26 παιδιά με δυσκολίες στην ανάγνωση (RD), εκτιμώνται οι αλληλεπιδράσεις μεταξύ περιοχών του εγκεφάλου σε προσεγγίσεις εσωτερικής, ενδιάμεσης και την κυρίαρχης συχνότητας, με τελικό σκοπό την επιτυχή κατηγοριοποίηση των ατόμων μεταξύ των ομάδων NI και RD. Αρχικά, γίνεται ο εντοπισμός των πηγών, χρησιμοποιώντας τεχνικές beamforming και χρήση ρεαλιστικού μοντέλου κεφαλής. Στην συνέχεια, με τη χρήση μετρικών συγχρονισμού φάσης, εκτιμώνται οι αλληλεπιδράσεις των πηγών σε εσωτερική και ενδιάμεση συχνότητα σε μεταβλητό χρόνο. Εκτιμάται επίσης, η κυρίαρχη συχνότητα για να αποκαλυφθεί περαιτέρω η μέγιστη αλληλεπίδραση των πηγών. Τέλος, κατασκευάζονται οι συμβολικές χρονοσειρές και υπολογίζεται ο δείκτης πολυπλοκότητάς του δικτύου. Πραγματοποιείται σύγκριση των προσεγγίσεων Ενδιάμεσης, Εσωτερικής και Κυρίαρχης συχνότητας, αναλύοντας τα εγκεφαλικά δίκτυα σε όλες τις περιοχές του εγκεφάλου, καθώς και στις καταστάσεις λειτουργικής συνδεσιμότητας(fcmstates). Από τα αποτελέσματα, φαίνεται ότι η κυρίαρχη συχνότητα (δ-β) παρέχει μια πιο ακριβή απεικόνιση των διαφορών μεταξύ των ομάδων σε όλες τις περιοχές του εγκεφάλου και τις καταστάσεις. Με τη χρήση αλγορίθμων μηχα-

νικής μάθησης Κ-Κοντινότεροι Γείτονες (k-NN) και Μηχανών Διανυσμάτων Υποστήριξης (SVM) στην κυρίαρχη συχνότητα, παρατηρείται υψηλή απόδοση κατηγοριοποίησης (Ακρίβεια $> 96\%$). Επιτυγχάνεται επίσης υψηλή ακρίβεια κατηγοριοποίησης σε όλες τις εξεταζόμενες μετρικές συγχρονισμού φάσης. Η παρούσα διπλωματική θέτει έτσι τις βάσεις για μελλοντικά μη επεμβατικά συστήματα διάγνωσης, για την ανίχνευση δυσκολιών στην ανάγνωση στην παιδική ηλικία.

Abstract

Reading Difficulties are the most common type of learning disability, often manifesting at a young age, including deficits in reading comprehension, word decoding, orthography, and phonology. Magnetoencephalography (MEG) is a neuroimaging technique that captures brain activity in millisecond precision. The source analysis of MEG recordings can provide an estimation of the underlying brain activity without being affected by volume conduction effects. An appropriate base to investigate functional connectivity patterns is thus established. In this thesis, resting state MEG recordings from 40 Non-Impaired (NI) children and 26 children with Reading Difficulties (RD) are analyzed to estimate the intra-, inter-, and dominant frequency-based brain interactions and successfully classify them between NI and RD groups. Initially, the source location is performed using beamforming techniques and realistic head modeling. Using intra-frequency and inter-frequency phase synchronization metrics in a time-varying fashion, source interactions are estimated. The dominant frequency coupling is also estimated to further reveal the maximum coupling source interaction. Symbolic time series and their complexity index are then estimated. A comparison of the Inter-, Intra- and Dominant frequency approaches is conducted, by analyzing the brain networks across brain regions, as well as their FCmstates. From the results, it is indicated that the dominant frequency ($\delta - \beta$) provides a more accurate depiction of the differences between groups across brain regions and FCmstates. By employing the machine learning approaches k-Nearest Neighbors (k-NN) and Support Vector Machine (SVM) on the dominant frequency, a high classification performance (Accuracy $> 96\%$) is observed. Highly accurate classification is also achieved across all the examined phase synchronization metrics. The present thesis thus paves the way for future non-invasive diagnostic systems for identifying reading difficulties in childhood.

Contents

List of Figures

List of Tables

Abbreviations

ANN Artificial Neural Network.

BEM Bountary Element Methhod.

CI Complexity Index.

CSF Cerebrospinal Fluid.

DFC Dynamic Functional Connectivity Graph.

DFCG Dominant Frequency Connectivity Graph.

DT Dwell Time.

EEG Electroencephalogram.

EPSC Ecxitatory Postsynaptic Current.

EPSP Ecxitatory Postsynaptic Potential.

FCmstate Functional Connectivity microstate.

FEM Finite Element Methhod.

FI Flexibility Index.

fMRI Functional Magnetic Resonance Imaging.

GCE Global Cost Efficiency.

ICA Independent Component Analysis.

IFCG Intra Frequency Connectivity Graph.

iPLV Imaginary Phase Locking Value.

k-NN K-Nearest Neighbours.

LCMV Linearly Constrained Minimum Variance.

MEG Magnetoencephalography.

MLP Multilayer Perceptron Network.

MRI Magnetic Resonance Imaging.

MST Minimum Spanning Trees.

mTBI Mild Traumatic Brain Injury.

MVAR Multivariate Autoregressive.

NG Neural Gas.

NI Non Impaired.

OMST Orthogonal Minimum Spanning Trees.

OT Occupancy Time.

PAC Phase Amplitude Coupling.

PCA Principal Component Analysis.

RC Rich Club.

RD Reading Difficulties.

ROI Region Of Interest.

SQUID Superconducting QUantum Interference Devices.

STS Symbolic Time Series.

SVM Support Vector Machines.

SW Small World.

TV-iPLV Time Variant imaginary Phase Locking Value.

Nomenclature

Term	Description	Units
B	Magnetic Field	T
E	Electric Field	NC^{-1}
J	Current Density	$\frac{Ampere}{meter^2}$
μ	Mean	as indicated
S	Power Spectral Density	$\frac{W}{Hz}$
s	Standard deviation	as indicated
σ	conductivity	$\frac{siemens}{m}$

Chapter 1

Introduction

1.1 Motivation

Learning Disorders are prevalent among children of scholar age, with studies showing that at least 5% of all public school students exhibit symptoms of learning disabilities [1]. Specifically, Reading Difficulties, characterized by deficits in Language Comprehension and Word Decoding, have been identified as the most common type among young children, with approximately 25% of schoolchildren diagnosed with such disorders [2]. An issue arising with reading problems, is the difficulty of identification, leading to delayed intervention. Children with such difficulties are often not diagnosed until the ages of 11-14. Reading Difficulties in Children are manifested through a spectrum of disabilities, often with overlapping symptoms rather than distinctive ones, making the diagnosis challenging. Given the difficulty of identification, implementing a data-driven model capable of successfully classifying children with reading difficulties from non-impaired ones is essential.

Reading Difficulties are foremost caused by nervous system impairments, which can be pinpointed in certain regions of the brain. Many studies associated the Reading Difficulties in Children with significant alterations primarily found in brain regions such as the Temporal and Parietal Lobes [3],[4]. In [5], [6], [7] Reading Disorders are linked with orthography and phonology difficulties in reading-related tasks. MEG is widely used in numerous studies for recording brain activity signals and analyzing its connectivity patterns, due to its precise portrayal of neuronal activity in the brain [8]. Specifically, using MEG at resting state offers

a depiction of the brain functionality, in the absence of task-related neural activations and has been extensively analyzed in many researches [3],[4].

This study utilizes established analysis techniques from prior studies, aiming to assess their efficiency when applied to data from Children with Reading Difficulties. The ultimate goal is to identify the alteration of the brain interactions in certain regions and FCmstates and subsequently to successfully classify between the two groups, NI and RD. A previous study, detailed in section 3.1, preprocesses the resting-state MEG data and analyses the functional connectivity networks at sensor level. Aim of this study is to build upon this research by using the preprocessed data and to extend it by analyzing the brain network at the source level. Analysis of the resting state MEG data at the source level can offer a precise depiction of the neuronal activity within the brain networks and help identify the exact brain regions associated with the disorder [9]. When neurons exchange information, they exhibit synchronization patterns in their oscillations [10], [11]. Phase synchronization techniques, extensively analyzed in prior studies [3], [12], detect synchronization patterns and construct functional connectivity networks in both intra- and inter-frequency. Recent studies in particular [13], proposed an optimization for localizing brain alterations caused by mild traumatic brain injuries by identifying the dominant frequency among Intra- and Inter- frequencies. This technique was based on the premise that the identified frequency exerts the greatest influence on brain networks. This study utilizes dominant frequency identification when analyzing the brain networks of children with reading difficulties. Further analysis of the brain networks has been found essential due to their highly non-stationary nature, even at rest[14]. Using symbolization techniques the frequency-dependent oscillations can be transformed into symbolic time series, helping characterize the dynamics and complexity of the time-varying brain networks and successfully classify Children with Reading Difficulties [15].

1.2 Contribution

The present study is the first study to analyze the given resting-state MEG recordings at the source level. Previous study *(Section 3.1)* successfully located the regions within the brain network showcasing abnormalities in Children with Reading Difficulties, by analyzing the same data at the sensor level. In another study [9], source localization of MEG data accurately

pinpointed the specific brain region exhibiting alterations. However, this study focused on subjects suffering from epilepsy upon receiving a stimulus. This research employs source analysis, in order to identify the brain regions responsible for Reading Disorders during resting state. Another contribution of this study is the identification of the dominant frequency of the brain networks, reinforcing the high classification accuracy. Previous studies focused primarily on the analysis of Intra- or Inter-frequency brain networks [3]. In our study as proposed in [13],[3], the dominant frequency of both Inter- and Intra-frequency is used in functional connectivity analysis. Because this frequency influences greatly the network interactions, the distinctions between NI and RD are accentuated, resulting in high classification performance. Overall, this research used various techniques that were utilized before successfully in prior studies and attained significant insights into the functioning of the brain networks in children with reading difficulties. The extracted information helped pinpoint the exact location of brain regions exhibiting alterations in children with reading difficulties and contributed to achieving significantly high classification performance between the two groups.

1.3 Thesis Structure

Chapter 2 introduces some theoretical knowledge of the topics covered in this thesis. It provides insights into Reading Difficulties, their causative factors, identifying symptoms, and the effects they can have on children. Additionally, states the reasons necessitating early identification. It introduces terms like resting-state MEG, Source Analysis, and Functional Connectivity of the neural activity among brain regions and ultimately their application in analyzing RD.

In **Chapter 3** the previous research upon which this study relies is detailed.

Chapter 4 describes the methods used in this current study. Initially, we introduce information about the subjects and also the experimental and recording design for the data acquisition. We apply source localization on the MEG data recorded, by solving the forward and inverse problem. We then, describe in detail the steps for the construction of the Functional Connectivity Microstates, which involve constructing the inter, intra, and dominant frequency connectivity graphs, applying data-driven thresholding, and finally implementing the Neural Gas algorithm. Finally based on the Complexity Index and Chronectomic values we imple-

ment the SVM, k-NN classification model.

The findings of this study are presented in **Chapter 5**. The brain networks across brain regions and FCmstates are analyzed and compared between NI subjects and RD. Furthermore, the classification performance based on Chronectomic features is presented.

In **Chapter 6**, we delve into the study's findings. Drawing from both the current results and previous research, we reach conclusions and provide suggestions for future studies.

Chapter 2

Background

2.1 Reading Difficulties

Reading Difficulties are the most common type of Learning Disabilities, in which a person exhibits Reading Comprehension deficits. This disorder can be classified into two main categories: Dyslexia, where a person experiences difficulty recognizing or sounding out written words, and hyperlexia, with advanced reading skills beyond their chronological age but an inability to understand what is read or spoken [16]. They are mainly associated with deficits, that often overlap, such as Language Comprehension, Word Decoding, Phonological Deficit, Orthographic Processing Deficit, and lack of Fluency. Reading Disorders can be developed, either to children in their early childhood or to adults after an injury affecting regions of the brain related to reading. In our research we analyze children with reading difficulties (dyslexia) in early adolescence (11 to 14 years old). Dyslexia is a sign of different brain processing between normal subjects and subjects with reading difficulties when it comes to certain tasks like reading or spelling, and not a sign of intellectual or developmental disorder. Recent studies showed that many children at early ages struggle with reading, specifically 10 million children on average[2].

Morton and Frith [17] in their book, use casual modeling on three different Levels to understand and give theoretical explanations on the factors that lead to Reading Disorders. The first Level is the *Biological level*, that attributes the risk factors in inheritance across individuals. Many researches have shown a correlation between parents with reading difficulties and

children with a high risk of developing disorders [18], [19]. In fact in [20] the candidate genes and their chromosome regions responsible for developing dyslexia were identified, giving insights about the genetic factors of the disorder. The second is the *Cognitive Level*, related to the ability of the individual in cognitive functions, such as memory, attention, and language skills. Lastly, the third Level is the *Behavioural Level*, manifested in children with social incompetence and behavioral problems. In [21] and [22] besides the above internal factors, cognitive and non-cognitive, the effects of external factors were studied as well. External factors are considered to be mainly related to a distressed family environment, characterized by parental absence, resulting in a lack of support and attention to children. Although cognitive factors were found in [21] to be correlated to a large extent with Reading Difficulties, non-cognitive factors added discriminatory value to the classification performance. External factors were found to affect the least classification accuracy, nevertheless, they shouldn't be overlooked when analyzing the causes of RD.

Children's reading difficulties can be associated with behavioral issues such as violent reactions or mental health challenges manifested through outbursts and excessive emotional responses as described in [22],[23]. In [24] children with difficulties in performing reading-related tasks, either cried or were unwilling to further participate in the class. Feelings of incompetence in children with reading difficulties, when compared to non-impaired children, can affect their mental well-being and lead to extreme reactions. It can also lead long-term to poor educational and social development.

Based on previous research [25] early identification of the problem can prevent the development of the disorder and its effects on the individual's life. Early treatment, while the subjects are still young, can lead to long-term social, emotional, and academic adjustment. More specifically 90-95 percent of children with reading disorders can overcome their problem in later years [2].

The problem resulting from the attempt for identification, is that this disorder is highly heterogeneous. Reading comprehension is a result of many cognitive disabilities that often overlap as referenced in [26] and have different symptoms and manifestations per individual, making the identification process hard to achieve. In [24] one child showed spelling deficits,

one reading comprehension deficits due to lower hearing ability and the last one showed difficulty understanding what was read affected by lack of parental attention and support in his studies. Given the disorder's heterogeneity and the large percentage of young children with Reading Disorders, coupled with the necessity of early identification, adopting a data-driven model for detecting RD is recommended.

2.2 Brain Structure

The Brain is the organ that controls and directs all functions of the body, physical and emotional. It consists of four major regions: (1)the cerebrum (cerebral cortex), the brain's largest component divided into right and left hemispheres, which is responsible for conscious control of our actions, (2)the diencephalon, which is part of the forebrain along with cerebrum and is responsible for sensations and emotions, (3)the cerebellum, located between the cerebrum and brainstem is related to muscle movement, speech coordination and balance and lastly (4)the brainstem, which connects the cerebrum and cerebellum with the spinal cord and is responsible for transmitting messages to and from the brain and the body[27] [28] [29].

In this research we study the function of the cerebrum for both NI and RD and we analyze the differences among its regions. The cerebrum is separated into 4 lobes [28] [29]. The *Frontal Lobe*, located in the front of the brain is the largest lobe. It is related with personality and behaviour characteristics, cognitive abilities like intelligence, concentration and organized thinking, judgement characteristics like decision making, and lastly speech (Broca's area) and movement. In the middle part of the brain, we find the *Parietal Lobe*, which controls the senses. Through this lobe the individual is able to sense touch, pain, to interpret signals received from vision and hearing, and identify their meaning based on memory. It also gives spatial and visual perception, the ability to understand the spatial relationships of one's body compared to others. In our research analysis, we use an extra brain Region called *Central* containing parts of both the Temporal and Frontal Lobes. The central Lobe processes and regulates emotion and memory while dealing with learning and is responsible for Behavior, motivation, and long-term memory. The *Occipital Lobe* is in the back of the brain and interprets vision, by processing stimuli like color, light, and movement. The fourth Lobe, *Temporal*, is located in the sides of the brain. This lobe is related with short term memory,

speech, sequencing, and organization.

In general, the left hemisphere of the brain is responsible for language and speech. The right hemisphere plays a large part in interpreting audio-visual information and spatial processing. In about one-third of left-handed people, speech function may be located on the right side of the brain [28]. Based on the information above, all 5 regions are likely to manifest deviations from normal functions, when a subject struggles with RD. In [7] dyslexia is associated with dysfunction in visual processing, in which the orthography to phonology conversion systems malfunction in the left occipitotemporal cortex. In children and adults with dyslexia, the left temporoparietal cortex is consistently under-activated during phonological processing tasks, regions associated with the development of phonological skills and consequently the ability to read [6] [5]. This under-activation was compensated with over-activation of the left frontal region [5], meaning possible overexertion of the brain to compensate for the reduced function of the temporoparietal cortex.

2.3 Neural Activity

The activity of the brain regions and the in-between communication is based on a network of nerve connections. Neurons are nerve cells composed of the cell body, dendrites, and an axon [30],[31]. Synaptic connections between dendrites, which receive and process signals, and the axon, which sends signals, construct the neural circuits responsible for transmitting information and communicating between different regions of the brain [32]. This communication relies on electrical and chemical signals [33]. The communication between two neurons is achieved with a chemical, released from pre-synaptic neurons, called neurotransmitter [34],[35]. The post-synaptic neurons, known as neurotransmitter receptors, receive the chemical signal and will either excite or inhibit. When the electrical signals, that rely on ion flow, within the cell are positively charged the postsynaptic potential is called Excitatory (EPSP) and is caused by Excitatory Postsynaptic Current (EPSC). The neuron is then charged positively, higher than -70mV to -65mV which indicates the resting state of the cell[35],[31]. Otherwise, Inhibitory Postsynaptic Currents (EPSC) cause a negatively charged flow or positive outflow, known as Inhibitory Postsynaptic Potentials (EPSC) [34]. EPSPs increase the likelihood a postsynaptic action potential will occur, by increasing the potential

past the threshold value(-40mV)[35]. Additional electricity is generated by the motion of free electrons. Brain signals indicate the action potentials, caused by ions flowing in and out of the neuron when processing and transmitting information.

Neural oscillations caused by synchronous, rhythmic, action potentials from inter-neural connections, can be categorized into 5 main frequencies bands. Based on their frequency range, brain waves are delta brain waves (1-4 Hz), theta (4-8 Hz), alpha (8-15 Hz), beta (15-30 Hz), and gamma (over 30 Hz). Analysis of the functional connectivity at distinctive frequency bands can provide insights into the cognitive differences between NI and RD. Dimitriadis in [36] found reduced temporal correlations in the b3 frequency band in Children with Reading Difficulties. The beta band is associated with fast brain activity and conscious and waking states. When analyzing the beta band we gain knowledge about the subject's concentration ability, decision-making, and anxiety. Unlike Beta, the Alpha band occurs in deep relaxation and is related to mental coordination, alertness, intelligence, and cognitive abilities. Delta and Theta bands are associated with sleep, the first one occurs in deep states of sleep while the second one on earlier states. Both of these states give us information about unconscious brain activity and cognitive abilities like memory, intuition, and learning. Lastly, the Gamma band is associated with cognitive tasks such as learning, problem-solving, and information processing between brain regions[37]. Study [38] highlights the importance of distinguishing and studying separately the Gamma sub-bands, low gamma (30-45 Hz), and high gamma (45-80 Hz). The distinction between the sub-bands lies in the measurement of one frequency while participants passively sit with their eyes either open or closed, and the measurement of another frequency in the presence of stimuli. In [39] in the case of hyperlexia, alterations were observed in both induced and evoked gamma band neural activity.

2.4 Magnetoencephalography

The electric currents created by synchronous activation of thousands of nerve cells inside the brain produce a magnetic field outside the head that can be measured by Magnetoencephalography [31]. Magnetoencephalography is a non-invasive brain imaging technique, for recording these magnetic fields. The magnetic field consists of two components, the primary and volume current. The primary contributors of the MEG are the membrane currents

(primary current), generated in the cells of the cortex, tangential to the head surface[31]. These currents due to the conductivity of the head tissues, impress the secondary (volume) currents that circulate through the tissues.

A helmet-shaped scanner, consisting of hundreds of superconducting sensors (SQUID), is placed around the head while the subject is sitting. The sensors can amplify the weak magnetic field from tangential currents and detect the brain activity [8]. Due to the distance between the sensor and the head the MEG isn't affected by head movement, inducing a very small percentage of signal distortion[40]. The procedure is usually performed in specially magnetically shielded rooms isolating the external noise, caused by the environment or the machinery [41]. The reduced noise and sensitivity to movements makes the MEG, compared to techniques like EEG and fMRI, a more accurate technique for spatial localization and reconstruction of the brain activity.

MEG has played an important role in the identification of structural and functional brain alterations in Children with Reading Difficulties. This technique provides a view of the neural activity in the millisecond time scale, making it possible to detect abnormal brain function in a resting state as well as abnormal brain activations when receiving a stimulus [41]. The way the brain works when receiving a stimulus has been widely studied in many researches. Studies [42],[43] and [44] identified differences in brain activations and neural correlations between children with no reading deficits and children with RD, during orthography and phonology tasks. Other studies [36],[3] using Resting-state MEG signals, gained insights into the brain alterations induced by Reading Disorders, particularly within specific brain regions or frequency bands. This research analyzed MEG data recorded during resting state, to gain an accurate and deep understanding of the intrinsically brain activity patterns and activations within the two groups.

2.5 RD and Source Analysis

It is possible to estimate the underlying neural activity from magnetic field sources and localize it to certain regions of the brain [45]. Source Localization indicates the exact region of the brain that contributes the most to the neural activity recorded from each sensor, during the

data acquisition using the MEG Scanner. It has been widely used in many brain researches and studies, combined with whole-brain networks, to detect or analyze the specific brain areas that are involved in an injury [46],[47] or are implicated in the execution of certain tasks [48].In this research, MEG source localization helps us diagnose and detect abnormalities in the resting state neural activities of the brain regions, that are related to reading deficits.
To achieve accurate source localization we solve the forward and inverse problem with the help of MRI data.

2.5.1 Forward Modeling

The forward problem refers to the difficulty of linking the MEG data recorded from the MEG sensors to the magnetic field on the surface of the head. The construction of a forward model that helps us map these electromagnetic fields outside the head to the ones on the surface, is an irremovable step for source localization. This problem can be solved with mathematical calculations based on the quasi-static approximation to Maxwell's equations [31].

As stated in previous sections the current density produced by neural activity consists of the primary and volume current described in 2.1.

$$J(r) = J^p(r) + J^v(r) \tag{2.1}$$

To compute the electric field E and the magnetic induction B caused by the density J^p, we use an approximation of the Maxwell's equations 2.2, 2.3,2.4

$$E = -\int V \tag{2.2}$$

$$B = \mu o J \tag{2.3}$$

$$J(r) = J^p(r) + \sigma(r)E(r) \tag{2.4}$$

in 2.4 σ is a constant value that denotes conductivity.

Given our MEG signals, our forward solution is restrained in the estimation of the magnetic field on the surface of the head. The magnetic field caused by an electric current J (2.4) is

given by the Biot-Savart Law

$$B(r) = Bo(r) - \frac{\mu o \sigma}{4\pi} \int_G V(r')n(r)\frac{R}{R^3}dS \tag{2.5}$$

Where $\frac{R}{R^3} = \frac{r-r'}{||r-r'||^3}$ with r the point the field is computed, with

$$Bo(r) = \frac{\mu o}{4\pi} \int_G J^p(r)\frac{R}{R^3}dv' \tag{2.6}$$

A more detailed analysis of the forward model is presented in [49], [50], [31].

Using an appropriate volume conductor (head) model, that assumes the geometry and conductivity of the brain tissues by applying a computational model to the MEG data, we can calculate the magnetic field (2.6) on the surface of the head.
The forward model solves the problem of infinite solutions by constraining the possible ones[49], allowing us to move forward with the inverse problem.

2.5.2 Inverse Model

The inverse problem is the problem of extracting as much information as possible for the source space of the MEG surface signals calculated in previous steps [49]. The problem we face in the inverse problem is that there are primary current distributions that are either magnetically silent, electrically silent, or both[31]. It is also possible for multiple different neural distributions to produce the same magnetic field measurements [51]. This non-uniqueness of the solution is what makes the problem ill-posed and can lead to inaccuracies.

Given the known magnetic field on the surface of the skull from the forward model calculations (2.5) the inverse problem is constrained to find the density $J^p(r)$ (2.3) [50].

Many techniques have been proposed from time to time for the distributed source estimation. Choosing the appropriate one is a challenging process that requires detailed information about the nature of the sources and the data. In [52], the approaches are separated in two categories: parametric and non-parametric. Parametric methods assume that the data depend linearly on the parameters, meaning the linear contribution of the sources in the studied

signal and accordingly a linear decomposition when reconstructing the source. In these models several dipole sources with fixed locations and possibly fixed orientations are distributed in the whole brain volume [53]. On the contrary, in the non-parametric methods, the data depend non-linearly on the parameters(sources) and have unknown dipole locations and orientations.

Earlier studies used non-linear dipole and multi-dipole modeling (MUSIC- MUltiple Signal Classification), using the current dipole as the primary source and localizing the dipoles whose field best fit the local measurements [51], [31]. Most recent studies used linear source estimations due to their simplicity and inexpensive calculations [54]. Widely used, are current distribution approaches that assume continuous current distribution across the whole source space and reconstruct the current density by minimizing the sum of the difference between the measured MEG data and those generated by the source estimate[55]. Some very popular and most used methods are algorithms using Minimum Norm solutions and their Regularizations, such as Minimum Norm Estimation, Weighted MNE, LORETA, sLORETA, and other linear algorithms like Standardized LeadField and Weighted Vector Norm[56], [54]. Regularization techniques introduce prior knowledge to the algorithm and make the ill-posed problem solvable[55]. An approach that performs in most cases more accurately than the traditional dipole fitting approaches and the MNE algorithm [57], is the non-linear dynamical modeling Bayesian approach [58],[59]. This approach uses the Bayes Thorem, for the posterior probability density function for the parameters [55].

Some other very popular methods, simple and effective, that will be used in this study are the Beamformers. They use an adaptive spatial filtering approach, that scans independently each location within a Region of Interest and reconstructs the data [60], using weights chosen based on statistics of the data [61]. Adaptive Beamforming is an algorithm of Statistically Optimum Beamforming. The main advantage of this approach is the ability to suppress the background interference from other locations achieving a better data reconstruction[62]. Induced changes in cortical oscillatory power that do not result in a strong average-evoked response can be identified and localized, providing a better sensitivity to deep focal activity compared to other methods like MNE [60]. In [63] Beamformers successfully detected weak signals, like hippocampal signals, in individual subjects despite demonstrating a bias in the

presence of strong brain noise backgrounds. They also offer spatial accuracy compared to dSPM (Dynamic statistical parametric maps) and sLORETA. While these methods enhance peak localization accuracy for deeper sources, they fall short in capturing the full spatial extent of the distribution [54]. Lastly, they require no prior knowledge of the number of sources, the main disadvantage of the dipole modeling approach [64].

There are several beamforming techniques compared and analyzed in extent in [61], [65],[66],[67]. Vector beamformers outperformed scalar beamformers, exhibiting a higher success rate in detecting deep focal signals [63]. In [68] the vector LCMV algorithm is used during source reconstruction, when examining the impact of phonological deficits on neural brain dynamics during spoken word recognition, aiming to test whether these deficits cause Reading Difficulties.

2.6 RD and Functional Connectivity Networks

2.6.1 Frequency Coupling

Many studies use graph theory in attempt to understand the way the brain regions communicate and identify abnormal interactions when studying Reading Difficulties. The analysis of brain connectivity through graphs can be achieved either with analysis of the effective or the functional connectivity [69]. Effective connectivity uses techniques, like casual modelling[70] and structural modeling [71], to measure the influence that one neural system exerts over another. In contrast, functional connectivity is widely used to describe the correlations and interactions between the neuronal activity of the studying regions.

Network-based analyses of resting state functional connectivity provide great insight in the brain alterations in Children with RD. The network approach is based on a pairwise matrix of connections between nodes. These connections can be estimated, by approximation of neuronal interactions between brain areas in specific frequency bands at the source level. Since these interactions are characterized by synchronization of the neuronal oscillations, the estimation of the brain connectivity is easily achieved with synchronization measures, either by assessing spectral coherence [72], the presence of a consistent phase delay [36],[73],[74],[75]

phase synchrony of brain signals [76], amplitude correlations [77], or the phase to amplitude coupling of oscillatory patterns [3],[78]. Recent studies [79] show, that low-frequency neural activity can contribute to the modulation of high-frequency activity. These findings have led to the widespread utilization of Phase to Amplitude coupling in cross-frequency for functional connectivity network [78]. In [3] cross-frequency functional connectivity showed a higher level of instability and lower level of predictability in students with RD. Distinctions in the brain connectivity were also observed in [80], showing overactivation in the delta band during inter-frequency analysis. Dominant frequency of both intra- and inter-frequency coupling is a technique used in most recent studies, for the identification and analysis of the neuronal interactions between brain areas in the specific frequency that contributes the most to the network. Study [13] analyzed the functional connectivity graphs of both intra-frequency and inter-frequency couplings, resulting in overactivations of the dominant brain networks, in mTBI patients. In [4], abnormal activity was observed in right temporoparietal brain areas in dominant frequency connectivity for children with RD.

Either in intra- or inter- or dominant frequency, techniques must be applied to capture the time-evolving connectivity estimates in dynamic time series. Techniques used in various studies for dynamic connectivity estimates are wave-let based methods [81] and the sliding window approach [12],[13], [3],[4]. Mostly used, is the sliding window approach, an approach with high performance in identifying dynamic connectivity in slow dynamic states. The limitation in this approach is the appropriate choice of window length, windows that are too short or too long will not capture the true temporal dynamics of the brain. Too short windows lead to results susceptible to noise, while too large windows fail to capture rapid changes in connectivity[82].

2.6.2 Topological Filtering

For reliable graph analysis, it is important to extract discriminative brain interactions from the fully connected functional connectivity graphs. Thresholding techniques allow us to filter out the non-significant information flow, by cutting off the weak connections between brain regions. With techniques like absolute and proportional [83] thresholding, connections with strength values below the threshold are considered weak and are removed from the graph.

The choice of threshold is important and may influence the outcome of the study. Studies [83] and [84] use density-based graph metrics such as path length and clustering coefficient of the overall network, coupled with thresholding techniques. For proportional thresholding, each density level indicates the percentage of the strongest connections. In [85] addition to Clustering Coefficient and Characteristic Path Length, metrics like Participation coefficient and SWI are used to present the correlation of graph metrics on different thresholds.

Earlier studies use Data-Driven approaches for network construction, to avoid subjectivity in the choice of threshold. In [85] the traditional thresholding methods are compared to the data-driven MST approach using the above density-based metrics for both networks, resulting in denser and potentially more meaningful networks in the case of data-driven thresholding. A thresholding method was proposed in [86],[75] using Orthogonal Minimum Spanning Trees as an improvement to the MST. There are four global graph measures for optimization, global efficiency (GE)[74], characteristic path length (CPL), transitivity (T), and synchronizability (S). Dimitriadis [86] uses the OMST thresholding approach and by maximizing the global cost efficiency (GCE), determines the optimal brain connectivity. In [87] both GCE-proportional thresholding and GCE- OMST thresholding techniques are analysed and compared.

2.7 RD and Functional Connectivity Microstates

MEG microstate analysis can potentially give insight into altered brain dynamics in Children with Reading Difficulties. Numerous recent studies have explored the dynamic brain network based on either the distinctiveness of the transitions between states [15], or either its connectivity patterns during these transitions [88]. The approaches commonly used to identify the Functional Connectivity states, are dictionary learning [89], dynamic community detection [90] and Principal Component Analysis [91]. Techniques like Independent Component Analysis have been used extensively to find functional networks based on common activation time courses in MEG[92],[93]. Another widely applied technique is K-means Clustering, used to identify patterns of Functional Connectivity that reoccur in time and across subjects, resulting in discrete neural states and transitions between states [94].

Complexity analysis of the resting state MEG data can give great insight into the intrinsic

activity and activations of the functional connectivity brain states in Children with Reading Difficulties. Using symbolization techniques on the clustered time series we estimate the complexity and diversity of the functional states. In [15] both Level-Zip and Neural Gas algorithms are utilized as techniques for complexity analysis of the brain network. The NG-based features outperformed the LZC features, particularly achieving high accuracy in classifying children with RD using the Complexity Index as a feature. In [86] Neural Gas algorithm was proven to be more robust to noise and produced stable symbolic time series. Study [88] analyzes the functional connectivity within different states in resting state MEG. Using the Neural Gas algorithm on the clustered DFCGs we gain insight into the complexity of the functional states during the resting state. He compares the connectivity patterns of each state between groups and achieves 85% accuracy in classifying mild cognitive impaired patients.

Chapter 3

Prior Work

Several previous studies have focused on topics such as source localization, connectivity analysis, and brain network analysis of resting state MEG. Below, we present research that contributed to the completion of this study. We present techniques, methodology as well as results, helping us acquire the appropriate methods for analyzing our signals and classifying with accuracy children with Reading Difficulties.

3.1 Data Preprocessing

In this study, preprocessing of our dataset using Independent Component Analysis (ICA) was conducted, aiming to remove non-cerebral brain activity and effectively address the Blind Source Separation problem. Resting-state MEG data were acquired from each subject (40 NI, 26 RD), followed by artifact removal during preprocessing. Initially, the data underwent a Fourier Transform, transitioning from the temporal to the frequency domain. Then, using an IIR lowpass Butterworth filter with a stop band at 73 Hz the dataset was constrained to the desired frequencies between 0 and 80 Hz. With a notch filter, the Power Line Noise was also removed at 60 Hz. Statistical analysis of the Energy Spectral Density showcased the differences between the two groups. Both Parametric and non-parametric tests were used depending on the normality of the dataset. In the case of normal distribution of the data, the parametric two-sample T-test and two-sample F-test were applied, otherwise, the two-sided Mann-Whitney test was used. To determine whether the data followed normal distribution one sample Kolmogorov-Smirnov was used. The significance level for all tests was set at

α=5%, indicating the probability of obtaining results due to chance. P-values higher than the threshold of 0.05 were not considered statistically significant, while values that didn't exceed the threshold were highly statistically significant. Following t-test and u-test analyses of the p-values, the study revealed group differences predominantly localized in the temporal lobe for the δ frequency and in both the parietal and temporal lobes for the θ frequency. No significant differences were observed in other frequencies.

ICA decomposes the data into individual independent components, separating artifact and signal in the process. Preprocessing of the data before applying ICA, ensures that the components are independent and uncorrelated. Whitening is a linear transformation, used in this study during ICA preprocessing, that employs a whitening matrix to transform the data into independent and uncorrelated vectors with zero expected value and unit variance. The whitening step is sped up using Principal Component Analysis (PCA), a dimensionality reduction algorithm. Based on the Percentage of Useful Information (PUI) 5% of the components, with minimum PUI values, were removed. After the preprocessing is done, the Infomax algorithm is used for Independent Component Analysis, an algorithm based on minimization of Mutual Information. Metrics like kurtosis, skewness, and Shannon Entropy are used, for identifying Cardiac, Ocular, and Gaussian Noise Artifacts. Independent Components (ICs) with metric values exceeding the upper bound in the segment approach, and those exceeding 30% in the global approach, were considered artifacts. The threshold is estimated based on the Chebysev's inequality. During artifact removal, the Empirical Mode Decomposition method is applied to maintain the integrity of the clean data and avoid loss of significant information. ICA decomposition was repeated for the cluster Independent Components using both K-means and hierarchical clustering. Clustering the Independent Components and reapplying ICA reveals artifacts missed in the initial attempt.

3.2 Brain Networks

The pipeline followed in this research was initially proposed in study [12]. In this study Dynamic Functional Connectivity analysis of source level resting state MEG is used, aiming to detect brain abnormalities involving Mild Traumatic Brain Injury. Given the significance of the results, we used the same methodology to assess its effectiveness, about children with

Reading Difficulties.

For source localization, the researcher utilized LCMV beamformer analysis, as a spatial filter, to reconstruct the Atlas-based 90 Regions of Interest from the 5061 sources of the spherical head model, allocated during the construction of the forward model. The LCMV beamformer weighted the contribution of each source, identifying the primary sources contributing the most to the brain activity as Regions of Interest (ROIs). Since the brain activity for each ROI was estimated, the next step was the construction of a Dynamic Connectivity Graph representing the brain interactions. The used DFC estimator was the imaginary side of the Phase Locking Value. Using the sliding window technique, the phase-to-phase interactions between brain regions of the same brain rhythm were computed, for each time series interval determined from the shifting window. The window length of each time interval was set to 2 s with an overlap of 10%. The final graph had a 3D dimension of 1,785 (segments) × 90 (sources) × 90 (sources) per subject and frequency band. Utilizing a topological filtering technique, the significant interactions of the DFC were extracted. An Orthogonal Minimal Spanning Tree was performed to identify the most dominant paths within every graph. Utilizing a cost-efficiency formula, the optimal OMST, comprising only strong connections, was selected.

In our research both intra-, inter- and dominant frequency couplings as estimated and analyzed. As described above, intra-frequency coupling was estimated using time-varying Phase Locking Value representing phase-to-phase synchronizations between brain regions of the same brain rhythm. Estimating the brain interactions between different brain rhythms, about Children with Reading Difficulties was recently proposed in a study [3]. Phase-amplitude coupling is a widely utilized technique in cross-frequency coupling analysis. The estimated iPLVs expressed the modulation of the amplitude of the High Frequency by the phase of the Low-Frequency oscillation. Study [13] introduced the dominant frequency of both intra- and inter-frequency couplings, which we used in this research to identify the predominant oscillatory rhythms of each brain region.

Study [12] utilized Complexity analysis and Chronnectomics, as features in the classification of mTBI patients. During Complexity analysis, the Neural Gas algorithm was used as a

symbolization technique, to transform the DFC graphs into network microstates. Initially, eigenvalue analysis on the normalized Laplacian transformations revealed the synchronization level of the original DFCs. A vector quantization process modeled the individual DFC graphs as NMstates. Using a stochastic gradient descent procedure, the total number of NMstates was fixed at k = 2 for both mTBI and control, minimizing the distortion error <2%. DFC network metrics, such as Flexibility Index, Occupancy Time, and Complexity Index, were calculated. A statistical procedure to estimate the significance level of the chronnectomic features for each brain region within and between the five brain subnetworks per frequency band and NMstate was utilized. The Kolmogorov-Smirnov test assessed the normality of the data, based on which the parametric t-test or the non-parametric Mann-Whitney u-test was applied. The significance threshold of the p-value was set to 95% and Chronnectomic features were statistically significant for P-values $p<0.05$. The k-nearest Neighbor classifier with an iterative 10-fold cross-validation procedure was adopted. The 10-fold cross-validation was repeated one thousand times and, in each iteration, cross-validation was repeated twice, separately for each NMstate. Antonakakis in this research achieved a Classification performance of 80% accuracy, 99% sensitivity, and 49% specificity based on chronnectomics and 91–97% accuracy, 100% sensitivity and 77–93% specificity when focusing on the microstates.

Dimitriadis in [15] demonstrated high accuracy in classifying children with reading difficulties, using also complexity analysis on the symbolized time series derived from the Neural Gas algorithm. With a reconstructed error <0.8 the total number of NMstates was set to k=6. K-NN and Support Vector Machines classifiers on a 10-fold cross validation scheme running over 100 iterations were utilized, achieving 80% accuracy.

Chapter 4

Methods

4.1 Subjects

For this research data are gathered from 66 subjects divided into two groups. The first group consists of 40 non-impaired subjects, 25 Males and 15 Females with a mean age of around 11 $\pm$ 2 years. The second group consists of 26 subjects with Reading Difficulties, 12 Males and 14 Females with a mean age of 12.2 $\pm$ 2.1 years. The classification into groups was based on the result of each subject on the Texas Assessment of Knowledge and Skills – TASK, a test designed to assess sufficient or insufficient knowledge and skill.

The assessment consists of sub-tests in various categories. In the following table, the values refer to tests that indicate the ability of students to identify letters in increasing difficulty words (Letter-Word Identification), to pronounce nonsense words of increasing complexity (Word Attack), to complete a test based on the combination of the two previous tests (Basic Reading Composite), to display acquired knowledge, verbal reasoning, and attention to verbal materials (Verbal IQ) and to display reasoning, spatial processing, attentiveness to details (WASI Performance IQ).

According to the results derived from the tests we can observe in table table 4.1 the differences between NI and RD. Specifically, the values from the RD groups are lower than the values from the NI group for each test, especially for the WJLWD, WJA, and WJC tests.

	Group	Mean	Standard Deviation	range
Age	NI	11	2	7-14
	RD	12.2	2.1	7-17
WJLWD**	NI	107	11	87-126
	RD	80.73	8.2	62-85
WJA**	NI	107	12	87-131
	RD	84.78	7.2	68-85
WJC**	NI	107	10	88-126
	RD	81.78	6.9	65-85
VIQ*	NI	108	17	86-147
	RD	90.76	13.3	81-128
PIQ	NI	100	10	80-117
	RD	95.39	12.6	80-129

Table 4.1: Statistical Significance of the group differences: *p¡ 0.01, **p¡ 0.001. WJLWD:Woodcock-Johnson III Letter Word Identification, WJA:Woodcock-Johnson III Word Attack, WJC:Woodcock-Johnson III Basic Reading Composite, VIQ:WASI Verbal IQ, PIQ:WASI Performance IQ

4.2 Experimental Design

Data were recorded using a 248-channel whole-head Magnes WH3600 system (4D Neuroimaging Inc., San 33 Diego, CA). During the recording, the subjects were in resting state and with their eyes closed, without receiving any stimulus. The recordings were 3 and 5 minutes of MEG signals. The NI group consists of 16 objects with 3-minute signals and 24 with 5-minute signals. The RD group consists of 17 and 9 subjects with signals of 3 and 5 minute duration accordingly. Data were collected at a sampling rate of 1017.25 Hz.

4.3 Data Preprocessing

The MEG Data underwent preprocessing using Matlab (The MathWorks, Inc., Natick, Massachusetts, United States) using the Fieldtrip software toolbox. Each sensor records a 3 or 5 minute signal depending on the subject, sampled with a frequency rate of 508.6250 Hz. Accordingly, we have a data set with size $\langle 40x91553 \rangle$ and $\langle 40x152588 \rangle$ for 40 components and 248 sensors. Firstly, an IIR low pass Butterworth filter was applied to the data to cut off frequencies higher than the frequency range (0-85 Hz) of the 6 brain rhythms, as well as a notch filter to remove the Power Line Noise at 60 Hz. With Blind Source Separation 10 artifacts, non-cerebral components, were identified and removed from the data. The data were initially whitened, reduced in dimensionality using Principal Component Analysis and

lastly, decomposed in Independent Components using Hierarchical Clustering Independent Component Analysis with Infomax algorithm. Metrics like Skewness, Kyrtosis, and Shannon Entropy were used to detect Ocular, Cardiac, and Gaussian Noise Artifacts. The Empirical Mode Decomposition algorithm ensured that no important information was lost during the artifact removal. After ICA and EMD, using channel reconstruction, data are projected from component $\langle 30x152588 \rangle$ and $\langle 30x91553 \rangle$ to channel $\langle 248x152588 \rangle$ and $\langle 248x91553 \rangle$.

4.4 Source Localization

4.4.1 Forward Modeling

The construction of the Forward Model consists of three essential steps: the design of the sensor array, the construction of the source model, and lastly the construction of the head model. The speed and accuracy of this process can also affect the performance of the inverse model since the inverse problem will predict the contribution of the sources on the magnetic field calculated during the forward modeling. The variables that can affect the accuracy of the source localization are the choice of the head model, the choices of dipole position and orientation, and the choice of source space [95] [96]. Co-registration errors, when adjusting the location of the head and source models with the sensors array, can lead to inaccurate localization and reconstruction of the brain activity [97]. In this research, we compute the head model, based on the segmented MRI using a fitting head volume conductor and we adjust it to the source model, constructed using an appropriate template, with respect to the sensor's location.

4.4.1.1 Sensor Analysis

Head positioning, during the MEG data acquisition, is estimated using the Head Positioning Indicator coils (HPI coils). The coils are placed at known locations on the scalp of the subject and generate a magnetic field that helps us to localize the position of the head in a three-dimensional space. Our data are recorded using a 248-channel whole-head magnetometer, with each sensor location consisting of a combined planar and axial gradiometer. We fitted the sensor model to the BTI coordinate system as shown in figure fig. 4.1. Gradiometers are ideal for measuring the gradient of the magnetic field. The axial gradiometer consists of two

magnetometers (superconductive coils) placed in series and is used to detect activation generated in deep brain structures, while the planar gradiometer consists of two magnetometers placed oppositely wound and is ideal for detecting weak signals. Planar gradiometer contributes to the detection of signals even with existing noise, in which the axial gradiometer shows sensitivity. After sensor analysis, all data are adjusted according to the sensors with a size of $\langle 248x91553 \rangle$

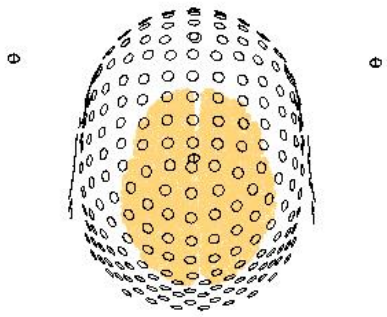

Figure 4.1: 248 sensor neighbor template in BTI system

4.4.1.2 MRI Preprocessing

Acquisition of detailed images of almost every internal structure in the human body, including the organs, bones, muscles, and blood vessels is achieved by Magnetic Resonance Imaging. MRI is a noninvasive imaging technique that can provide anatomical or functional information. This can be used to build a more detailed and anatomically realistic head model. In this research, the same MRI template is used for all subjects and is adjusted to the sensor coordinates. The template is an averaged asymmetric Brain Scan from 152 Children of age 10-14 years old. In 4.2 we see the T1-weighted MRI template(4.2a), the template after Realignment (4.2b) where the fiducials RPA, LPA and NAS (NAS = nasion, LPA = left ear, RPA = right ear) are interactively coordinated to the sensor locations in BTI coordinate System and after Reclising (4.2c) where the x, y,z axes of the MRI are aligned and the voxels

are isotropic.

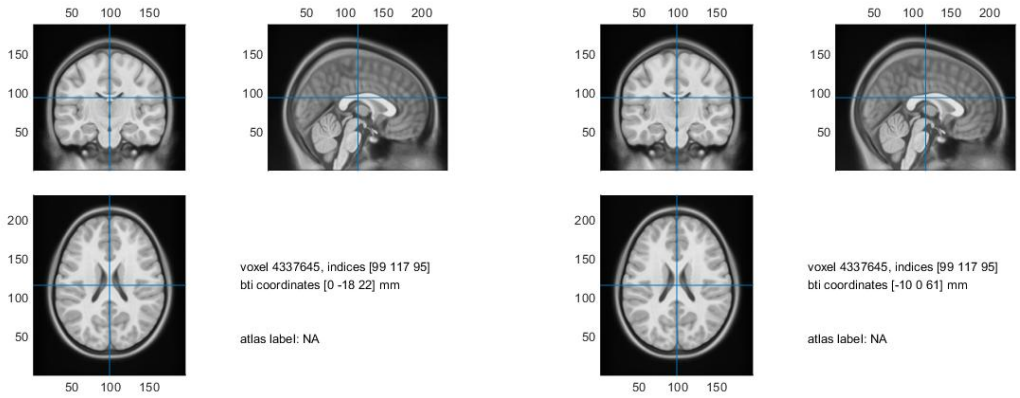

(a) Children MRI template

(b) Children MRI Realigned

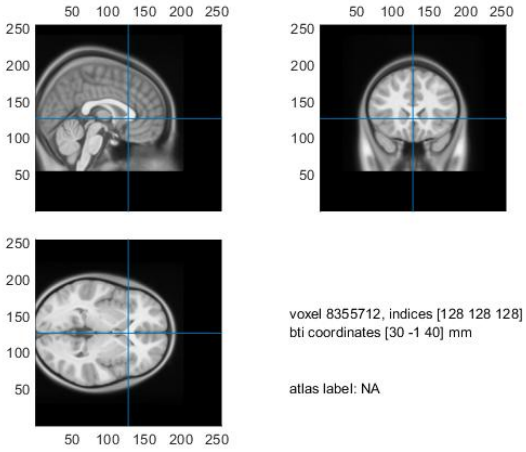

(c) Children MRI Resliced

Figure 4.2: Comparison of the T1-weighted MRI template after realigning and reslicing

Multi-tissue segmentation of the MRI is an essential first step in the construction of a realistic head model [98]. The anatomical structure is segmented into 3 main tissue types, Grey Matter(GM), White Matter (WM), and Cerebrospinal Fluid (CSF), and also the scalp and skull (4.3). White Matter is found in the deeper tissue of the brain and is a network of long axons that allow the exchange of information and communication between regions of the brain. It is also the tissue through which messages pass within areas of grey matter and the nervous system. The Grey matter has a large number of neuronal bodies and is the tissue, externally of the WM, where the information processing is happening. CSF is the fluid that flows in the brain and the spinal cord contributing to the function of the central nervous system.

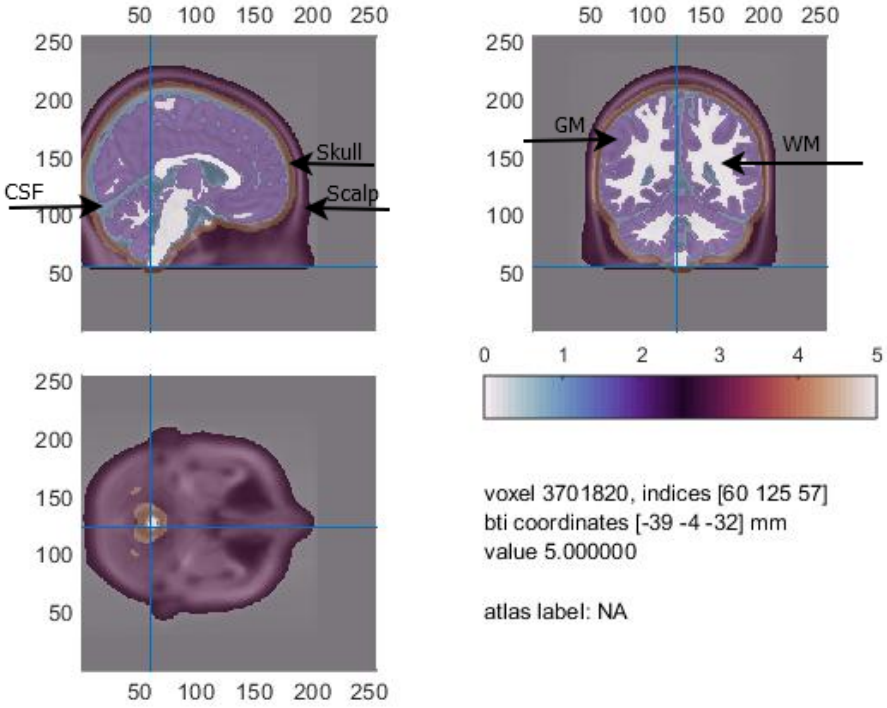

Figure 4.3: Image of MRI segmentation of Human Brain into Anatomical regions: Gray Matter, White Matter, CSF, Skull Compacta and Spongiosa, Scalp

The segmented brain structures are used as compartments to the head volume conductor for semi-realistic construction of the head model and accurate reconstruction of the magnetic field on the surface of the head.

4.4.1.3 Source & Head Modeling

The volume conductor model uses a mathematical construction to predict the electromagnetic field produced by the sources at a given sensor [96], based on computations on the external magnetic fields recorded from the MEG and describes the geometry and conductivity of the brain tissues [99]. The external magnetic field is computed based on the channel configuration described in the previous section, as well as the given source space. The source model describes the distribution of the sources on the brain surface. We use an adult-based template, which allocates a large number of sources to grid points over the whole brain surface and we later adjust it to the head and sensor model we have created based on children. The source model consists of a 3D grid of 5061 sources.

For estimating the geometry and conductivity of the brain tissues, several head modeling techniques with different constraints have been proposed. In this research, a single layer spherical model is chosen for each subject. Although it lacks the accuracy of the BEM or FEM models the spherical model is suggested, due to its simplicity, easier and faster calculations, and sufficient head geometry accuracy provided by spheres [99] [100]. We use the local spheres spherical model, in which an optimal sphere is fitted on the local surface close to each field measurement individually(overlapping spheres). The spheres fit best the local curvature of the brain areas, minimizing the approximation error of the magnetic field detected in each sensor location[101]. The estimation of the magnetic field on the surface of the head, described in Chapter Two 2.6, can be described for the spherical model with the below equation:

$$B_{dipole}(r) = Bo(r)e_r = Bo(r)\frac{r}{|r|} \tag{4.1}$$

based on the knowledge of the radial component, combined with the Maxwell equation [49], [31], [102].

In [98],[103] CSF was found to be the most effective conductor for MEG signal topography due to its high conductivity between gray and white matter and the modeling of skull was neglected due to its low conductivity and high conductivity uncertainties [104]. In our case, the volume conductor chosen for the one-layer model is the low conductivity skull compartment, since MEG ignores tissue conductivity values [103] and focuses on spatial accuracy. This means that the magnetic field will give the same MEG value for a particular sensor, regardless of the conductivity of the layers. The skull allows us to define the outline of the brain volume and construct a more accurate head model.

4.4.2 Inverse problem-Source Analysis

Given the known magnetic field on the surface of the head, we apply source analysis to reconstruct the magnetic field of the sources. In this research, we use linearly constrained minimum variance, a vector-type Beamformer, as a spatial filtering technique for solving the inverse problem.

With the beamformer we try to reconstruct the contribution of a single source (ROI) to the

measured magnetic field, while simultaneously suppressing the contributions from all other sources and noise captured in the data. LCMV, in our case, is done in the time domain using the covariance matrix [64]. Our covariance matrix is a square matrix of size $\langle 248x248 \rangle$ giving the covariance between the data of each pair of sensors, calculated using timelock analysis. The advantage of this algorithm is the implementation without apriori knowledge of the number of sources, since the localization is performed using the spatial covariance matrix [64], and based on the assumption that two distinct regions can generate partial-coherent scalp potentials, not perfectly linearly correlated in their activation time series, making it easy to distinguish [60], [64]. If the sources are 100% correlated the efficiency of the beamformer isn't known.

The beamformer offers an optimization by calculating the optimum weight w_k that minimizes the variance for each source location $r_k = [x_k, y_k, z_k]$

$$min_{w_k} tr[w_k C_i w_k^T] \tag{4.2}$$

where C is the covariance matrix $\langle 248x248 \rangle$ and w the beamformer coefficient vector $\langle 5061x248 \rangle$, that represents the contribution of each of the 248 sensors in the 5061 sources [105].

We apply 5% regularization into our linear estimator (beamformer) to suppress the noise added in the system [54],[106]. The mathematical model of the algorithm is analyzed in extent in many studies [64], [60], [67],[65], [62].

We apply a more specific, more complex, spatial filtering technique for reconstructing the sources. By applying the obtained spatial filters $\langle 5061x248 \rangle$ to the MEG data $\langle 248x91553 \rangle$, the result of the analysis is a time series $\langle 5061x91553 \rangle$ representing the activity of each source.

$$y_k = w_k x \tag{4.3}$$

Utilizing a 90 Regions of Interest template Atlas for all subjects we cluster our sources, assigning each cluster to one of the 90 Regions of Interest. Based on the Spectral Power S (4.5) of each one of the sources within the clusters, we estimate the final source that

contributes the most to each ROI (4.6)

$$\sum_{i=1}^{90}\sum_{m=1}^{N} X(\omega, i, m) = \sum_{i=1}^{90}\sum_{m=1}^{N}\int x(t, i, m)e^{j\omega t}\vartheta t \tag{4.4}$$

$$\sum_{i=1}^{90}\sum_{m=1}^{N} S(\omega, i, m) = \sum_{i=1}^{90}\sum_{m=1}^{N} |X(\omega, i, m)|^2 \tag{4.5}$$

$$\sum_{i=1}^{90} ROI(i) = \sum_{i=1}^{90} max(S(\omega, i, m)) \tag{4.6}$$

where N is the number of sources within each of the 90 clusters.

We result in 90 Regions of Interest with reconstructed data y_k $\langle 90x91553 \rangle$ for each subject.

4.5 Functional Connectivity Networks

4.5.1 Frequency Coupling

We use Frequency Coupling to measure the synchronization of the neural oscillations between ROIs. With Time Varying Phase Locking Value (TV-iPLV) we estimate the phase-to-phase oscillations of the sources over segmented time intervals for each brain rhythm and each subject. With PAC we estimate the phase-to-amplitude (PAC) interactions between brain rhythms. Firstly, source-space data were filtered into delta (1-4 Hz), theta (4-8 Hz), alpha (8-15 Hz), beta (15-30 Hz), low gamma (30-45 Hz), high gamma (45-80 Hz) bands. Sliding window correlation is the most commonly used method for dynamic functional connectivity analysis. Based on [91] the minimum window length should be at least equal to 1/fmin, where fmin is the minimum frequency of the signal. With a sliding time window of 1 minute and a step of 0.1 minutes, we estimated the intra-frequency and inter-frequency phase coupling values of the filtered time series, over segmented time intervals.

4.5.1.1 Intra- Frequency Coupling

For Intra- Frequency Coupling graph we estimate the TV-iPLV values for each pair of sources Xi, Xj (ij=1, ...90) using Hilbert transform [107],[108].

$$IFCG_{i,j} = \frac{1}{N}\sum_{1}^{N} e^{-(\phi f,j - \phi f,i)} \tag{4.7}$$

Where N refers to 1785 slides, resulting from the time window and step chosen earlier, and ϕf to the phase time series extracted via the Hilbert Transform for each i,j source.

$$\phi f, i = tan^{-1}\{HT(X_{f,i})\} \tag{4.8}$$

while the imaginary part of TV-iPLV is given by

$$Im\{IFCG_{i,j}\} = \frac{1}{N}\left| Im\left\{\sum_{1}^{N} e^{-(\phi f,j - \phi f,i)}\right\}\right| \tag{4.9}$$

We result in 1785 intra-frequency fully connected functional connectivity graphs of size $\langle Rois \times Rois \rangle$.

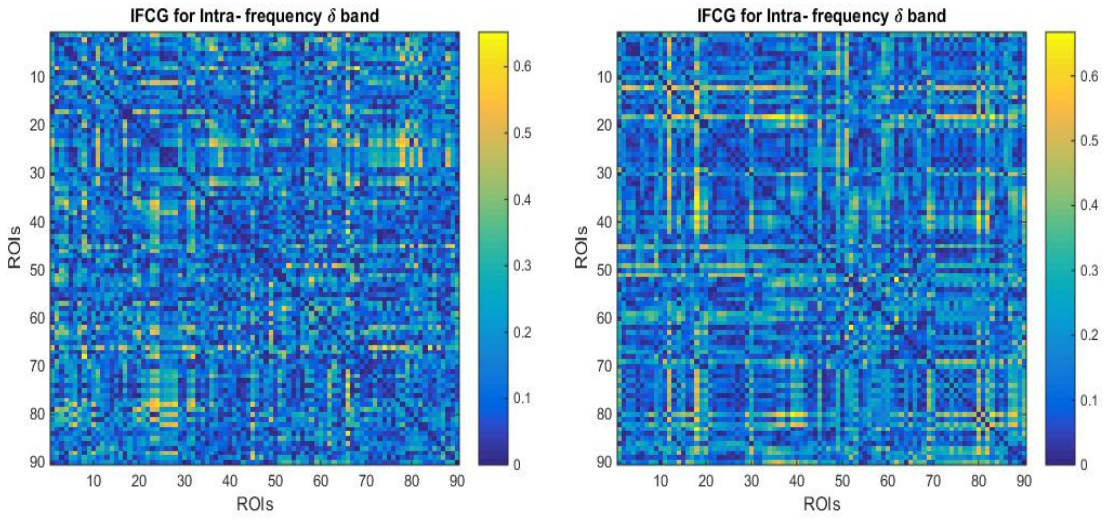

(a) Non Impaired (b) Reading Difficulties

Figure 4.4: Comparison of the δ band Intra-frequency Functional Connectivity Graphs for NI (4.7a) and RD (4.7b). This figure demonstrates the last snapshots of the first subjects NI and RD accordingly.

4.5.1.2 Cross Frequency Coupling

Phase-to-amplitude coupling is the most suitable for estimating brain connectivity in cross-frequency bands [3]. We estimate the PAC values for each pair of frequencies

$$CFCG_{i,j} = \frac{1}{N}\sum_{1}^{N} e^{-(\phi lf - \phi low-to-highf)} \tag{4.10}$$

where the imaginary part of the PAC is given by

$$Im\left\{CFCG_{i,j}\right\} = \frac{1}{N}\left|Im\left\{\sum_{1}^{N} e^{-(\phi lf - \phi low-to-highf)}\right\}\right| \tag{4.11}$$

where ϕ_{lf} the phase of the slow frequency and $\phi_{low-to-highf}$ the phase of the modulated low-to-high frequency extracted from the Hilbert Transform on the envelope of the fast oscillation. In cross-frequency coupling, the phase of the lower frequency oscillation for each i source modulates the amplitude of the higher frequency oscillation for each j source. Like in IFCG, the result is a matrix with dimensions $\langle 1785 \times 90 \times 90 \rangle$.

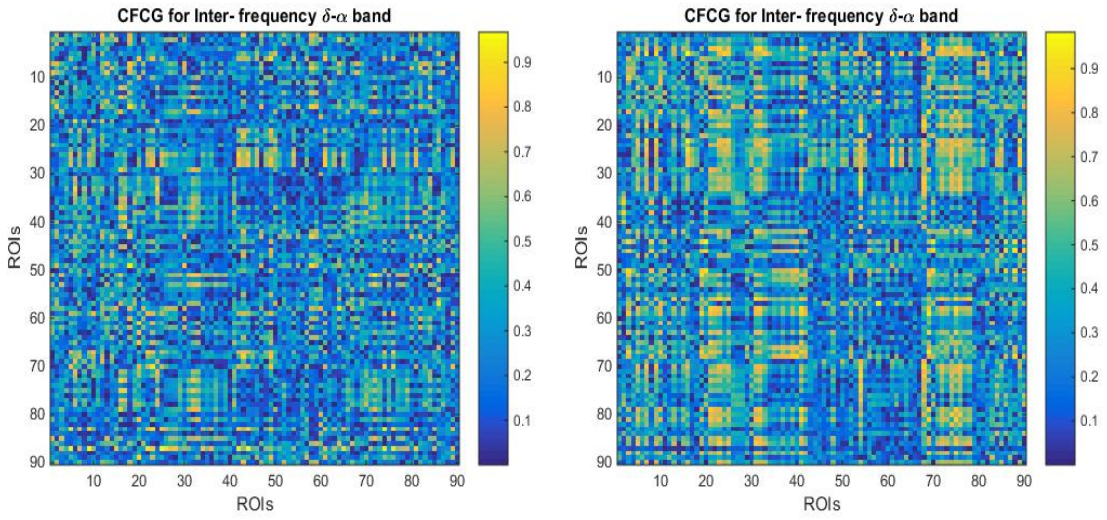

(a) Non Impaired (b) Reading Difficulties

Figure 4.5: Comparison $\delta - \alpha$ Inter- frequency Functional Connectivity Graphs for NI (4.7a) and RD (4.7b) subjects.This figure demonstrates the last snapshots of the first subjects NI and RD accordingly.

4.5.1.3 Dominant Frequency

For the DFCG we identify the optimal frequency coupling, from both intra and inter- frequency, to subsequently give us the optimal graph results. We estimate the dominant frequency, by getting the maximum value from 21 frequency couplings, 6 intra-frequency couplings and 15 inter-frequency couplings [13].

$$DFCG_{i,j} = max_{f=\{\alpha\beta\delta\theta\gamma1\gamma2\}.fc=(\alpha,\beta),\ldots,(\delta,\theta)} IFCG(i,j), CFCG(i,j) \tag{4.12}$$

The dominant frequency graph $\langle 1785 \times 90 \times 90 \rangle$ maximizes the group differences between NI and RD. The $\delta - \beta$ cross-frequency coupling emerged as the predominant frequency within the dominant frequency graph.

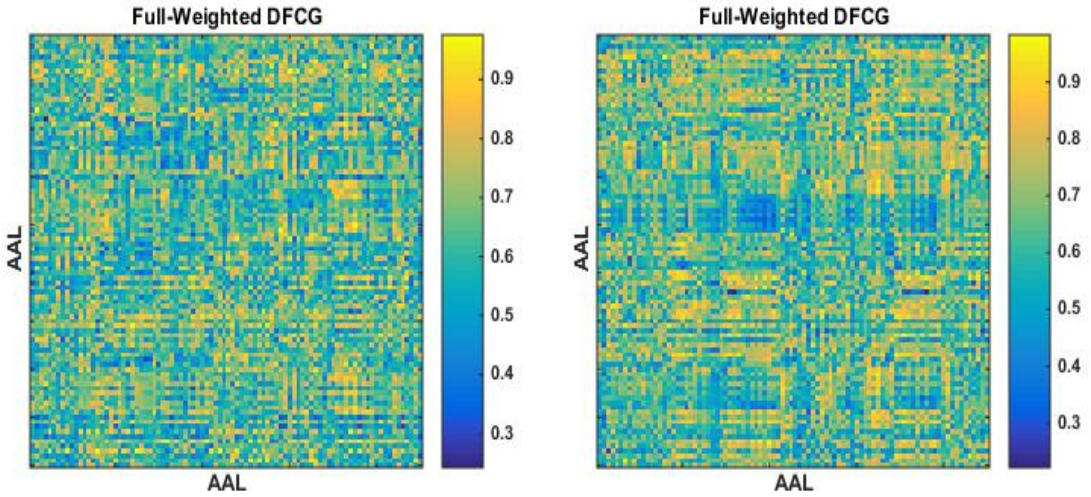

(a) Non Impaired (b) Reading Difficulties

Figure 4.6: Comparison of the Full-Weighted Dominant Functional Connectivity Graphs for NI (4.6a) and RD (4.6b) subjects

4.5.2 Topological Filtering

Fully connected graphs are more complex and difficult to analyze. A data-driven topological filtering technique is applied to our Functional Connectivity Graphs to detect the strongest interactions within brain regions. This technique is useful for maximizing the synchronization between brain areas and allowing the extraction of the significant information flow. Many brain network analyses consider important information to be found in the shortest paths between cerebral regions. In DB West's book [109] graph metrics for finding the shortest

path, like Prim's algorithm, Kruskal's, Dijkstra's, and BFS are described in detail. Using the Kruskal algorithm on the connectivity graph of each subject in intra-, inter-, and dominant frequency, we estimate the MSTs consisting of the minimum-weight subgraph [108]. To better sample the brain network, we orthogonalize each MST, by creating 15 MSTs while zeroing their connections in each repetition. From the constructed OMSTs, we choose the Optimal that maximizes the formula (global efficiency - cost)

$$J = \frac{E(mst)}{E(G)} - cost(mst) \tag{4.13}$$

where E is the average communication efficiency of the graph defined as the average efficiency, inversely proportional to the distance of nodes i,j ε G

$$E(G) = \frac{1}{N(N-1))} \sum \frac{1}{d_{ij}} \tag{4.14}$$

and cost the mean number of links connecting the graph

$$cost(omst) = \frac{depth(omst)}{depth(G)} \tag{4.15}$$

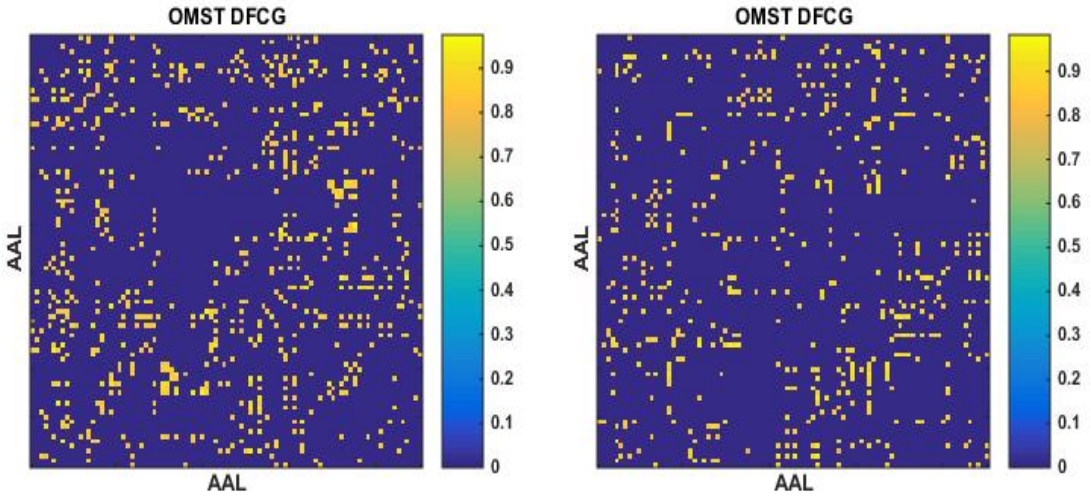

(a) Non Impaired (b) Reading Difficulties

Figure 4.7: Comparison of the Data-Driven Thresholded Dominant Functional Connectivity Graphs for NI (4.7a) and RD (4.7b) subjects. This figure demonstrates the last snapshots of the first subjects NI and RD accordingly.

4.6 Functional Connectivity Microstates

4.6.1 Neural-Gas Algorithm

We use a microstate-based method to explore the functional connectivity pattern associated with each microstate class. To extract the differences in microstate dynamics between the two groups, we construct a group study with time series $\langle 90 \times [slides \times subjects] \rangle$, $\langle 90 \times 71400 \rangle$ for NI and $\langle 90 \times 46410 \rangle$ for RD, representing the degree/strength of each group's functional connectivity graphs[12]. Using Vector Quantization techniques on the reconstructed time series we transform our MEG time series into symbolic time series.

The Neural Gas algorithm helps us map our time series to the symbolic time series, using k prototypical microstates[15],[110]. Each repetition consists of the following steps:

1. The initial prototype values $\langle 1 \times 90 \rangle$ are randomly selected from the range of each attribute over all samples. With every repetition the prototype values $\langle k \times 90 \rangle$ are recalculated, according to the number of clusters k.

2. The clustering of the time series data points to symbols is achieved by calculating the Euclidean Distance of the time series from the k prototypes. The constructed time series are $\langle 1 \times 71400 \rangle$ for NI and $\langle 1 \times 46410 \rangle$ for RD, indicating the microstates of each subject.

3. The repetitions stop when the optimal number of clusters is found and the end condition is met. The average distortion error between the original time series and the reconstructed one is estimated. The end condition is met when the error is higher than the chosen threshold.

For a better point of comparison between microstates, we choose a constant number of symbols for both groups and frequencies. To achieve this constant number of symbols we apply different threshold values. Setting the threshold for the reconstructed error rate approximately at <1.5% for intra- and dominant frequency and <2% for inter-frequency we result in the k=5 symbols for both NI and RD in inta-, inter- and dominant frequency. The symbolic time series STS^{NG} consist of symbols i (i=1, ..., 5) with size $\langle 1 \times 71400 \rangle$ for NI and $\langle 1 \times 46410 \rangle$ for RD.

4.6.2 Chronnectomic Features

Useful information on brain states is to be found when analyzing their transition probabilities. The transitions between FCmstates are estimated based on the interchanges between the following indicators of the codebook created in the previous section 4.6.1 using NG. The indicators are initially sorted, based on the eigenvalues derived from the Laplacian matrices. With calculations on the functional connectivity graph $\langle 5 \times 5 \rangle$ of the FCmstates, the Laplacian matrices are estimated. The term chronnectomics is used to describe the calculation metrics of the dynamic connectivity network. Based on the patterns of transitions and connectivities between states we are able to estimate metrics, such as the complexity index (CI), flexibility index (FI), the occupancy time (OT) and dwell time (DT)[108]. The complexity of a network is defined as the distribution of distinct words up to a specific length of letters-symbols, normalized by randomized versions of the symbolic time series [15]. We estimate the symbol distribution within segmented symbolic time series for each subject with the given formula[12]

$$CI = \sum_{i=1}^{N} c^i(STS^{NG}) \tag{4.16}$$

where N=5 is the length of the symbols. CI values were then normalized using 5 randomized versions of the original symbolic sequence. The resulting matrix $\langle 90 \times 66 \rangle$ represents the complexity of the network.

We estimate the FI, OT and DT based on the ranked FCmstates. The flexibility Index describes the cumulative transitions between the following indicators, thus the transition probabilities among states

$$FI = \frac{number\ of\ transitions}{number\ of\ indicators} \tag{4.17}$$

Occupancy time per symbol describes the cumulative time that the brain spends in each state, while dwell time per symbol describes the consecutive period of time that the brain spends in each state.

$$OT = \frac{frequency\ of\ occurance}{number\ of\ indicators} \tag{4.18}$$

$$DT = \frac{frequency\ of\ consecutive\ occurance}{number\ of\ indicators} \tag{4.19}$$

4.6.3 Statistical Analysis

Statistical testing helps us analyze our data and informs decisions about the distributions and differences of the two groups. For each test applied, we define a corresponding null hypothesis, which we either accept or reject based on the selected significance level. The significance level α, is a measure of strength, that quantifies the likelihood that the observed results are not due to random chance. The results of the statistical tests, P-values, that don't exceed the significance level are considered statistically significant and accept the null hypothesis, while those greater than α are attributed to chance and reject the hypothesis.

We applied statistical tests in both the degree\strength time series and the chronnectomics. Initially, a normality test is applied to determine whether the data are normally distributed. The Kolmogorov-Smirnov test is a non-parametric test that decides the distribution of a sample based on the empirical distribution.

$$D = sup_x \{F_n(x) - F(x)\} \tag{4.20}$$

where $F_n(x)$ the empirical distribution, $F(x)$ the cumulative distribution of the data and sup_x, the minimum upper bound. With null hypothesis of normally distributed data, p-values from (4.20) greater than α reject that hypothesis.
In the case of normally distributed data we use the parametric two-sample f-test to compare the variances of the two groups

$$F = \frac{s1^2}{s1^2} \tag{4.21}$$

where $s1$,$s1$ the variances. The null hypothesis that the two data groups have equal variances is rejected if $F > F_{\alpha/2,N11,N21}$, where $F_{\alpha/2,N11,N21}$ the critical value of the F distribution with N1-1 and N2-1 the degrees of freedom and the significance level of α.
For data with both equal and not equal variances the two-sample t-test is used. This test is used to determine if two population means are equal

$$T = \frac{\mu 1 - \mu 2}{\sqrt{\frac{s1^2}{N1} + \frac{s2^2}{N2}}} \tag{4.22}$$

where $\mu 1$,$\mu 2$ the mean values of the populations. For not equal variance the equation (4.22) is reduced to

$$T = \frac{\mu 1 - \mu 2}{\sqrt{s\frac{1}{N1} + \frac{1}{N2}}} \tag{4.23}$$

The null hypothesis is rejected if $|T| > t_{1-\alpha/2,\nu}$ with $t_{1-\alpha/2,\nu}$, is the critical value of the t distribution with degrees of freedom.

In the case of abnormal distribution, the non-parametric Wilcoxon signed-rank test is applied. We test the distribution of the data by estimating the sums of the ranks derived from a positive and a negative difference of the two samples.

4.7 Machine Learning Algorithms for Classification

Classification algorithms help predict the mental state of the subjects, based on extracted information of their brain activity. Many studies have widely researched Children with Reading Difficulties in resting state MEG using Machine Learning algorithms for classification. To gain insight into the underlying neural interactions and thoroughly examine the behavior of each classifier, both the K-Nearest Neighbours (k-NN) and Support Vector Machines (SVM) algorithms were employed in our research[111]. This strategic approach enhances our understanding and yields comprehensive insights into the dataset's dynamics.

4.7.1 K-Nearest Neighbours

The k-Nearest Neighbors (KNN) algorithm operates by predicting output values based on a set of input values, through the identification of the K nearest neighbors to each data point, determined by a specified distance metric. This algorithm is simple, highly accurate, and highly appropriate for our research, given our relatively small and noise-free dataset. k-NN is also a non-parametric and supervised algorithm, which means it uses labeled datasets and does not require any assumptions about the underlying data distribution.

In our study, the classification is binary and only two classes have to be distinguished. The dataset used is a matrix $\langle 66 \times 4 \rangle$ representing all 4 chronnectomics estimated from the previous section (flexibility index, Complexity index, Occupancy Time and mean Dwell Time) per subject. Initially, data are sampled for training and testing, using K-fold cross-validation

[15]. The data set is split into k sets, from which one by one the data points are categorized in training and test. Usually, as well as in this research, the fold value is k=10. Cross-validation is an important step for the classification, that helps avoid over-fitting and assess the performance of the model. Training and testing datasets were split based on a ratio 90\10, where 90% of the dataset was used for training and 10% for testing.

During the training phase, we predict the class of the data points. During the testing phase, each test data point is classified based on the training model, using Euclidean Distance as the decision boundary.

$$distance(x, x_j) = \sqrt{\sum_j |x - x_j|^2} \tag{4.24}$$

The algorithm selects the k-trained data points that have the shortest distances to the test data point and assigns to it the class that is the most frequent among the k-trained data points. We employ a 100-iteration iterative scheme to enhance classification performance.

Lastly, we applied the k-NN classifier one more time, in this case by extracting the most informative features using a Laplacian score[12] [15]. We estimate a cut-off threshold, based on 1000 Laplacian values estimated from randomized sequences of the features. The features extracted for k-NN classification, are the features with Laplacian scores higher than the cut-off threshold. Utilizing Laplacian score-based feature selection optimizes the classifier, resulting in highly accurate performance outcomes.

4.7.2 Support Vector Machines

Employing the same methodology, we apply a 100-iteration 10-fold cross-validation classification, for both no-feature selection and Laplacian scores feature selection, using SVM algorithm. SVM is also a supervised algorithm effective for small, limited training samples. It is a widely used algorithm with high classification performance. Compared to k-NN where the decision boundary is based on the similarity of its features to the features of its k nearest neighbors, SVM is based on the concept of the hyperplane. During training a linear kernel is used as a decision boundary, to classify the linearly separable training data into classes. Based on the distance of the data points from the hyperplane, data are assigned in class one

or two

$$y = +1, \vec{x}.\vec{w} + b \geq 1$$
$$y = -1, \vec{x}.\vec{w} + b \leq 1 \tag{4.25}$$

where x is the data point and vectors $\vec{x}$ and $\vec{w}$ perpendicular to the hyperplane, while b is the decision boundary. If the dot product is greater than 'b' then training data is classified to class 1, otherwise the data point is classified to class 2.

During testing each test data point is classified based on the training data set.

4.7.3 Classification performance

The classification performance is evaluated using metrics that assess the ratio between the correctly classified and predicted data points. Such metrics are the accuracy of the performance, the sensitivity, as well as the specificity. The formulas for calculating the evaluation metrics are given by

$$Sensitivity = \frac{TruePositives}{TruePositives + FalseNegatives} \tag{4.26}$$

$$Specificity = \frac{TrueNegatives}{TrueNegatives + FalsePositives} \tag{4.27}$$

$$Accuracy = \frac{TruePositives + TrueNegatives}{N} \tag{4.28}$$

where True Positives are the data correctly predicted in the positive class and True Negatives are the data correctly predicted in the negative class. While False Positives are the data incorrectly predicted in the positive class and False Negatives are the data incorrectly predicted in the negative class.

Chapter 5

Results

5.1 Network Analysis

5.1.1 Network Dynamics of Brain Regions at Dominant Frequency

Firstly, we investigated the functional connectivity dynamics of our 5 brain regions: Frontal, Temporal, Central, Parietal, and Occipital. *Figure 5.1* demonstrates the differences between the two groups, NI and RD, regarding the degree\strength of the connectivity network at Dominant Frequency($\delta - \beta$), across each distinct brain region. We present the mean node degree and strength values, alongside their statistically significant differences. Statistical analysis is done utilizing the Wilcoxon rank-sum test, chosen due to the non-normal distribution of both groups, with the level of significance α set at 0.005. We observe highly significant differences at two brain regions, Frontal and Parietal, for both degree\strength time series (***p$<$ 0.005, after FDR correction), while no statistical differences are found in the Temporal region for both time series, and in the Occipital region for the degree time series.

5.1.2 Network Dynamics of Functional Connectivity microstates at Dominant Frequency

After analyzing the connectivity dynamics of each distinct Brain Region, we analyze our network based on functional Connectivity microstates. In this phase of the analysis, we estimate 5 distinct microstates, utilizing the Neural-Gas symbolization algorithm. *Figure 5.2*

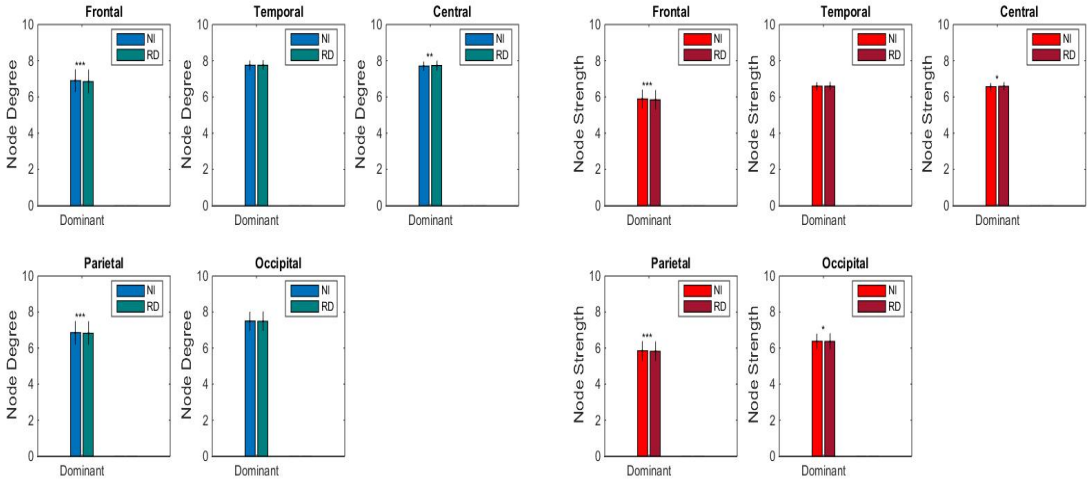

ht (a) Degree time series per brain region (b) Strength time series per brain region

Figure 5.1: Comparison of Children's with Reading Difficulties degree\strength time series per brain region. (5.1a) degree time series for Non Impaired(blue barplot) and Reading Difficulties(dark blue barplot) for the 5 brain regions: Frontal, Temporal, Central, Parietal and Occipital(5.1b) strength time series for NI(red barplot) and RD(dark red barplot) for the 5 brain regions.(***p< 0.005, **p< 0.001,*p< 0.01)

illustrates the differences of the two groups, regarding the degree\strength of the Dominant Frequency connectivity graph, of each microstate across the brain regions. The constant number of network microstates in both NI and RD is determined using a suitable threshold, as an optimal measure of comparison between groups. The Wilcoxon rank-sum test with a level of significance α set at 0.005, is used again. In this case, high statistically significant differences are evident in the two groups across all states and regions.

5.1.3 FCmstate Transition Probabilities at Dominant Frequency

Following the construction of Functional Connectivity microstates utilizing the Neural-Gas symbolization algorithm, we estimate the in-between transitions. As described in Section 4.6.2, the transitions are based on the interchanges between the following indicators of Symbolic Time Series created by NG. The transition dynamics between ranked FCmstates for Non-Impaired 5.4a and subjects with Reading Difficulties 5.4b, are compared in *Figure 5.4*. In this figure, only the transitions that were considered significant, with values exceeding the threshold set at 0.05, are shown. The significant transitions were identified by estimating the mean value across 100 shuffled transition probabilities. We observe, that regarding the

children with RD, a decreased likelihood of transitioning between states is exhibited.

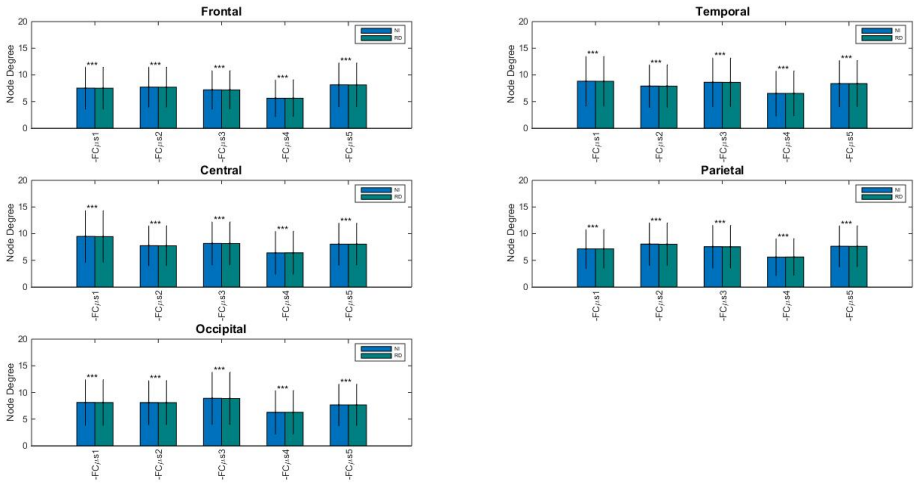

(a) Degree symbolic time series of FCmstates per brain region

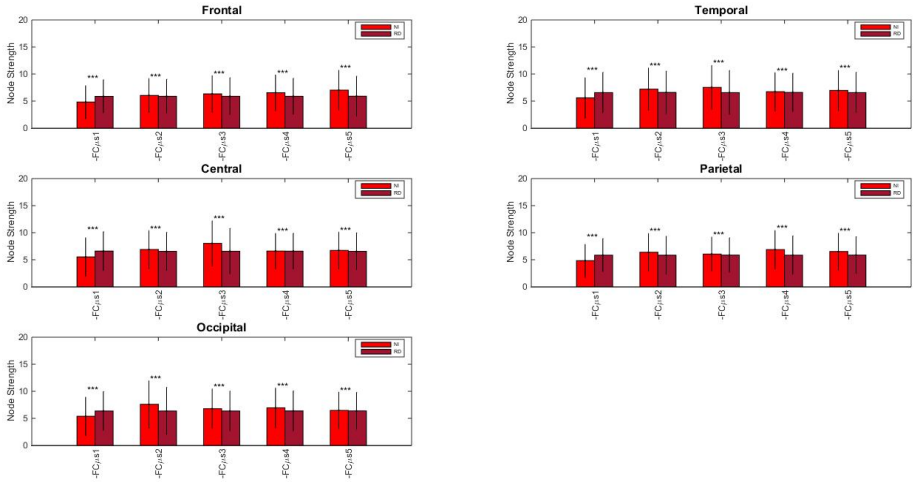

(b) Strength symbolic time series of FCmstates per brain region

Figure 5.2: Comparison of Children's with Reading Difficulties degree\strength time series of the 5 different states per brain region. (5.1a) degree FCmstates time series for Non Impaired(blue) and Reading Difficulties(dark blue) for the 5 brain regions: Frontal, Temporal, Central, Parietal, and Occipital. (5.1b) strength FCmstates time series for NI(red) and RD(dark red).

5.1.4 Chronnectomic Features

As an attempt to identify the differences between groups, we analyze the Chronnectomic features of the STS, Complexity Index, and Dwell Time. *Figure 5.5* compares the Complexity Index for Non-Impaired and subjects with Reading Difficulties at the Dominant Frequency. We observe notable higher, mean complexity, values among Children exhibiting reading dif-

ficulties for both the degree and strength symbolic time series.

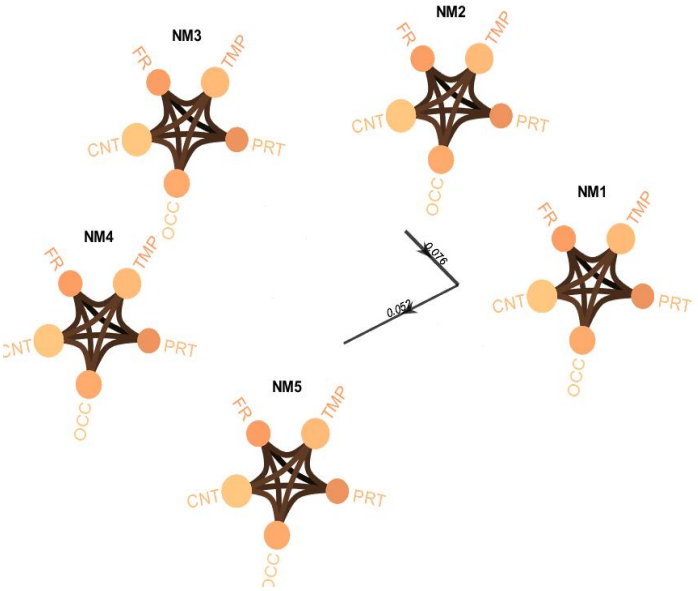

(a) Strength FCmstates for Non Impaired

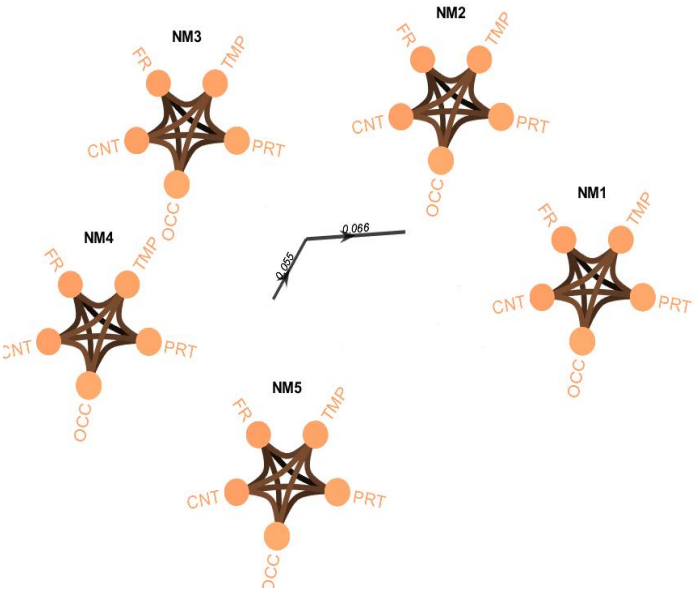

(b) Strength FCmstates for Reading Difficulties

Figure 5.3: Comparison of Children with Reading Difficulties on the significant transitions between Functional Connectivity microstates. The threshold for the significant transition is set at 0.05.

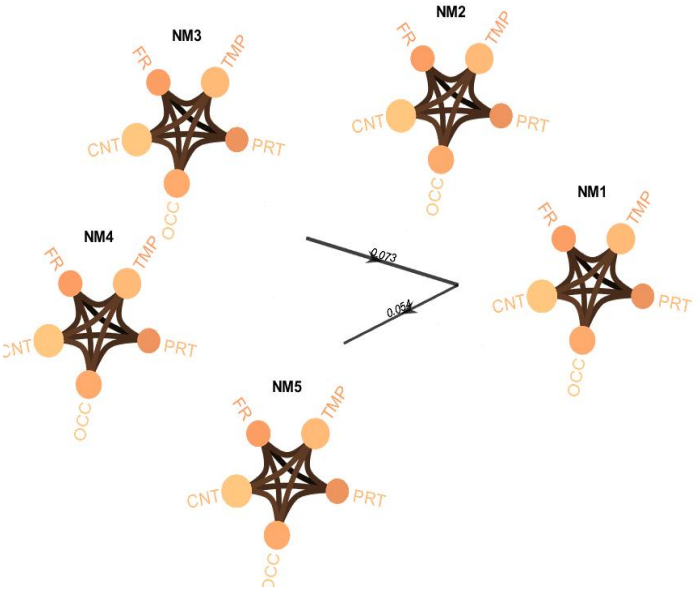

(a) Degree FCmstates for Non Impaired

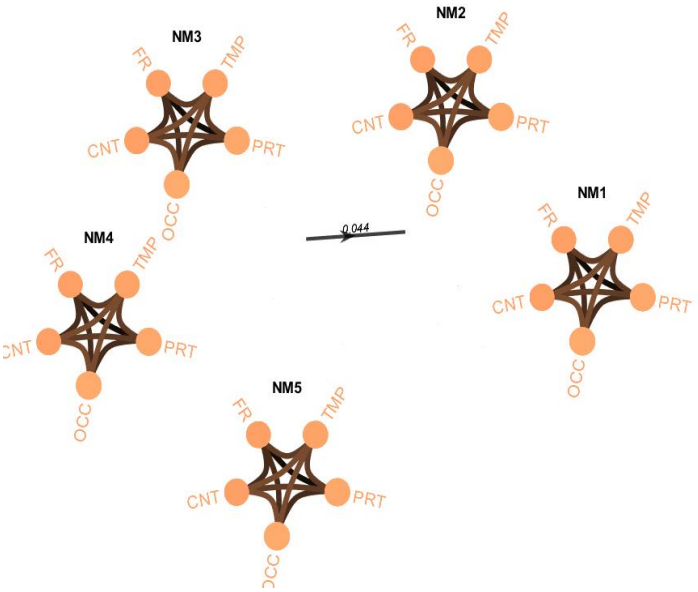

(b) Degree FCmstates for Reading Difficulties

Figure 5.4: Comparison of Children with Reading Difficulties on the significant transitions between Functional Connectivity microstates. The threshold for the significant transition is set at 0.05.

Further analysis of the statistical differences of the complexity between the two groups revealed significant differences in all frequencies(inter,- intra-, and dominant frequencies) among the 5 brain regions, except for the θ band, where the strength symbolic time series displayed no significant statistical difference. *Table 5.1* presents the P-values resulting from statistical analyses using the Wilcoxon rank-sum test, as well as the Q-values following FDR correction. This technique is used to correct the p-values that falsely appear significant. The mean values of the Complexity Index for both the degree and strength time series are shown in *Figure 5.6*, along with their Q-values (***p< 0.005, **p< 0.001, *p< 0.01).

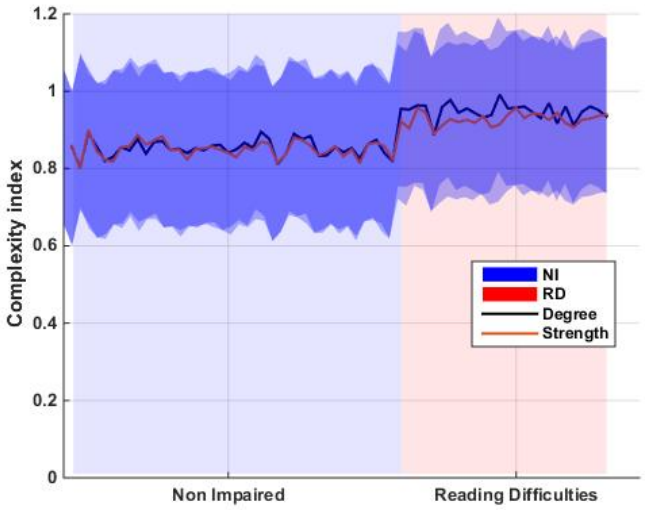

Figure 5.5: Comparison of the Complexity Index for Non-Impaired (left) and Reading Difficulties (right) for both degree and strength symbolic time series of the Dominant frequency.

The mean time the brain dwelled on each microstate for both the degree and strength symbolic time series are shown in Figure 5.7. Despite observing differences in the mean dwell time between the two groups, statistical analysis using the Wilcoxon rank-sum test yielded no statistical difference.

	Frontal		*Temporal*		*Central*	
Frequency	P-values	Q-values	P-values	Q-values	P-values	Q-values
Dominant	1.01×10^{-11}	2.53×10^{-11}	1.01×10^{-11}	2.53×10^{-11}	1.01×10^{-11}	2.53×10^{-11}
δ	2.20×10^{-16}	1.66×10^{-15}	1.11×10^{-16}	1.66×10^{-15}	1.11×10^{-16}	1.66×10^{-15}
θ	0.40	0.41	0.41	0.41	0.41	0.41
α	6.63×10^{-11}	1.10×10^{-10}	6.63×10^{-11}	1.10×10^{-10}	6.63×10^{-11}	1.24×10^{-10}
β	1.59×10^{-12}	5.96×10^{-12}	1.47×10^{-12}	4.42×10^{-12}	1.90×10^{-12}	7.13×10^{-12}
γ_{low}	1.02×10^{-10}	1.53×10^{-10}	9.40×10^{-11}	1.14×10^{-10}	1.02×10^{-10}	1.65×10^{-10}
γ_{high}	2.42×10^{-10}	3.30×10^{-10}	2.42×10^{-10}	3.30×10^{-10}	2.42×10^{-10}	3.30×10^{-10}
$\delta-\theta$	1.01×10^{-11}	2.53×10^{-11}	1.11×10^{-12}	4.17×10^{-12}	1.01×10^{-11}	2.53×10^{-11}
$\delta-\gamma_{low}$	2.22×10^{-16}	1.66×10^{-15}	2.22×10^{-16}	1.66×10^{-15}	3.33×10^{-16}	2.49×10^{-15}
$\delta-\gamma_{high}$	2.81×10^{-13}	1.40×10^{-12}	2.82×10^{-13}	1.14×10^{-12}	3.38×10^{-13}	1.69×10^{-15}
$\delta-\alpha$	1.91×10^{-11}	4.10×10^{-11}	2.09×10^{-11}	4.48×10^{-11}	1.91×10^{-11}	4.10×10^{-11}
$\theta-\beta$	5.92×10^{-04}	5.92×10^{-04}	6.92×10^{-04}	6.92×10^{-04}	6.28×10^{-04}	6.28×10^{-04}
$\alpha-\beta$	2.76×10^{-09}	3.32×10^{-09}	2.55×10^{-09}	6.92×10^{-09}	3.02×10^{-09}	3.77×10^{-09}
$\alpha-\gamma_{high}$	2.88×10^{-09}	3.32×10^{-09}	2.42×10^{-08}	2.60×10^{-08}	2.88×10^{-08}	3.32×10^{-08}
$\beta-\gamma_{low}$	7.10×10^{-09}	7.60×10^{-09}	6.61×10^{-09}	7.63×10^{-09}	7.37×10^{-08}	7.90×10^{-08}
$\gamma_{low}-\gamma_{high}$	6.63×10^{-11}	1.10×10^{-10}	6.63×10^{-11}	1.10×10^{-10}	1.10×10^{-10}	1.65×10^{-10}

	Parietal		*Occipital*	
Frequency	P-values	Q-values	P-values	Q-values
Dominant	1.01×10^{-11}	2.84×10^{-11}	1.01×10^{-11}	2.84×10^{-11}
δ	2.22×10^{-16}	1.55×10^{-15}	1.11×10^{-16}	1.55×10^{-15}
θ	0.40	0.41	0	0
α	7.23×10^{-11}	1.26×10^{-10}	6.63×10^{-11}	1.16×10^{-10}
β	1.49×10^{-12}	5.24×10^{-12}	1.53×10^{-12}	5.37×10^{-12}
γ_{low}	9.40×10^{-11}	1.46×10^{-10}	9.24×10^{-11}	1.43×10^{-10}
γ_{high}	2.42×10^{-10}	3.39×10^{-10}	2.41×10^{-10}	3.37×10^{-10}
$\delta-\gamma_{low}$	2.22×10^{-16}	1.55×10^{-15}	2.22×10^{-16}	1.55×10^{-15}
$\delta-\gamma_{high}$	2.17×10^{-13}	1.01×10^{-12}	1.92×10^{-13}	8.97×10^{-13}
$\delta-\alpha$	1.91×10^{-11}	4.46×10^{-11}	2.09×10^{-11}	4.88×10^{-11}
$\theta-\beta$	5.42×10^{-04}	5.42×10^{-04}	6.11×10^{-04}	6.11×10^{-04}
$\alpha-\beta$	2.68×10^{-09}	3.41×10^{-09}	2.87×10^{-09}	3.65×10^{-09}
$\alpha-\gamma_{high}$	3.07×10^{-08}	3.31×10^{-08}	2.81×10^{-08}	3.03×10^{-08}
$\beta-\gamma_{low}$	6.15×10^{-09}	7.17×10^{-09}	6.95×10^{-09}	8.11×10^{-09}
$\gamma_{low}-\gamma_{high}$	6.63×10^{-11}	1.26×10^{-10}	6.63×10^{-11}	1.16×10^{-10}

Table 5.1: Statistical analysis of the Complexity index of the symbolic degree time series

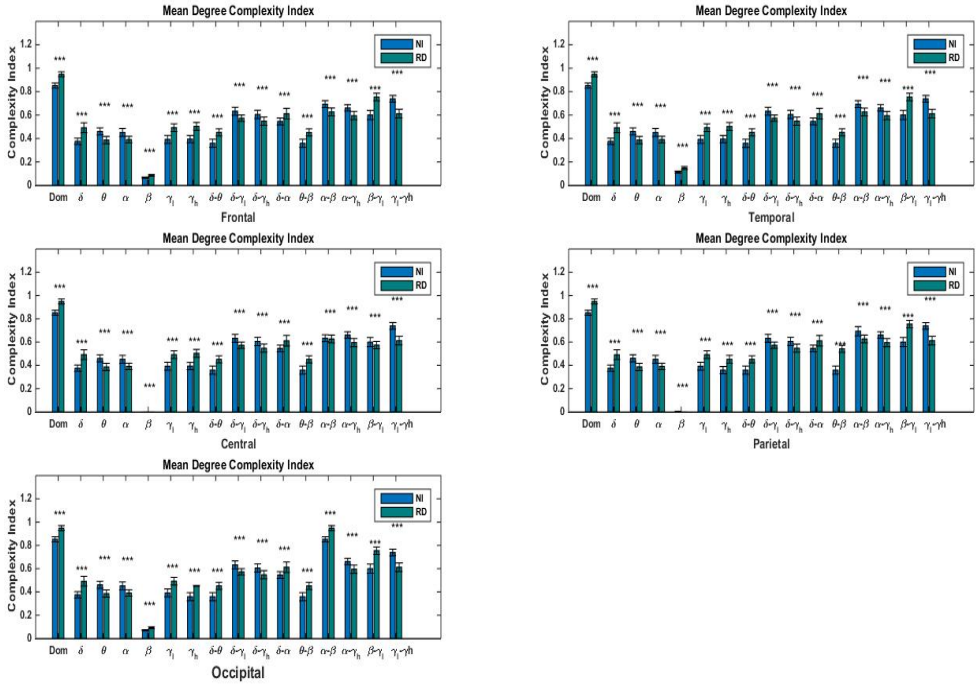

(a) Complexity Index of the degree symbolic time series after symbolization for all frequencies and brain regions

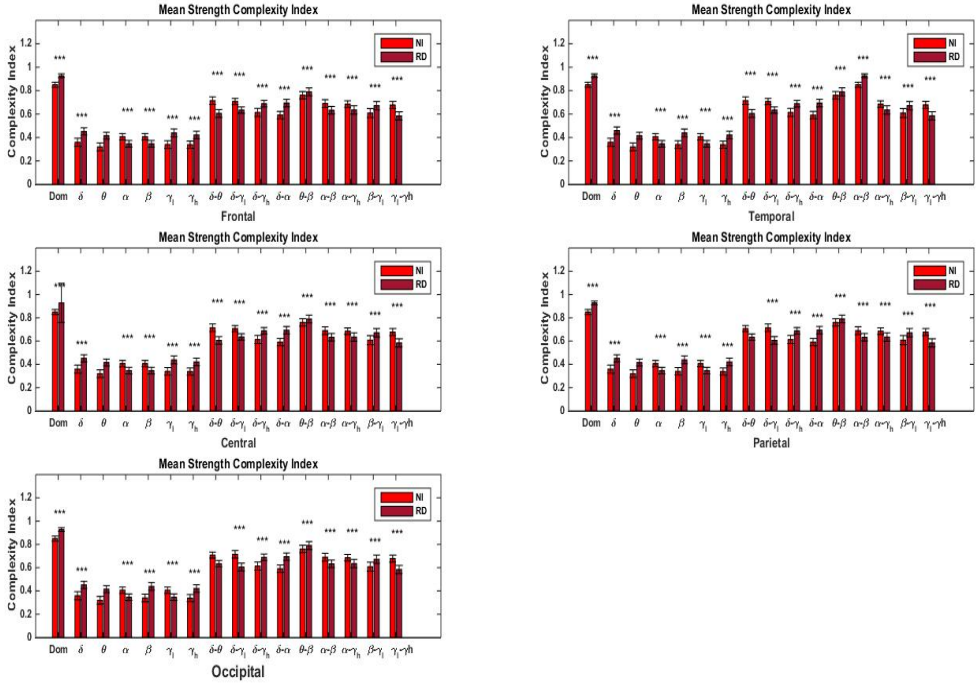

(b) Complexity Index of the strength symbolic time series after symbolization for all frequencies and brain regions

Figure 5.6: Statistical Significance of the group differences: *p< 0.01, **p< 0.001, ***p<0.05, for the complexity Index of the degree\strength symbolic sequences for intra-, inter- and dominant frequencies per net.(5.6a) Complexity Index of the symbolized degree time series for Non Impaired(blue) and Reading Difficulties(dark blue). (5.6b) Complexity Index of the symbolized strength time series for NI (red) and RD (dark red).

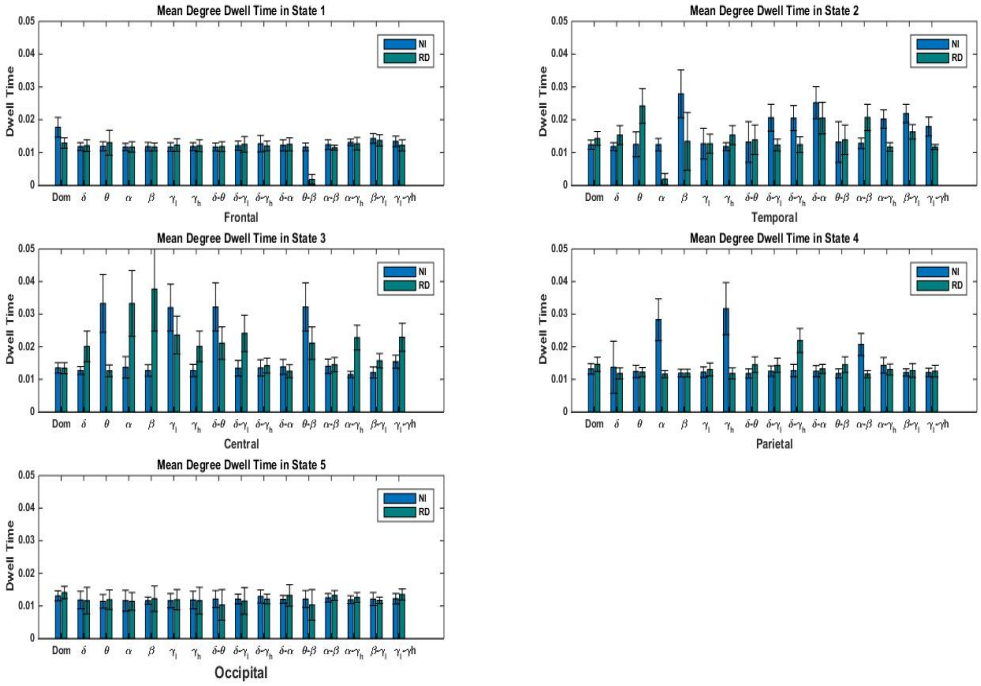

(a) Mean Dwell time of the degree symbolic time series after symbolization for all frequencies in each State

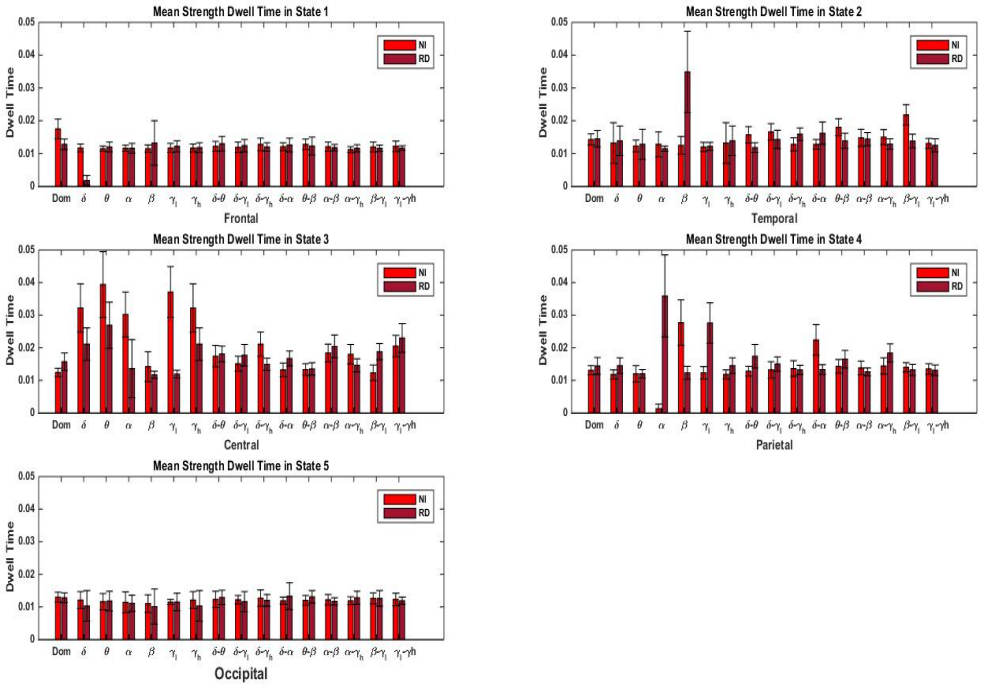

(b) Mean Dwell Time of the strength symbolic time series after symbolization for all frequencies in each state

Figure 5.7: Statistical Significance of the group differences: *p< 0.01, **p< 0.001, ***p<0.05, for the Dwell Time of the degree\strength symbolic sequences for intra-, inter- and dominant frequencies per state.(5.7a) Mean Dwell Time of the symbolized degree time series for Non Impaired(blue) and Reading Difficulties(dark blue). (5.7b) Mean Dwell Time of the symbolized strength time series for NI (red) and RD (dark red).

In *Figure 5.8* we compare the Chronnectomic features of Non-Impaired and subjects with Reading Difficulties. The mean value of the metrics, Flexibility Index, Complexity Index, Occupancy Time, and Dwell Time, along with the statistical differences, are presented. For both algorithms, significant statistical differences are observed between the two groups regarding flexibility and complexity indices across degree and strength FCmstates. On the contrary, no statistical difference is observed in the other two metrics: occupancy time and dwell time.

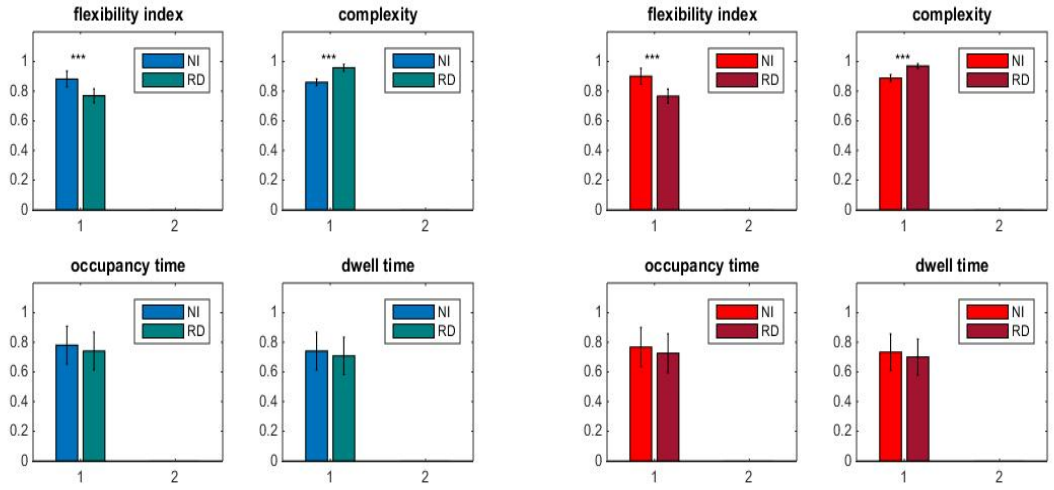

(a) Chronnectomic features of the degree symbolic time series

(b) Chronnectomic features of the strength symbolic time series

Figure 5.8: Statistical Significance of the group differences: *p< 0.01, **p< 0.001, ***p<0.05. Statistical analysis of the 4 features: Flexibility Index, Complexity Index, Occupancy time, and Dwell Time, of the degree symbolic sequence for the dominant frequency.(5.8a) Mean values of the degree symbolic time series features for Non Impaired(blue) and Reading Difficulties(dark blue). (5.8b) Mean values of the strength symbolic time series features for NI (red) and RD (dark red).

5.2 Classification Performance at Dominant Frequency using k-NN and SVM Algorithms

5.2.1 Classification Performance of Functional Connectivity microstates

We analyzed and compared the Classification Performance of both k-NN and SVM algorithms for each FCmstate. To improve the efficiency of the classification between groups, we utilized a 100-iteration 10-fold cross-validation technique and used as features all four

Chronnectomics: Flexibility Index, Dwell Time, Complexity Index, and Occupancy Time. *Table 5.3*, displays the Classification Performance: Accuracy, Sensitivity, and Specificity. Both algorithms achieve accuracy>93%, sensitivity >96% and specificity>86% in both degree and strength FCmstates, with SVM exhibiting slightly higher performance for all three metrics compared to k-NN. Degree FCmstates achieve higher accuracy and specificity values compared to strength FCmstates, however lower values of sensitivity. Extremely high sensitivity values are evident in both algorithms across microstates.

	$k-NN$			SVM		
	Accuracy	Sensitivity	Specificity	Accuracy	Sensitivity	Specificity
State 1	98±0.11	100±0	96±0.79	99±0.14	100±	99±0.33
State 2	98±0.11	100±0	96±0.79	99±0.1	100± 0	96±0.69
State 3	98±0.91	100±0	94±2.46	96±0.68	96±1.06	96±0.77
State 4	93±1.17	98±0.87	86±2.75	96±1.29	97±1.77	95±1.75
State 5	97±0.16	100±0	92±1.12	96±0.87	98±1.32	92±1.45

Table 5.2: Classification Performance for Degree symbolic time series with k-NN SVM Classifier per state

	$k-NN$			SVM		
	Accuracy	Sensitivity	Specificity	Accuracy	Sensitivity	Specificity
State 1	99±0.25	99±0.17	100±0	99±0.55	99±0.32	100±0
State 2	97±0.4	97±0.49	96±0.73	96±0.97	95±1.03	96±1.97
State 3	95±0.89	100±0	87±3.46	99±0.33	98±0.14	100±0
State 4	96±1.72	98±0.43	92±3.46	98±0.51	97±0.91	100±0
State 5	94±0.79	97±0.43	90±2.13	97±0.59	97±0.91	96±0.89

Table 5.3: Classification Performance for Strength symbolic time series with k-NN SVM Classifier per state

In *figure 5.9* we compare the Accuracy of the k-NN and SVM algorithms across degree and strength FCmstates. No statistical difference is found, from the Wilcoxon rank-sum test with a significance level set at α 0.005.

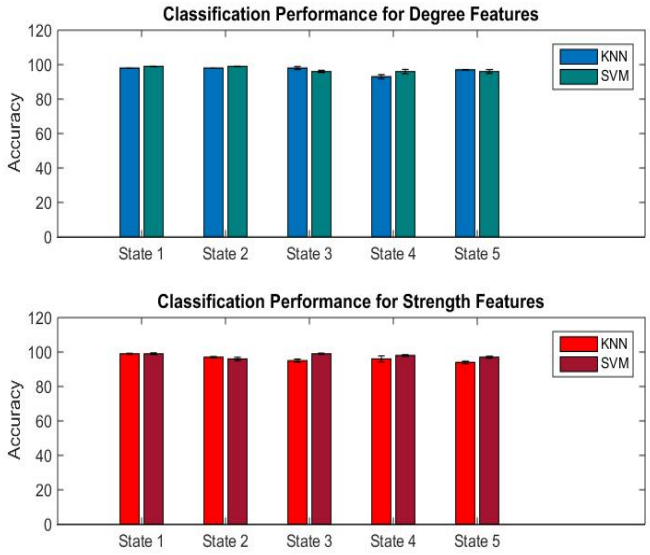

Figure 5.9: Comparison of the Accuracy of all 4 Classification features: flexibility index, complexity index, occupancy time and dwell time for k-NN and SVM Classifiers in dominant frequency per state.

In *figures 5.10* and *5.11* we present the Accuracy, Sensitivity, and Specificity of the k-NN and SVM algorithms across degree and strength FCmstates.

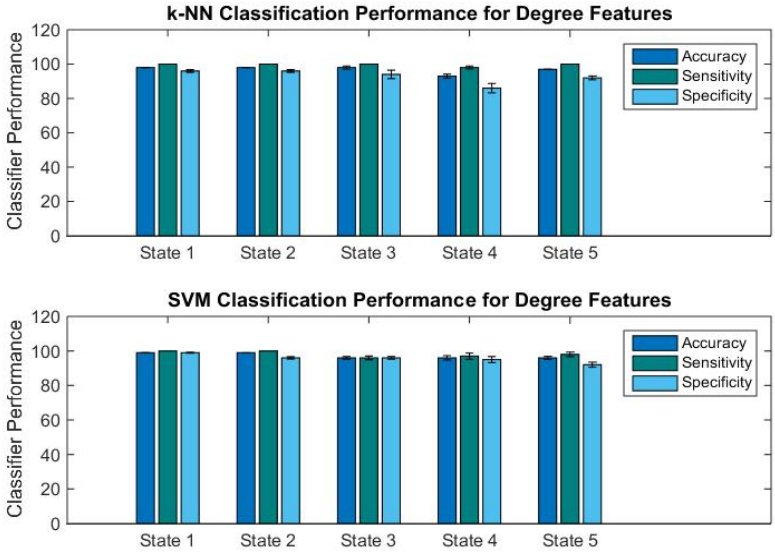

Figure 5.10: Comparison of the Classification performance: Accuracy, sensitivity, specificity, of all 4 Classification features: flexibility index, complexity index, occupancy time and dwell time for k-NN and SVM Classifiers in dominant frequency per state.

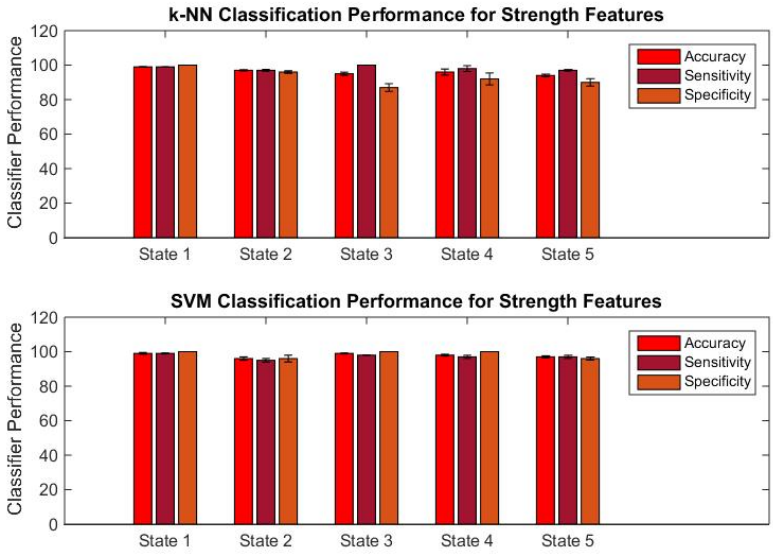

Figure 5.11: Comparison of the Classification performance: Accuracy, sensitivity, specificity, of all 4 Classification features: flexibility index, complexity index, occupancy time and dwell time for k-NN and SVM Classifiers in dominant frequency per state.

5.2.2 Classification Performance at Dominant Frequency with feature selection

Lastly, we assess the Classification Performance of both k-NN and SVM algorithms, after feature selection. We use Laplacian Scores to set a cut-off threshold, retaining only the most significant features. Similarly to before, a 10-fold cross-validation technique is applied to the most discriminative features. *Table 5.4*, highlights the classification performance: Accuracy, Sensitivity, and Specificity. Both algorithms achieve accuracy>96%, sensitivity >97% and specificity>95% in both degree and strength FCmstates, with SVM classifier demonstrating higher performance than k-NN. We observe that the performance slightly diminishes after feature selection, indicating that without feature selection, overfitting had occurred, which is now addressed.

	$k-NN$			SVM		
	Accuracy	Sensitivity	Specificity	Accuracy	Sensitivity	Specificity
Degree	98.12±0.66	100±0	95.1±.89	98.45±0.27	99.95±0.35	96±0.82
Strength	96.95±0.18	97.5±0	96±0.82	97.01±0.33	97.5±0	96.17±1.12

Table 5.4: Classification Performance for Degree\Strength symbolic time series with k-NN SVM Classifier after feature selection using Laplacian Scores

In *figure 5.12* we illustrate the Accuracy, Sensitivity and Specificity of the k-NN and SVM algorithms across degree and strength FCmstates.

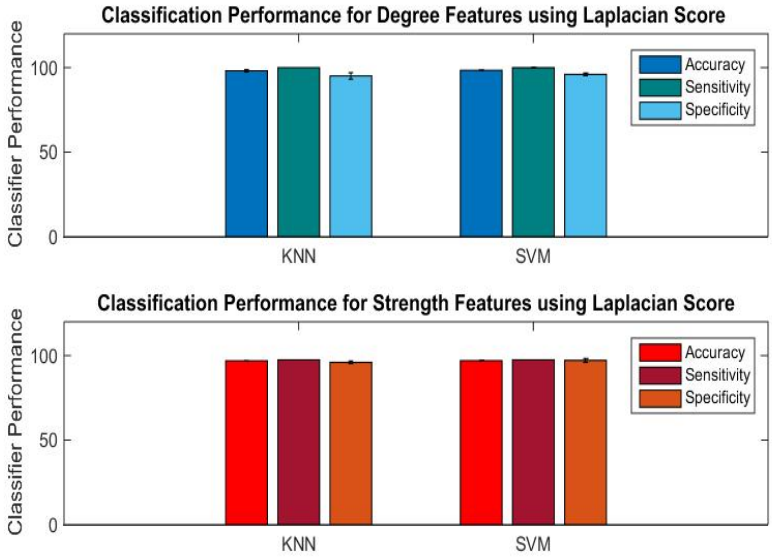

Figure 5.12: Comparison of the Classification performance: Accuracy, sensitivity, specificity, of all 4 Classification features: flexibility index, complexity index, occupancy time and dwell time for k-NN and SVM Classifiers in dominant frequency after feature selection using Laplacian Scores.

Chapter 6

Discussion & Conclusions

6.1 Discussion

This study highlights the differences in the brain networks within the source space, particularly at Dominant Frequency, between Children with Reading Difficulties and Non-Impaired.

Previous studies analyzing brain networks, have utilized dynamic Phase Locking Value to gain insights into the Intra-[107],[12] and Inter- [3] frequency connectivity graphs. Employing a sliding time window to compute phase-to-phase interactions within the same frequency and phase-to-amplitude interactions across frequency pairs, offers a depiction of the multi-layered brain interactions in each subject. In our study, the single-layered connectivity graphs of the 90-region brain network in inter- *(Figure 4.5)* and intra-frequency *(Figure 4.4)*, revealed notable distinctions between NI and RD. A thresholding technique utilizing Optimal Minimum Spanning Trees is applied to the fully weighted connectivity graphs, which otherwise exhibit greater complexity and lesser effectiveness. After the data-driven threshold is applied, the discrimination between NI and RD is enhanced. The correlations between regions were more frequent, stronger, and exhibited higher values within the brain network of Non-Impaired Children *(Figure 7.1)*. On the contrary, frequencies β and θ exhibited more frequent interactions *(Figure 7.1a)*, while frequencies α and θ stronger interactions *(Figure 7.1b)* in RD comparing to NI. In [13] a new technique, that estimates the dominant frequency across the 6 Intra- Frequencies and 15 Inter- Frequency pairs, is presented. In Dominant Frequency, before *(Figure 4.6)* and after OMST thresholding technique *(Figure 4.7)*, the distinctions

between NI and RD appear more evident, with NI subjects exhibiting slightly more frequent and strong correlations.

Analysis of the brain network across brain regions at Dominant Frequency *(Figure 5.1)* exhibited stronger interactions at Central, Temporal and Occipital Lobes. The difference between NI and RD is more evident in the Frontal and Parietal lobes and less evident in the Central and Occipital. Overall, NI demonstrates higher degree and strength values across the regions, except from the Central Lobe where the interactions are stronger in Children with Reading Difficulties. The Temporal Lobe exhibits no difference between the two groups. In the case of inter- *(Figure 7.2)* and intra- *(Figure 7.3)* frequency we observed similarly, slightly stronger interactions at Central, Temporal, and Occipital Lobes. Overall, NI subjects show increased degree and strength values across brain regions, except in the β, θ, δ and α frequency bands. In RD subjects, interaction frequency within the β band notably increased in the Frontal and Central regions. Meanwhile, θ frequency band showed higher contrast in the Central Lobe for both degree and strength time series, with minor variations in the Occipital region regarding the strength of the interactions. In δ and α bands both degree and strength time series exhibit significantly elevated values in the Occipital Lobe.

Prior studies have suggested that distinct microstate classes reflect the transitioning in dynamic phase synchronization patterns [112] and that these connectivity patterns contribute to describing differences in brain functionality [88]. In our study we analyzed the brain networks in Functional Connectivity microstates, aiming to identify the microstate connectivity patterns that differentiate the NI and RD groups. We employed the Neural-Gas symbolization algorithm to construct five Functional Connectivity microstates for each group. In dominant frequency *(Figures 5.4 and 5.3)* we see stronger transition between states in NI subjects compared to RD. In *(Figure 5.2)*, notable distinctions emerge between NI and RD in the FCmstates' brain networks across all brain regions. Specifically, in *Figure 5.2b* RD exhibit elevated strength values in state 1, contrasting with considerably lower values in all other states. The transitions between FCmstates were more frequent or significant in RD subjects, in both Intra-frequency and Inter-frequency, in specific frequency pairs, such as $\alpha, \beta, \gamma_{high}, \gamma_{low}, (\alpha - \gamma_{high})$, $(\delta - \gamma_{low})$, $(\alpha - \beta)$,$(\theta - \beta)$, $(\delta - \theta)$,$(\beta - \gamma_{low})$,$(\delta - \gamma_{high})$ and $(\delta - \alpha)$*(Figures 7.6 - 7.23)*. In β frequency the distinctions between the groups are

also evident in the brain networks within each FCmstate across brain regions *(Figure7.4)*. Additionally, within the Central Lobe, subtle group disparities are observed in the δ and γ_{low} frequency bands. In Inter frequency *(Figure7.5b)* differences are observed in all states and frequencies across brain regions.

To distinguish between subjects with NI and RD, a classification at Dominant Frequency is chosen, resulting in optimal outcomes. Utilizing both k-NN and SVM algorithms, alongside a 100-iteration 10-fold cross-validation technique to ensure the robustness of the results, we are able to classify with high accuracy our subjects. In strength, symbolic time series, both algorithms achieve the highest classification performance in state 1 with accuracy at 99%, sensitivity 99%, and specificity 100% *(Table5.3)*. Meanwhile, in degree time series, both states 1 and 2 demonstrate strong classification performance with accuracy $>$ 98%, sensitivity reaching 100%, and specificity $>$ 96%. Overall, subject classification demonstrates high values, with accuracy>93%, sensitivity>96% and specificity>86% with SVM exhibiting slightly higher performance for all three metrics compared to k-NN 5.9. To avoid the observed overfitting resulting from the notably high classification performance, we implement feature selection, based on Laplacian Scores, on our dataset. In line with prior research [15], Laplacian scores SVM have consistently demonstrated superior performance in classification compared to k-nearest neighbors (k-NN). In our study, the degree symbolic time series exhibits higher classification performance, across all states, with accuracy $>$ 98 %, sensitivity reaching 99% and specificity 95 %, with SVM surpassing in performance the k-NN algorithm *(Table 5.4)*. Our observations suggest that feature selection effectively mitigates overfitting.

The classifier's performance can be explained by analyzing the features employed in the classification process. In *Figures 5.6a and 5.6b* we observe statistically significant differences in the Complexity Index feature between the two groups for both degree and strength symbolic time series. In the Dwell Time feature *(Figures 5.7a and 5.7b)*, while the differences in mean values between NI and RD are apparent, no statistically significant difference is observed. These results are depicted in Figure 5.8, where differences between groups are evident across all four features. Particularly notable are the Flexibility and Complexity Index, which exhibit the most significant statistical differences. Complexity Index, Flexibility Index, and certain

states of the Occupancy Time were found to be the most informative features in the classification scheme *(Figures 7.24 and 7.25)*, attributed to the distinct differences observed between the two groups.

6.2 Conclusions

This study investigated the evident impact of Reading Difficulties on the functional connectivity of the time-varying brain networks at the source level. Employing a range of analysis techniques including complexity analysis and symbolization, our aim is to achieve high classification performance between the groups. Analysing the resting-state, source-space MEG brain networks we observed that Non-Impaired subjects exhibited slightly more frequent and robust interactions within brain regions. Particularly, identification of the brain network in Dominant Frequency enhances the differences between NI and RD subjects and offers a better depiction of the brain networks across brain regions and FCmstates. In Dominant Frequency ($\delta - \beta$) NI subjects demonstrated more frequent and robust interactions within brain networks. Lower values in the Frontal, Parietal, and Occipital Lobes and four out of five states, indicate reduced brain activity in children experiencing Reading Difficulties. The under-activation of those regions shows reduced cognitive and judgment abilities related to the Frontal Lobe in Children with Reading Difficulties. Additionally, there is a reduced capacity to interpret signals received from vision and hearing and identify their meaning based on memory related to the Parietal and Occipital lobes. On the contrary, the Central Lobe displays overactivation and heightened brain interaction in children with RD, manifesting heightened emotions and behavioral responses. The least susceptible Lobe is found to be the Temporal Lobe, with no differences between the groups. The utilization of Dominant frequency yields optimal results compared to both inter- and intra-frequency analysis. Utilizing all four features, Complexity Index, Flexibility Index, Dwell, and Occupancy Time, of the Dominant Frequency symbolic time series provides high classification performance. Both k-NN and SVMdemonstrated strong performance, with accuracy>93%, sensitivity reaching 96% and specificity>86%. SVM showed slightly higher performance across all three metrics compared to k-NN, specifically in states 1,3 and 4. After feature selection, both algorithms, k-NN and SVM, demonstrate slightly reduced performance values, suggesting a more ro-

bust classification algorithm. However, they still achieve an exceptionally high classification performance, with accuracy $> 96\%$, sensitivity $> 97\%$ and specificity $> 96\%$.

6.3 Future Work

This study focused on large-scale functional brain connectivity architecture. An interesting future approach would be the analysis of the functional connectivity of the brain networks in rich club and small word organizations [113]. The terms "small-world" and "rich club" refer to the topological properties of brain networks, where subgraphs are constructed to include nodes that are indirectly connected over short distances and strongly interconnected accordingly. Extracting RC and SW network metrics, representing the backbone of brain networks (the most significant information flow between regions), could optimize the identification of altered brain regions and subsequently classify with high accuracy children with reading difficulties.

Another suggestion for future work would be the use of Time-varying Multivariate Auto regressive models (MVAR) as an optimization to estimate dynamic interactions. Due to the multivariate nature of neuronal interactions, multivariate models are proposed to describe the directed functional connectivity and phase synchrony with better accuracy[114]. The MVAR model can also be useful in analyzing the effective connectivity of brain networks. In our research, we analyze the functional connectivity, by estimating the correlations among brain regions using various measures of synchrony, correlation, or coherence. On the contrary, effective connectivity refers explicitly to the influence that one neural system exerts over another [69]. Granger causality and Bayesian models are techniques used for measuring the causal relationships between brain regions and, subsequently, effective connectivity [115]. These techniques have been rarely investigated in studies of resting-state MEG, especially in the context of reading difficulties.

Finally, a possible research direction could involve using neural networks for classification. Neural networks are a newer classification technique not yet widely used for children with reading difficulties. Most studies on reading difficulties focus on using deep learning on MRI or fMRI data [116]. Very few researchers have examined deep learning approaches, such as

MLP [117] and ANN [118], using cognitive skills as features. Specifically study [117], used Reading Fluency and Reading Comprehension as features, proving that MLP can achieve high classification performance, even surpassing linear and mixture models. A research based on our data would be an interesting approach to follow, to analyze the intrinsic brain patterns and successfully classify the subjects. It would also allow, us to examine the benefits and limitations of neural network classification when applied to Reading Difficulties in Children.

Chapter 7

Appendix A

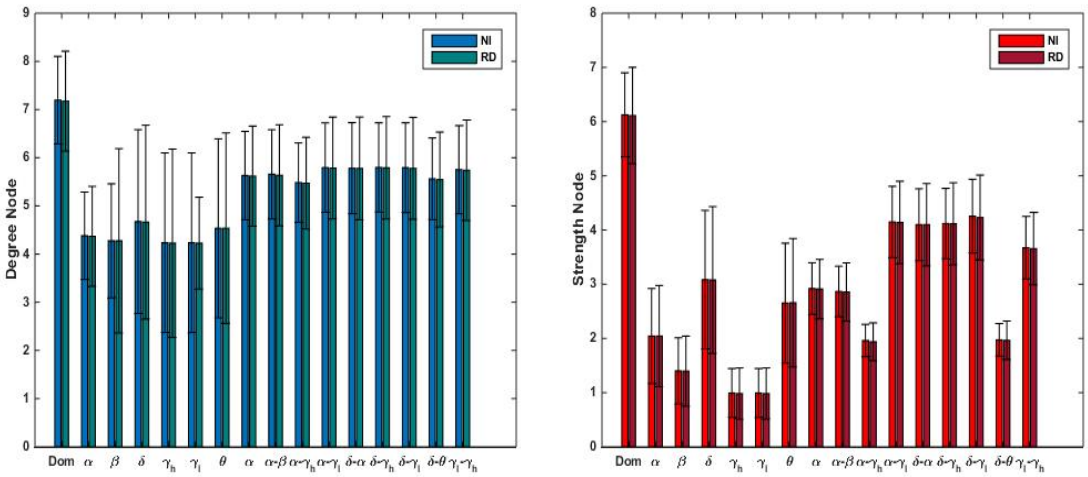

(a) Degree time series

(b) Strength time series

Figure 7.1: Comparison of Children's with Reading Difficulties degree\strength time series for frequencies and brain regions.(7.1a) degree time series for Non Impaired(blue barplot) and Reading Difficulties(dark blue barplot) ,(7.1b) strength time series for NI(red barplot) and RD(dark red barplot).(***p$<$ 0.005, **p$<$ 0.001,*p$<$ 0.01)

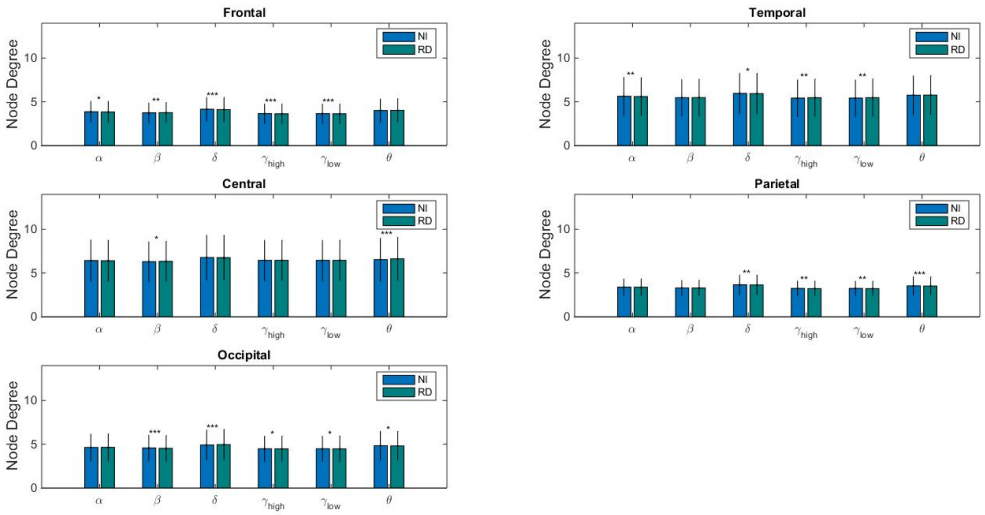

(a) Degree time series per brain region at Intra-Frequency

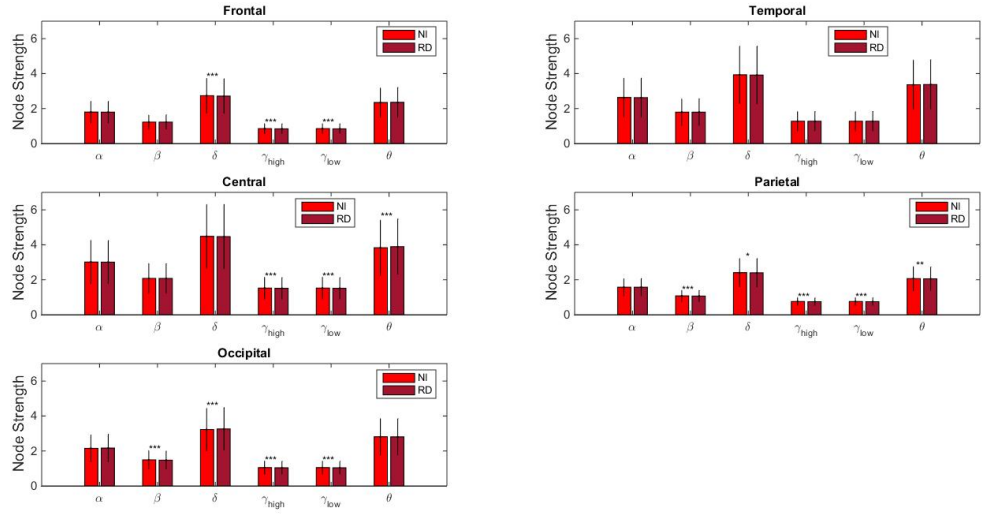

(b) Strength time series per brain region at Intra-Frequency

Figure 7.2: Statistical Significance of the group differences: *p< 0.01, **p< 0.001, ***p<0.05, for the degree\strength time series per brain region in Intra- Frequency.(7.2a) degree time series for Non Impaired(blue barplot) and Reading Difficulties(dark blue) for the 5 brain regions: Frontal, Temporal, Central, Parietal and Occipital(7.2b) strength time series for NI(red barplot) and RD(dark red) for the 5 brain regions.

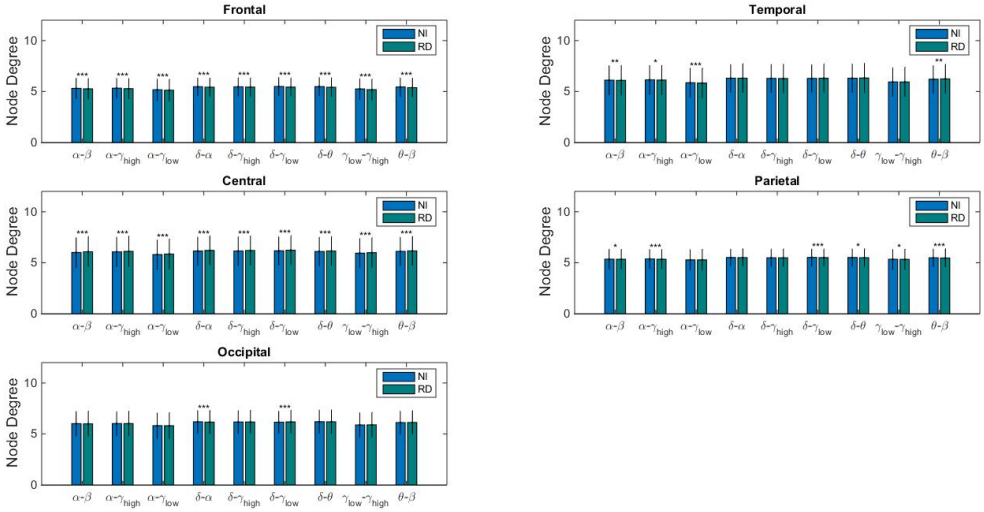

(a) Degree time series per brain region at Inter-Frequency

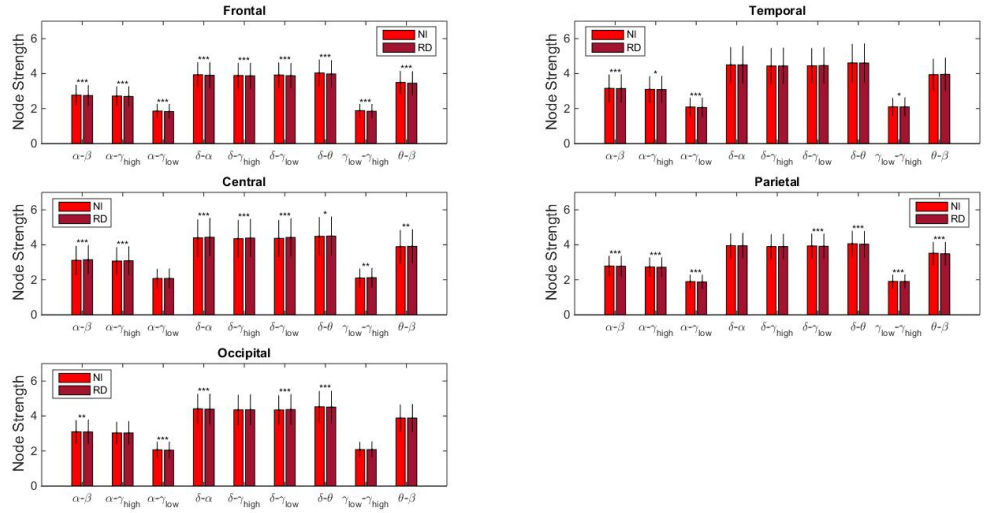

(b) Strength time series per brain region at Inter-Frequency

Figure 7.3: Statistical Significance of the group differences: *p< 0.01, **p< 0.001, ***p<0.05, for the degree\strength time series per brain region in Inter- Frequency.(7.3a) degree time series for Non Impaired(blue barplot) and Reading Difficulties(dark blue) for the 5 brain regions: Frontal, Temporal, Central, Parietal and Occipital(7.3b) strength time series for NI(red barplot) and RD(dark red) for the 5 brain regions.

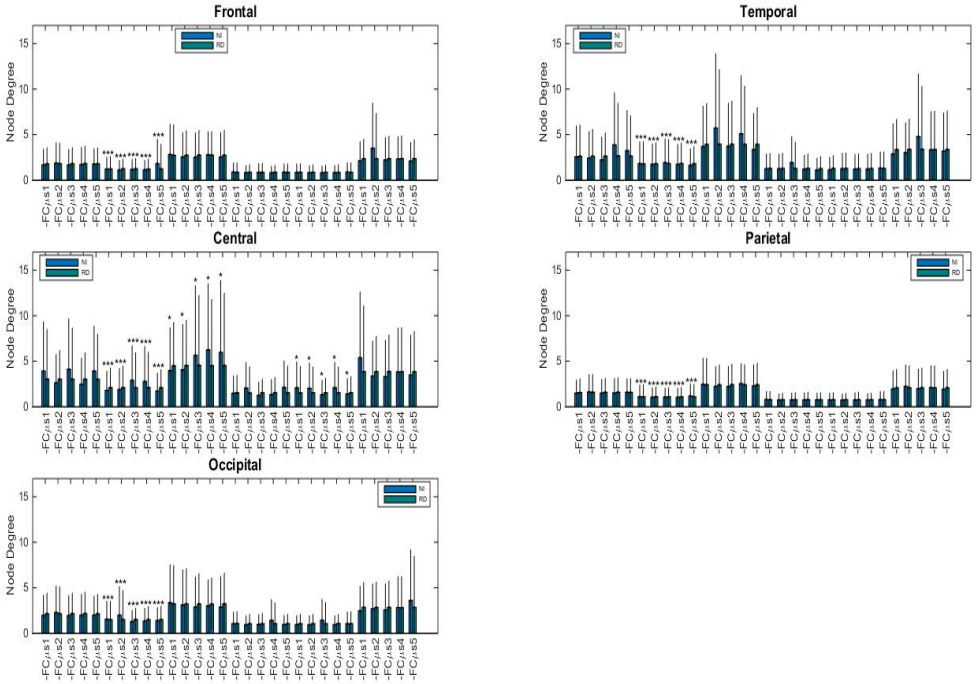

(a) Degree time series per brain region at Intra-Frequency

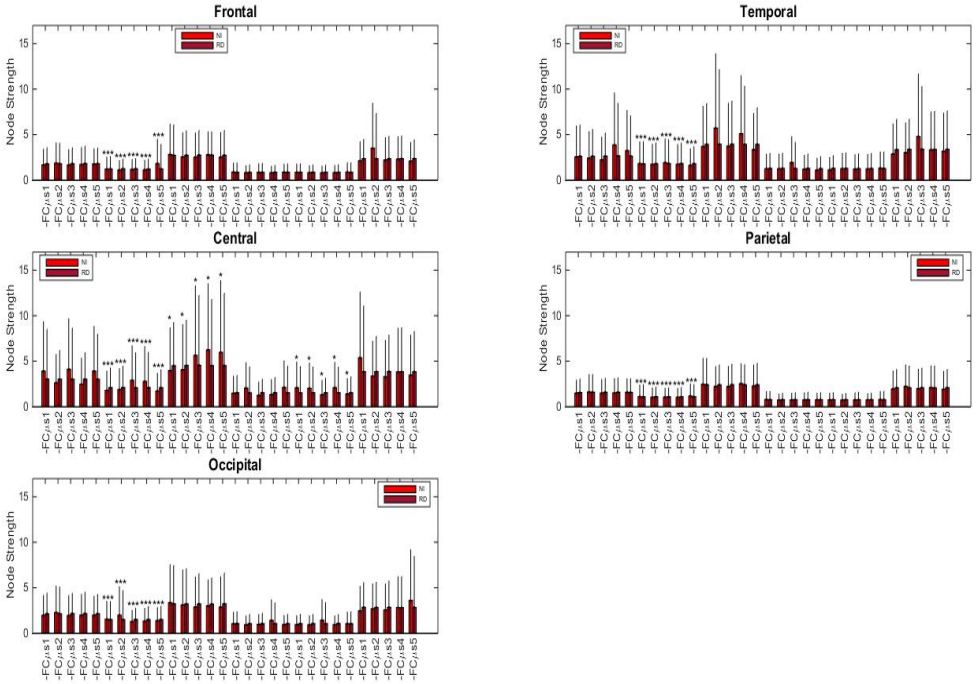

(b) Strength time series per brain region at Intra-Frequency

Figure 7.4: Statistical Significance of the group differences: *p< 0.01, **p< 0.001, ***p<0.05, for the degree\strength time series per brain region and FCmstates in Intra-Frequency.(7.4a) degree time series for Non Impaired(blue barplot) and Reading Difficulties(dark blue) for the 5 microstates per frequency band, (7.4b) strength time series for NI(red barplot) and RD(dark red).

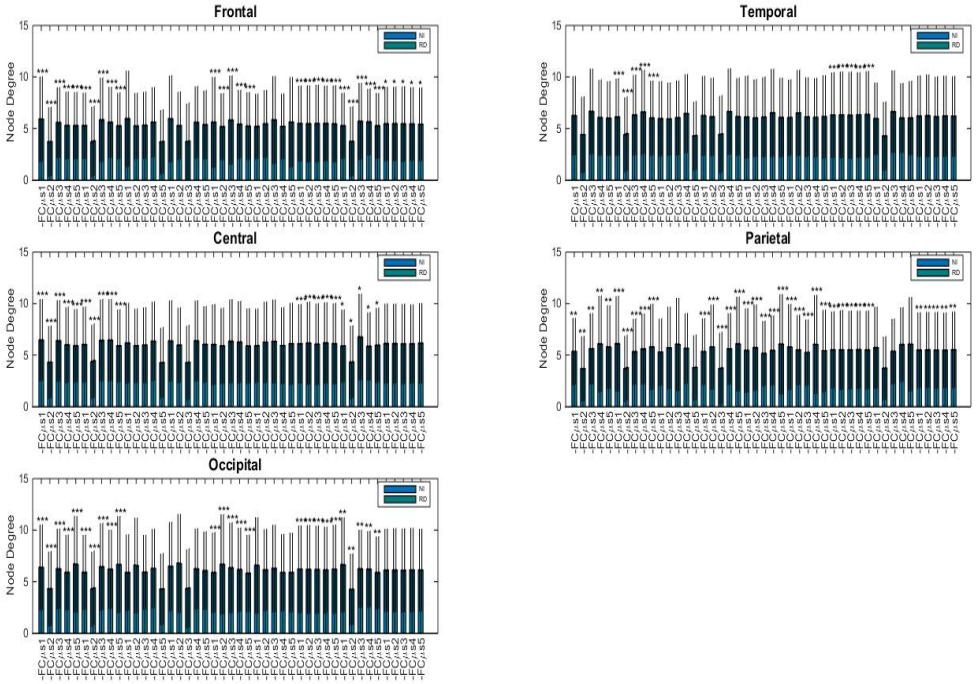

(a) Degree time series per brain region at Inter-Frequency

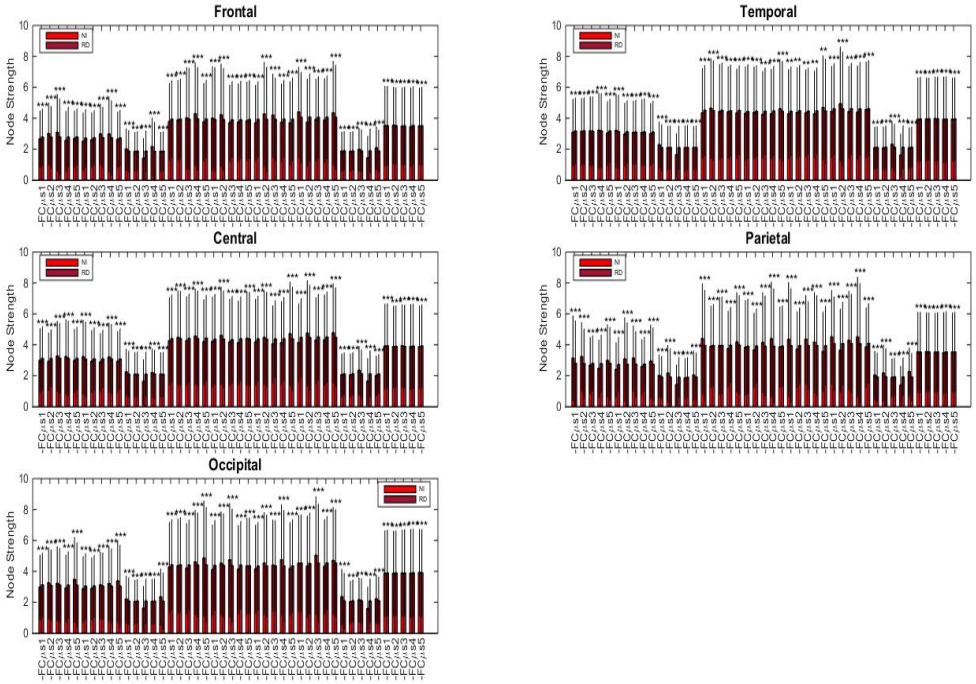

(b) Strength time series per brain region at Inter-Frequency

Figure 7.5: Statistical Significance of the group differences: *p< 0.01, **p< 0.001, ***p<0.05, for the degree\strength time series per brain region and FCmstates in Inter-Frequency.(7.5a) degree time series for Non Impaired(blue barplot) and Reading Difficulties(dark blue) for the 5 microstates per frequency pair, (7.5b) strength time series for NI(red barplot) and RD(dark red).

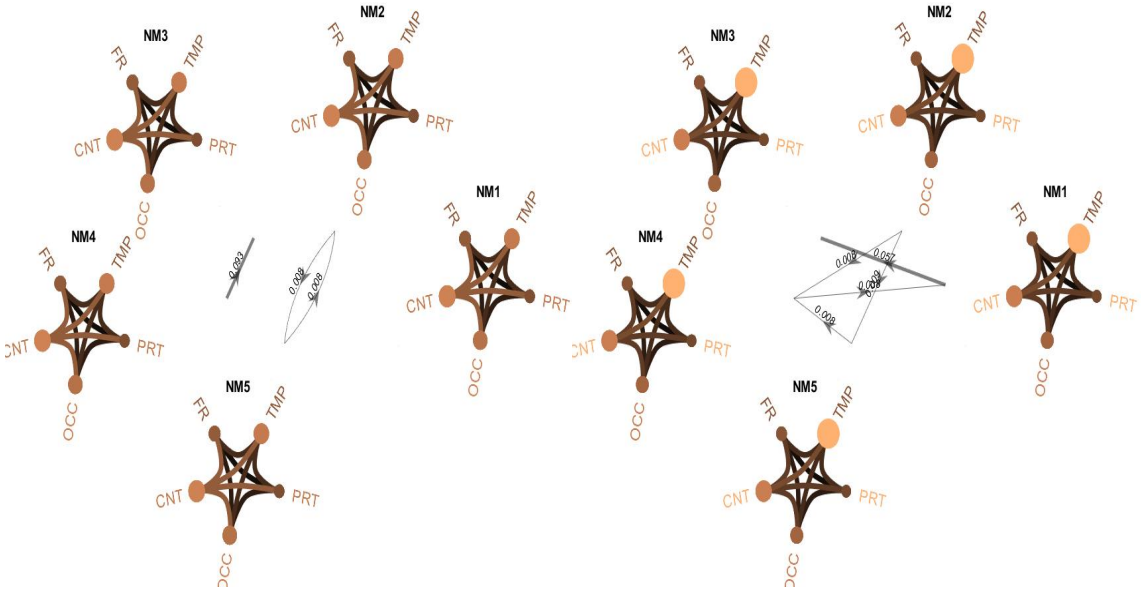

(a) Non-Impaired (b) Reading Difficulties

Figure 7.6: Comparison of degree time series in α frequency band for NI (7.6a) and RD (7.6b).

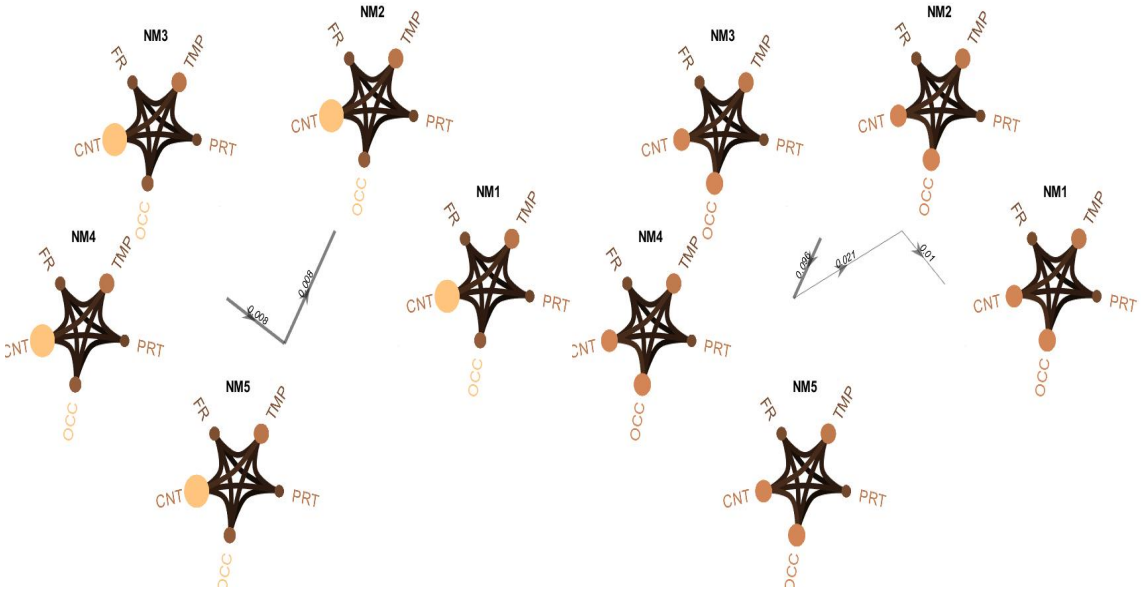

(a) Non-Impaired (b) ReadingDifficulties

Figure 7.7: Comparison of degree time series in γ_{high} frequency band for NI (7.7a) and RD (7.7b).

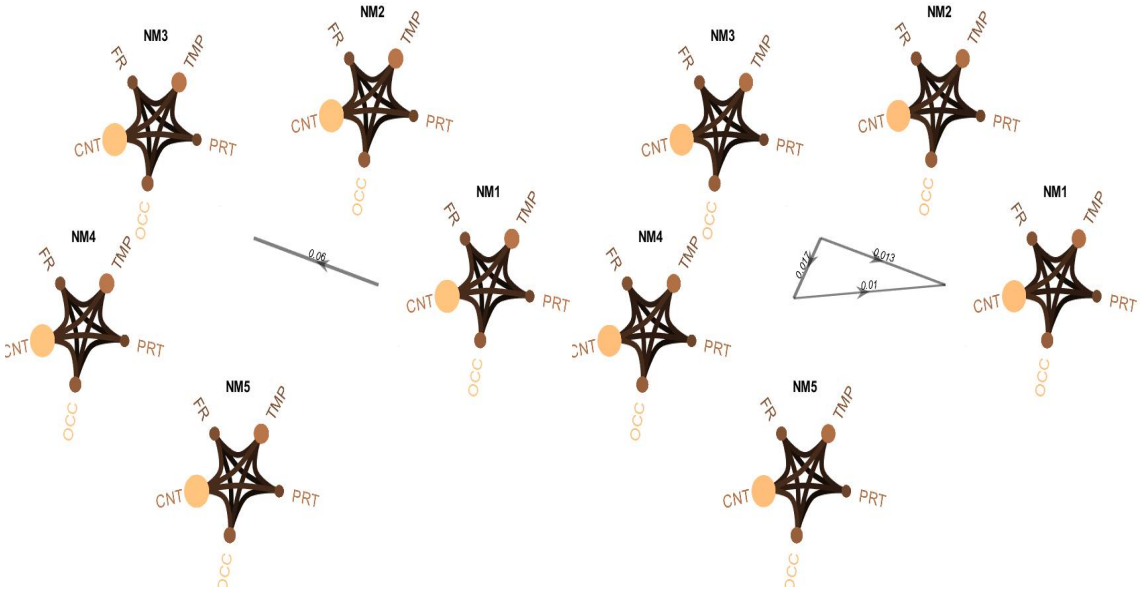

(a) Non-Impaired (b) Reading Difficulties

Figure 7.8: Comparison of degree time series in γ_{low} frequency band for NI (7.8a) and RD (7.8b).

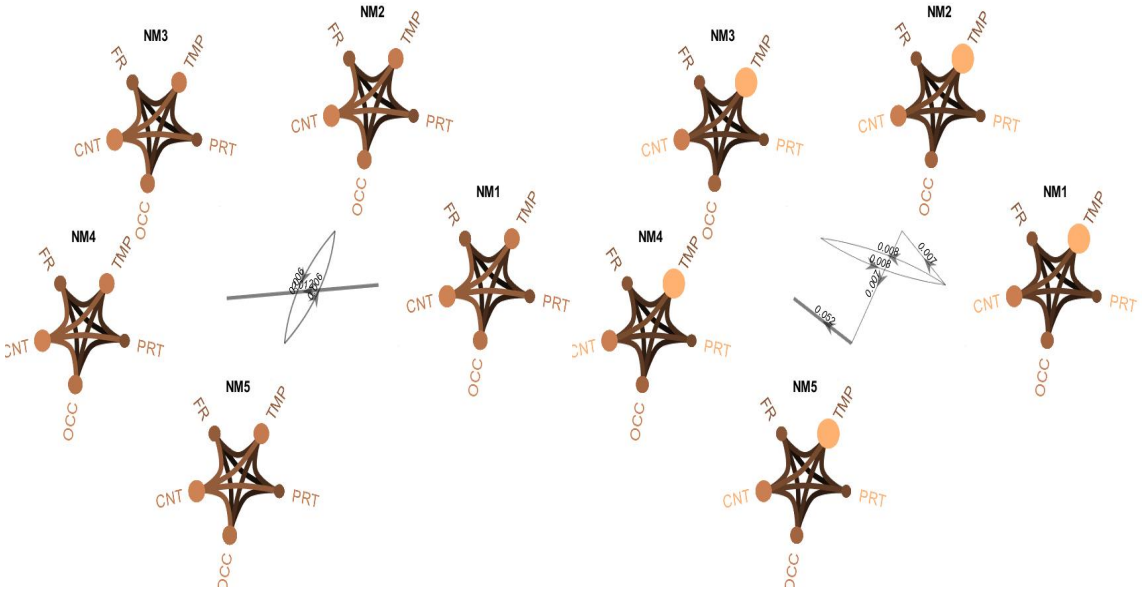

(a) Non-Impaired (b) Reading Difficulties

Figure 7.9: Comparison of strength time series in α frequency band for NI (7.9a) and RD (7.9b).

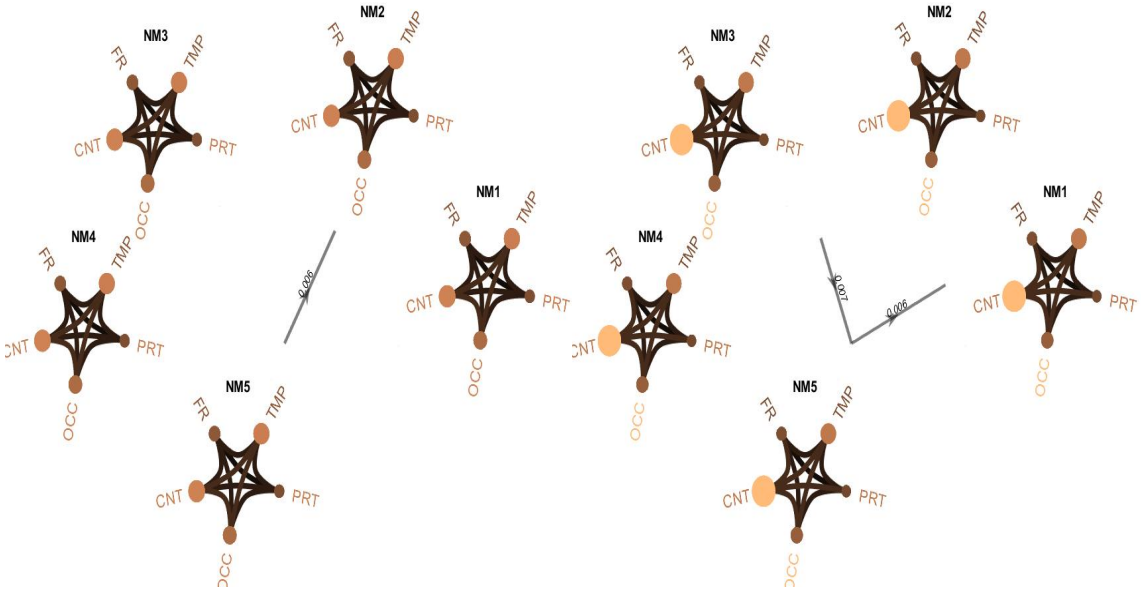

(a) Non-Impaires (b) Reading Difficulties

Figure 7.10: Comparison of strength time series in β frequency band for NI (7.10a) and RD (7.10b).

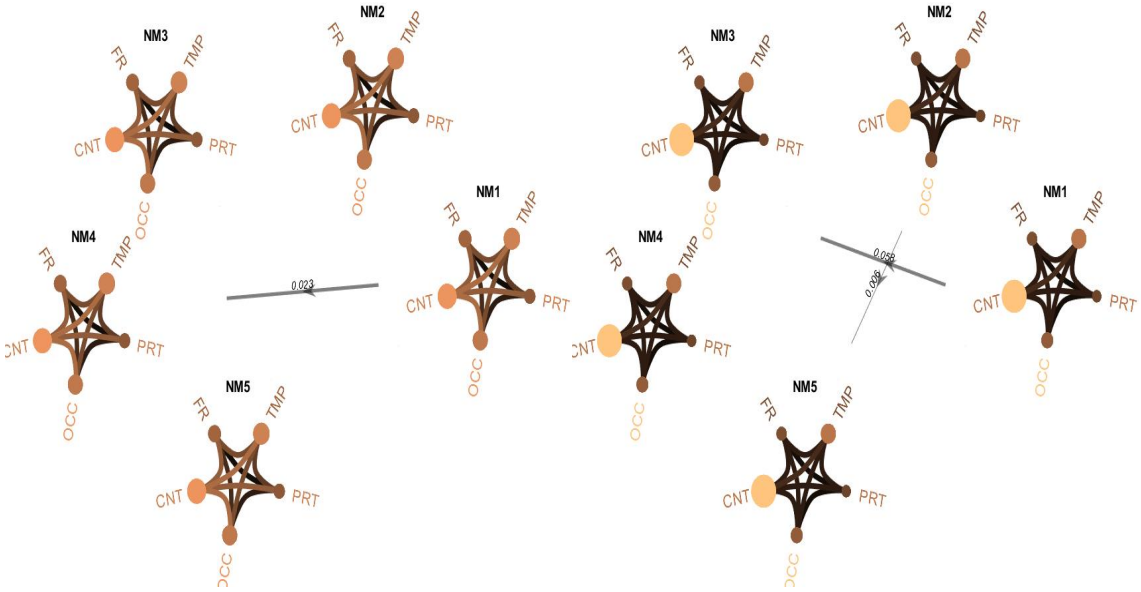

(a) Non-Impaired (b) Reading Difficulties

Figure 7.11: Comparison of strength time series in γ_{high} frequency band for NI (7.11a) and RD (7.11b).

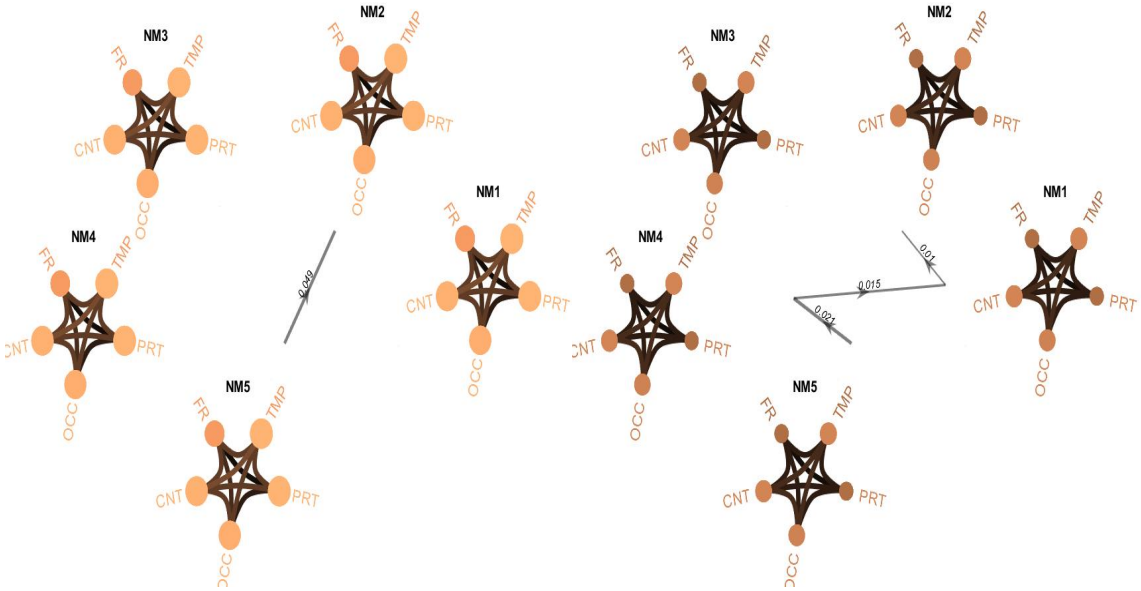

(a) Non-Impaired (b) Reading Difficulties

Figure 7.12: Comparison of degree time series in α - γ_{high} frequency band for NI (7.12a) and RD (7.12b).

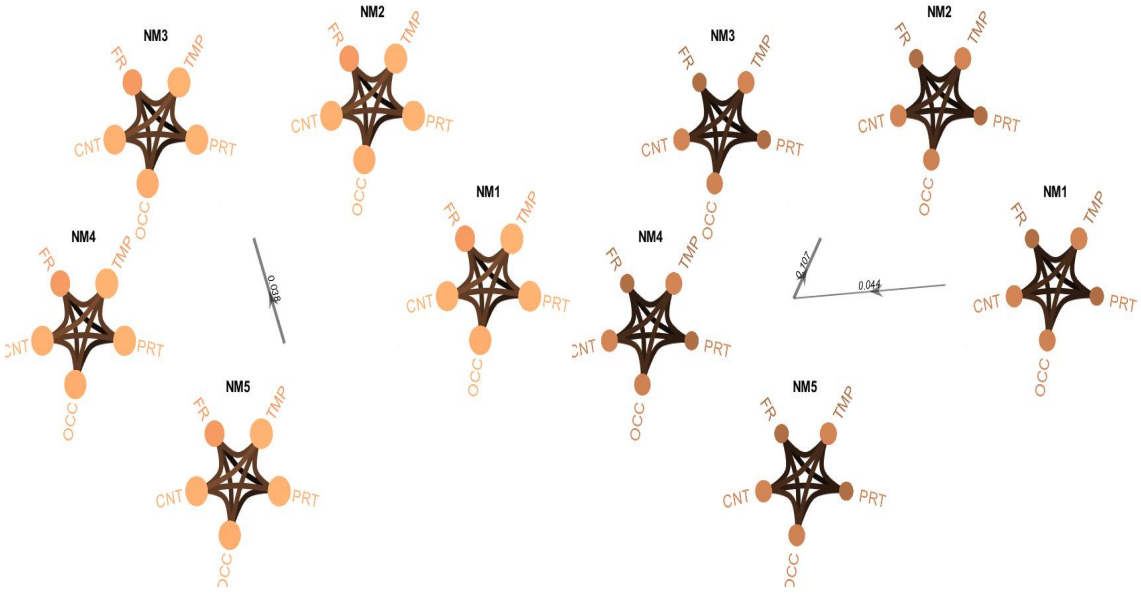

(a) Non-Impaired (b) Reading Difficulties

Figure 7.13: Comparison of strength time series in α - γ_{high} frequency band for NI (7.13a) and RD (7.13b).

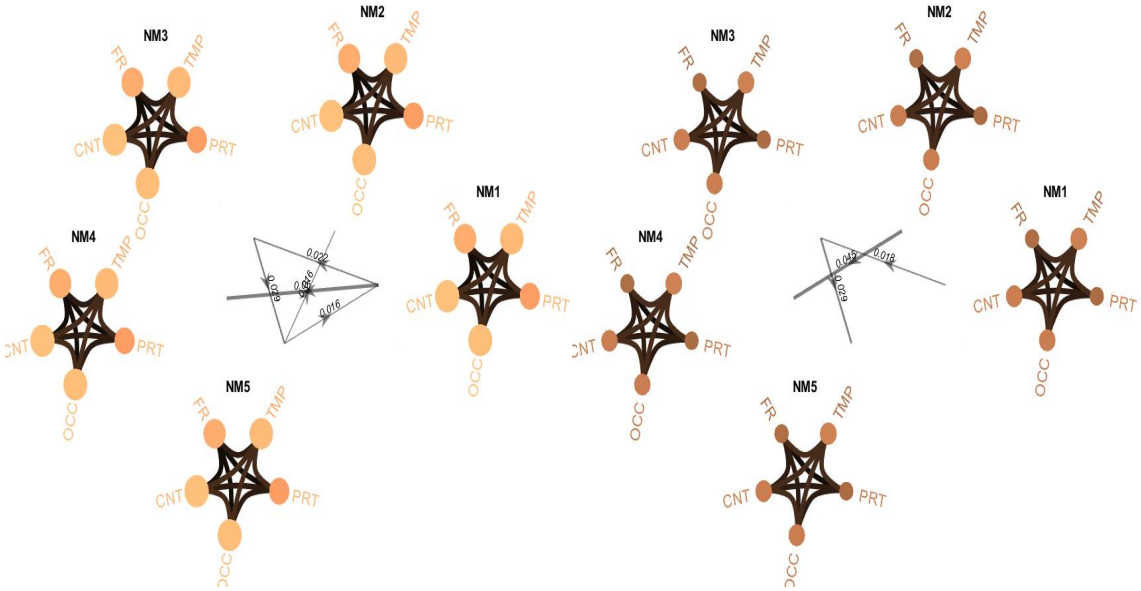

(a) Degree time series (b) Strength time series

Figure 7.14: Comparison of degree time series in α - β frequency band for NI (7.14a) and RD (7.14b).

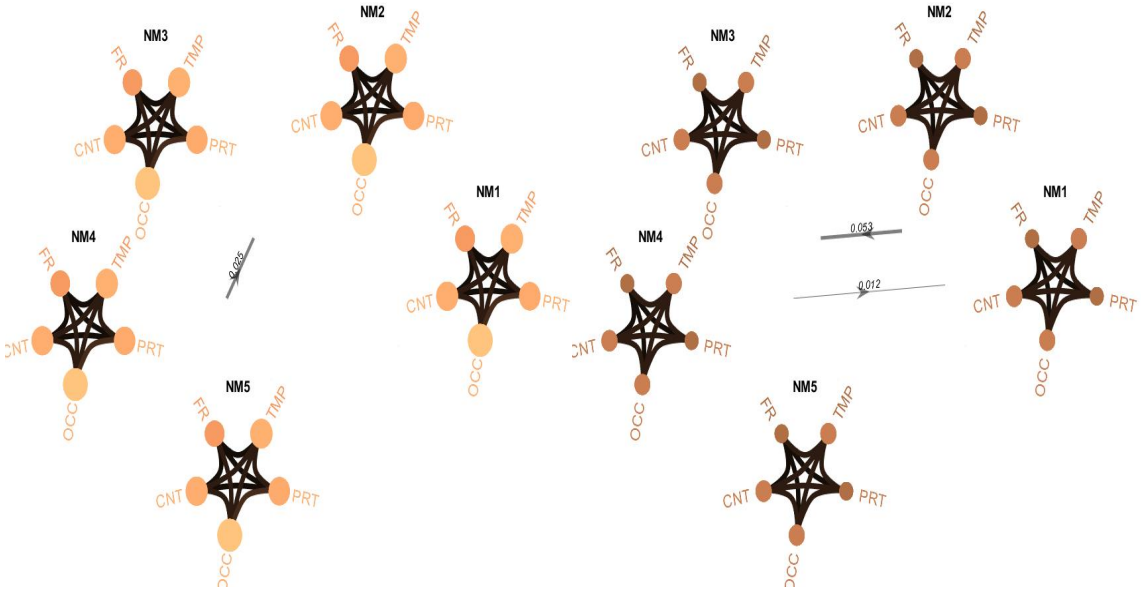

(a) Non-Impaired (b) Reading Difficulties

Figure 7.15: Comparison of degree time series in γ_{low} - γ_{high} frequency band for NI (7.15a) and RD (7.15b).

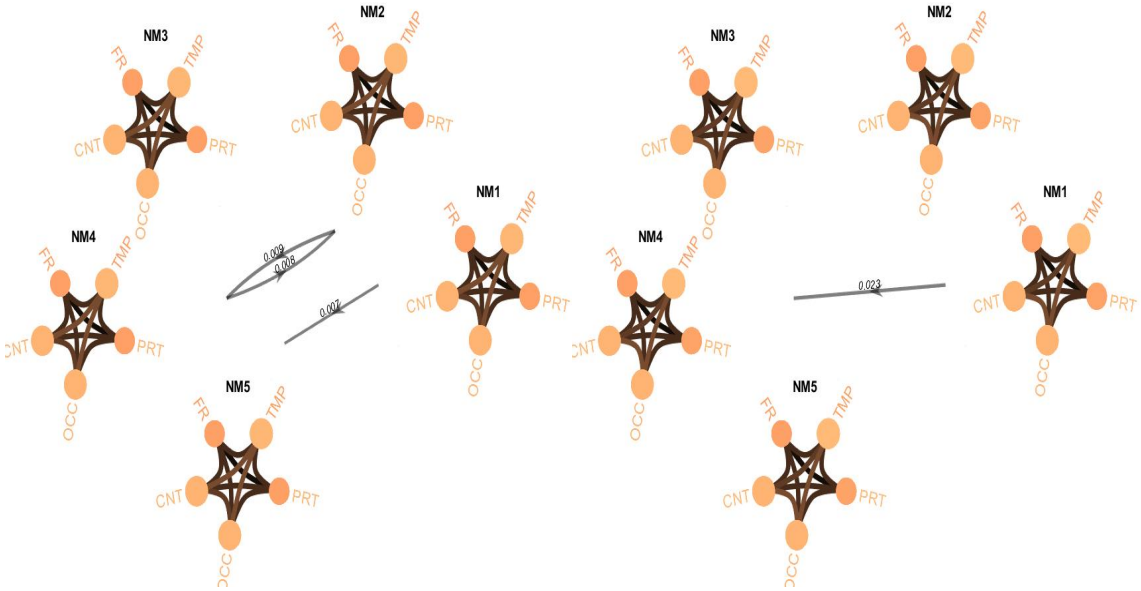

(a) Non-Impaired (b) Reading Difficulties

Figure 7.16: Comparison of degree time series in θ - β frequency band for NI (7.15a) and RD (7.15b).

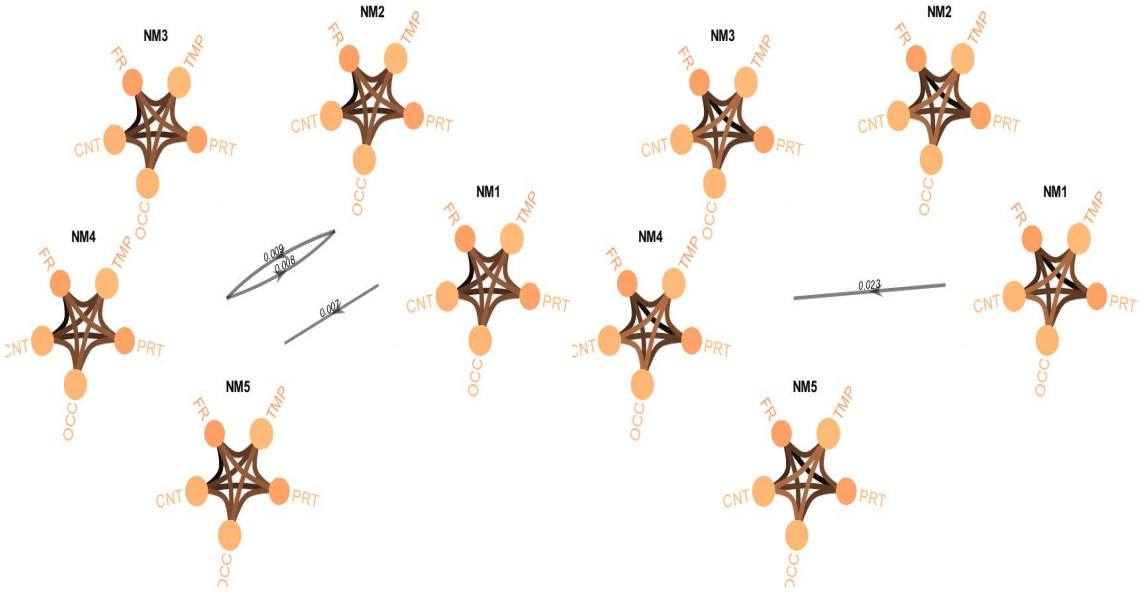

(a) Non-Impaired (b) Reading Difficulties

Figure 7.17: Comparison of degree time series in δ - θ frequency band for NI (7.17a) and RD (7.17b).

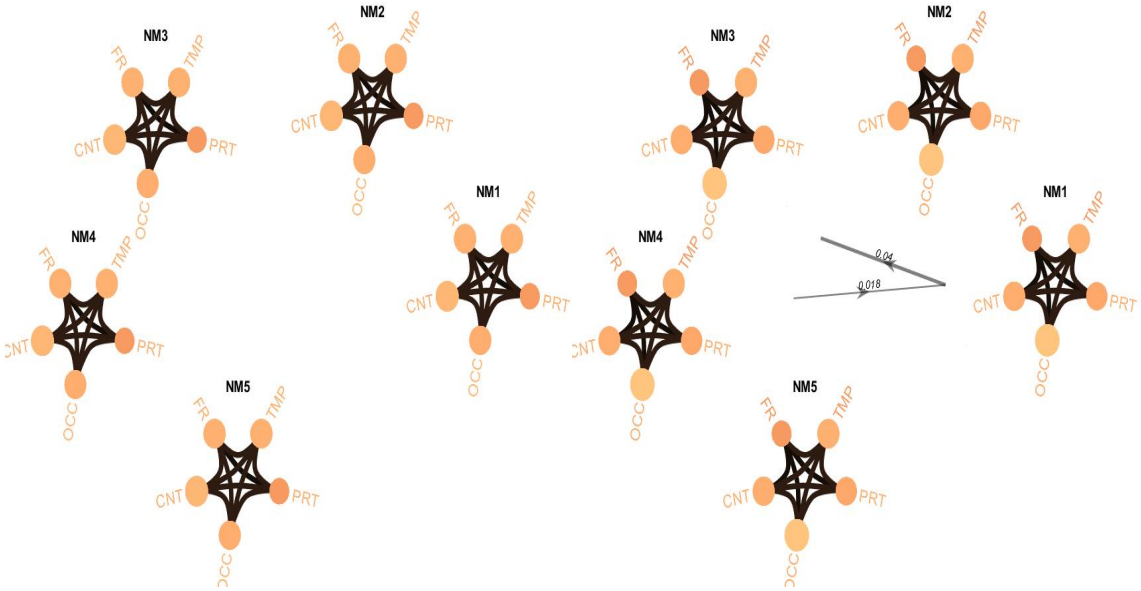

(a) Non-Impaired (b) Reading Difficulties

Figure 7.18: Comparison of strength time series in β - γ_{low} frequency band for NI (7.18a) and RD (7.18b).

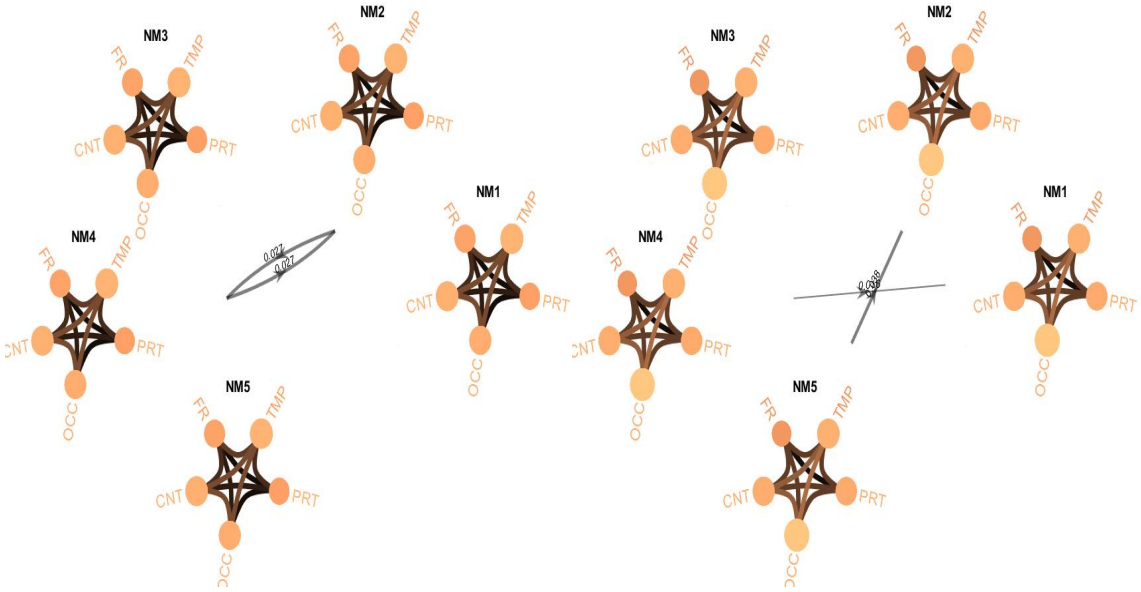

(a) Non-Impaired (b) Reading Difficulties

Figure 7.19: Comparison of strength time series in δ - γ_{high} frequency band for NI (7.19a) and RD (7.19b).

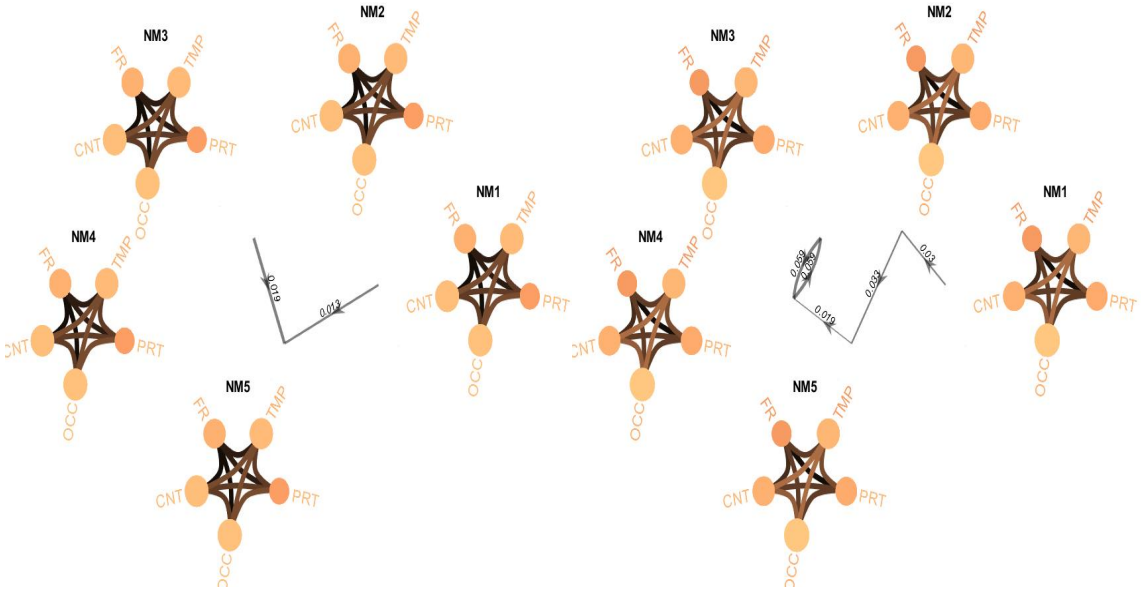

(a) Non-Impaired (b) Reading Difficulties

Figure 7.20: Comparison of strength time series in δ - α frequency band for NI (7.20a) and RD (7.20b).

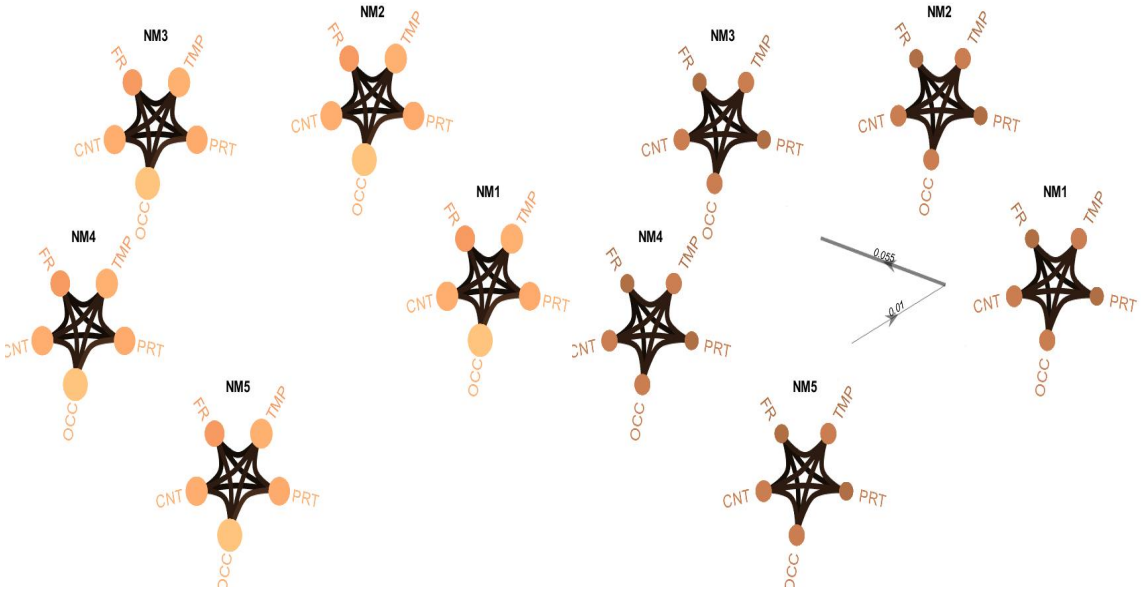

(a) Non-Impaired (b) Reading Difficulties

Figure 7.21: Comparison of strength time series in δ - α frequency band for NI (7.21a) and RD (7.21b).

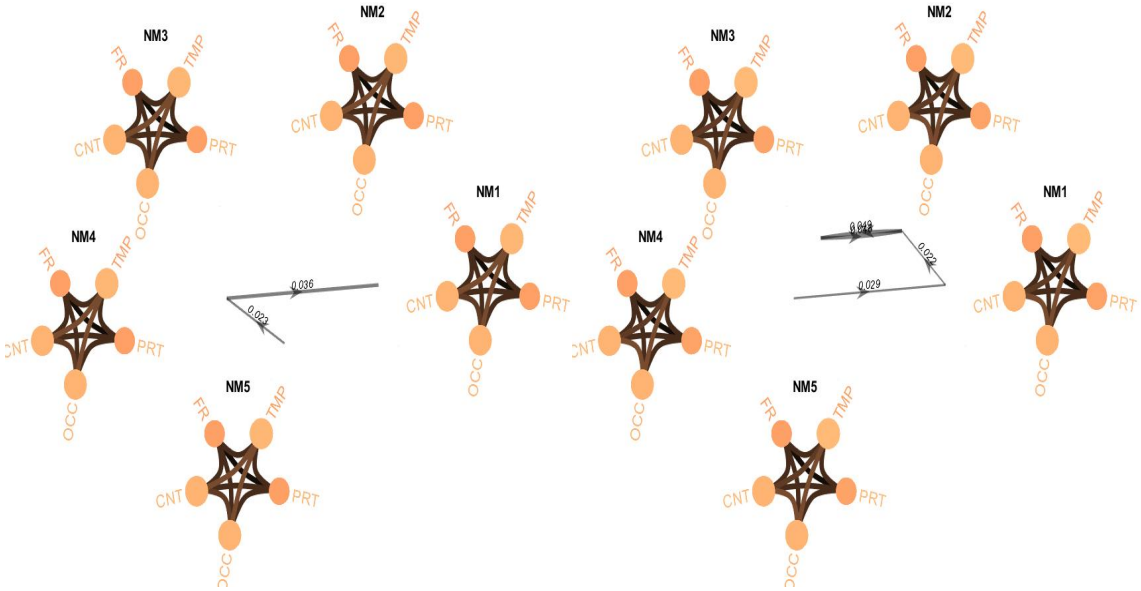

(a) Non-Impaired (b) Reading Difficulties

Figure 7.22: Comparison of strength time series in θ - β frequency band for NI (7.22a) and RD (7.22b).

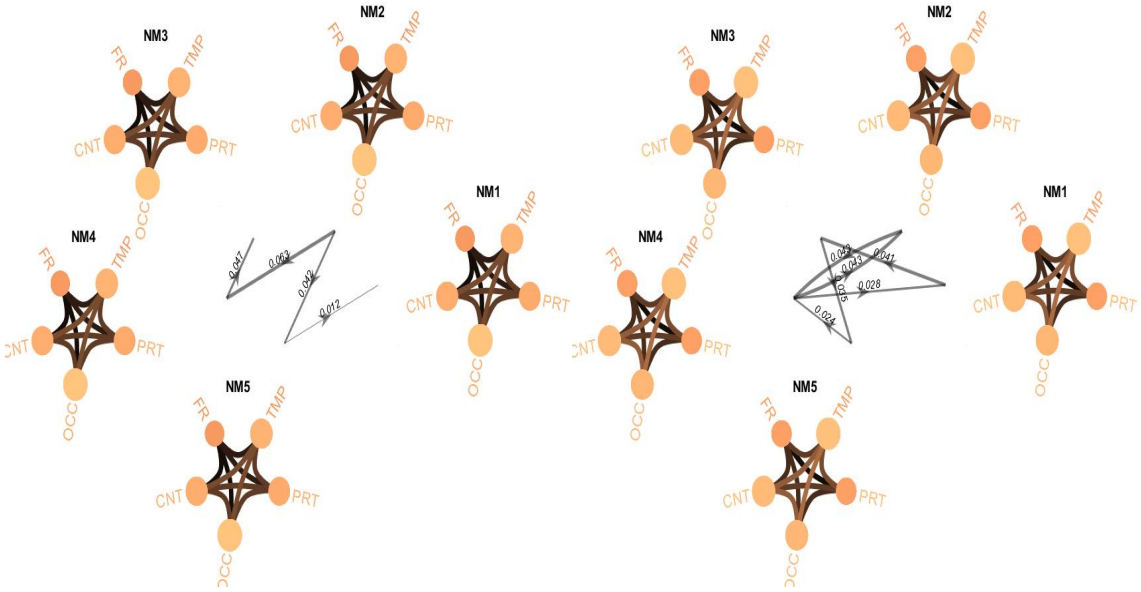

(a) Non-Impaired (b) Reading Difficulties

Figure 7.23: Comparison of strength time series in δ - γ_{low} frequency band for NI (7.23a) and RD (7.23b).

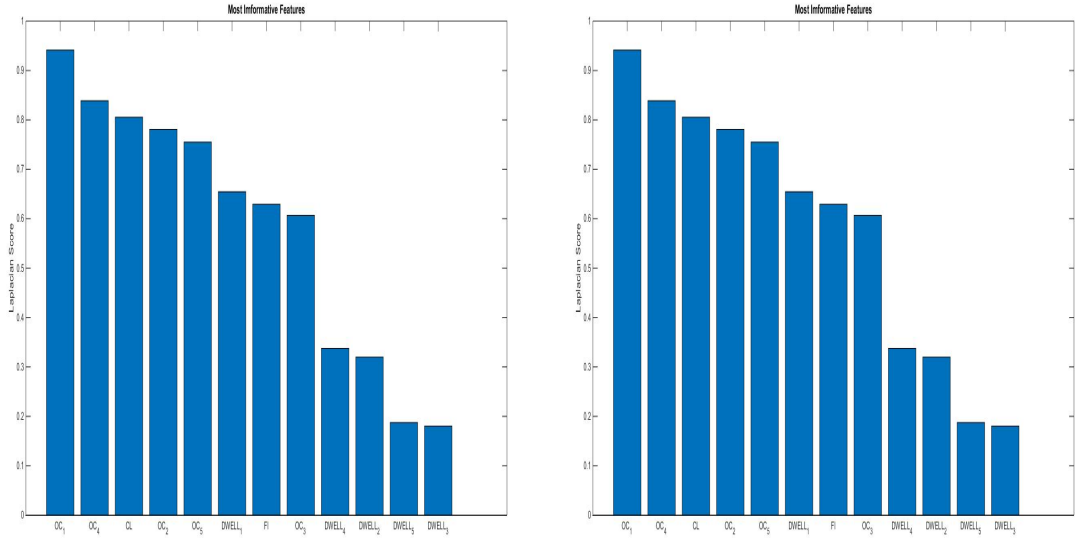

(a) k-NN Classifier (b) SVM Classifier

Figure 7.24: Ranking the most informative degree features for k-NN (7.24a) and SVM classification(7.24b) after feature selection.

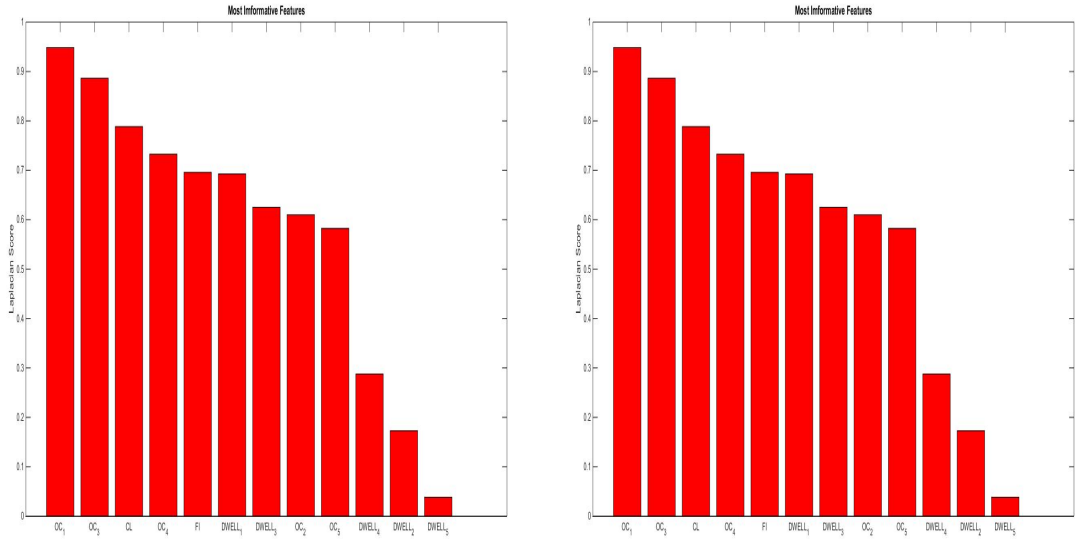

(a) k-NN Classifier (b) SVM Classifier

Figure 7.25: Ranking the most informative strength features for k-NN (7.25a) and SVM classification(7.25b) after feature selection.

References

[1] G. Reid Lyon. Learning disabilities. *The Future of Children*, 6(1):54–76, 1996.

[2] About reading disabilities. https://www.readingrockets.org/topics/struggling-readers/articles/about-reading-disabilities-learning-disabilities-and-rea

[3] Stavros I. Dimitriadis, Nikolaos A. Laskaris, Panagiotis G. Simos, Jack M. Fletcher, and Andrew C. Papanicolaou. Greater repertoire and temporal variability of cross-frequency coupling (cfc) modes in resting-state neuromagnetic recordings among children with reading difficulties. *Frontiers in Human Neuroscience*, 10, 2016.

[4] Stavros I. Dimitriadis, Panagiotis G. Simos, Jack . Fletcher, and Andrew C. Papanicolaou. Aberrant resting-state functional brain networks in dyslexia: Symbolic mutual information analysis of neuromagnetic signals. *International Journal of Psychophysiology*, 126:20–29, 2018.

[5] Fumiko Hoeft, Ann Meyler, Arvel Hernandez, Connie Juel, Heather Taylor-Hill, Jennifer L. Martindale, Glenn McMillon, Galena Kolchugina, Jessica M. Black, Afrooz Faizi, Gayle K. Deutsch, Wai Ting Siok, Allan L. Reiss, Susan Whitfield-Gabrieli, and John D. E. Gabrieli. Functional and morphometric brain dissociation between dyslexia and reading ability. *Proceedings of the National Academy of Sciences*, 104(10):4234–4239, 2007.

[6] E Temple. Disrupted neural responses to phonological and orthographic processing in dyslexic children: an fmri study. *Neuroreport*, 12, 2001.

[7] Eraldo Paulesu. Reading the dyslexic brain: multiple dysfunctional routes revealed by a new meta-analysis of pet and fmri activation studies. *Frontiers in Human Neuroscience*, 8, 2014.

[8] Intro to meg. https://imaging.mrc-cbu.cam.ac.uk/meg/IntroEEGMEG.

[9] Marios Antonakakis. The effect of experimental and modeling parameters on combined eeg/meg source analysis and transcranial electric stimulation optimization of somatosensory and epilepsy activity. 2021.

[10] C von der Malsburg. Internal rept. 81–2, dept. of neurobiology, max planck institute for biophysical chemistry, göttingen. *Fed. Rep. Germany.[taDHB]*, 1981.

[11] Charles M Gray and Wolf Singer. Stimulus-specific neuronal oscillations in orientation columns of cat visual cortex. *Proceedings of the National Academy of Sciences*, 86(5):1698–1702, 1989.

[12] Marios Antonakakis, Stavros Dimitriadis, Michalis Zervakis, Andrew Papanicolaou, and George Zouridakis. Alterations in dynamic spontaneous network microstates in mild traumatic brain injury: A meg beamformed dynamic connectivity analysis. 04 2019.

[13] Marios Antonakakis, Stavros I. Dimitriadis, Michalis Zervakis, Andrew C. Papanicolaou, and George Zouridakis. Reconfiguration of dominant coupling modes in mild traumatic brain injury mediated by δ-band activity: A resting state meg study. *Neuroscience*, 356:275–286, 2017.

[14] R Matthew Hutchison, Thilo Womelsdorf, Joseph S Gati, Stefan Everling, and Ravi S Menon. Resting-state networks show dynamic functional connectivity in awake humans and anesthetized macaques. *Human brain mapping*, 34(9):2154–2177, 2013.

[15] Stavros Dimitriadis, Nikos Laskaris, Spiros Fotopoulos, Jack Fletcher, David Linden, and Andrew Papanicolaou. Classifying children with reading difficulties from non-impaired readers via symbolic dynamics and complexity analysis of meg resting-state data. 12 2016.

[16] Types of reading difficulties. https://www.nichd.nih.gov/health/topics/reading/conditioninfo/disorders.

[17] John Morton and U. Frith. Causal modelling a structural approach to developmental psychopathology. *Manual Dev. Psychopathol.*, 1, 01 1995.

[18] C Hulme and MJ Snowling. Reading disorders and dyslexia. *Current opinion in pediatrics*, 2016.

[19] Oskar Ankkuriniemi and Petrus Kuusisto. Resting-state functional connectivity in reading-related brain regions : a meg study in monozygotic twins. 2023.

[20] S Paracchini, T Scerri, and AP Monaco. Reading disorders and dyslexia. *Annual review of genomics and human genetics*, 2007.

[21] Jayne Newbury, Laura Justice, Hui Jiang, and Mary Beth Schmitt. Cognitive, noncognitive, and home environment correlates of reading difficulties in primary-grade students with language impairment. *Journal of Speech, Language, and Hearing Research*, 63:1–14, 06 2020.

[22] Indo Dini, Wita Seftiani, and Zakariyah. Understanding and expressing the factors causing difficulties of children in learning, especially in the field of reading. *International Journal of Education and Teaching Zone*, 2:221–232, 06 2023.

[23] J. D. Scarborough, H. S. & Parker. Matthew effects in children with learning disabilities: Development of reading, iq, and psychosocial problems from grade 2 to grade 8. *Annals of Dyslexia*, 2003.

[24] Jr Ocampo and J. M. Children's reading difficulty and their perceived misbehavior. *SIPATAHOENAN*, 2015.

[25] Alyse Sukovieff and Richard S. Kruk. Reading difficulty and socio-emotional adjustment: Internalizing patterns depend on age of identification. *Cogent Education*, 8(1):1910162, 2021.

[26] Emma James, Paul A. Thompson, Lucy Bowes, and Kate Nation. Heterogeneity in children's reading comprehension difficulties: A latent class approach. *JCPP Advances*, 2023.

[27] The human brain: Anatomy and function. https://www.visiblebody.com/learn/nervous/brain.

[28] Brain anatomy. https://mayfieldclinic.com/pe-anatbrain.htm.

[29] Brain anatomy and how the brain works. https://www.hopkinsmedicine.org/health/conditions-and-diseases/anatomy-of-the-brain.

[30] An easy guide to neuron anatomy with diagrams. https://www.simplypsychology.org/neuron.html.

[31] Matti Hämäläinen, Riitta Hari, Risto J. Ilmoniemi, Jukka Knuutila, and Olli V. Lounasmaa. Magnetoencephalography—theory, instrumentation, and applications to noninvasive studies of the working human brain. *Rev. Mod. Phys.*, 65:413–497, Apr 1993.

[32] Neural circuits. https://www.ninds.nih.gov/health-information/public-education/brain-basics.

[33] How is electricity generated by neurons in our brain. https://www.scienceabc.com/humans/electricity-generated-neurons-brain.html.

[34] Marc D. Binder, Nobutaka Hirokawa, and Uwe Windhorst. *Encyclopedia of Neuroscience*. Springer, 2009.

[35] Dale Purves, George J Augustine, David Fitzpatrick, Lawrence C Katz, Anthony-Samuel LaMantia, James O McNamara, , and S Mark Williams. *Neuroscience*. Sinauer Associates, 2001.

[36] S.I. Dimitriadis, N.A. Laskaris, P.G. Simos, S. Micheloyannis, J.M. Fletcher, R. Rezaie, and A.C. Papanicolaou. Altered temporal correlations in resting-state connectivity fluctuations in children with reading difficulties detected via meg. *NeuroImage*, 83:307–317, 2013.

[37] Brainwave frequencies. https://nhahealth.com/brainwave-frequencies-what-are-they/.

[38] Suresh D Muthukumaraswamy. High-frequency brain activity and muscle artifacts in meg/eeg: a review and recommendations. *Frontiers in human neuroscience*, 7(138), 2013.

[39] Donald C. Rojas, Keeran Maharajh, Peter Teale, and Sally J. Rogers. Reduced neural synchronization of gamma-band meg oscillations in first-degree relatives of children with autism. *BMC Psychiatry*, 8(66), 2008.

[40] A. Kanno, N. Nakasato, and M. Oogane. Scalp attached tangential magnetoencephalography using tunnel magneto-resistive sensors. 2022.

[41] SP Ahlfors and Mody M. Overview of meg. 2016.

[42] Sendy Caffarra, Clara D. Martin, Mikel Lizarazu, Marie Lallier, Asier Zarraga, Nicola Molinaro, and Manuel Carreiras. Word and object recognition during reading acquisition: Meg evidence. *Developmental Cognitive Neuroscience*, 24:21–32, 2017.

[43] Amy S. Desroches, Nadia E. Cone, Donald J. Bolger, Tali Bitan, Douglas D. Burman, and James R. Booth. Children with reading difficulties show differences in brain regions associated with orthographic processing during spoken language processing. *Brain Research*, 1356:73–84, 2010.

[44] Panagiotis G Simos. Neural correlates of sentence reading in children with reading difficulties. *Neuroreport*, 22:674–8, 2011.

[45] Source localization. https://www.sciencedirect.com/topics/computer-science/source-localization.

[46] Ming-Xiong Huang, Sharon Nichols, Ashley Robb, Annemarie Angeles, Angela Drake, Martin Holland, Sarah Asmussen, John D'Andrea, Won Chun, Michael Levy, Li Cui, Tao Song, Dewleen G. Baker, Paul Hammer, Robert McLay, Rebecca J. Theilmann, Raul Coimbra, Mithun Diwakar, Cynthia Boyd, John Neff, Thomas T. Liu, Jennifer Webb-Murphy, Roxanna Farinpour, Catherine Cheung, Deborah L. Harrington, David Heister, and Roland R. Lee. An automatic meg low-frequency source imaging approach for detecting injuries in mild and moderate tbi patients with blast and non-blast causes. *NeuroImage*, 61(4):1067–1082, 2012.

[47] J. Zhang, K. Safar, Z. Emami, G. M. Ibrahim, S. E. Scratch, and B. T. da Costa, L.and & Dunkley. Local and large-scale beta oscillatory dysfunction in males with mild traumatic brain injury. *Journal of neurophysiology*, 124, 2020.

[48] Rose Bruffaerts, Alvince Pongos, Cory Shain, Benjamin Lipkin, Matthew Siegelman, Vincent Wens, Martin Sjøgård, Dimitrios Pantazis, Idan Blank, Serge Goldman, Xavier De Tiège, and Evelina Fedorenko. Functional identification of language-responsive

channels in individual participants in meg investigations. *bioRxiv : the preprint server for biology*, 03 2023.

[49] Jan De Munck, Carsten Wolters, and Maureen Clerc. *EEG and MEG: forward modeling*. 01 2012.

[50] J Sarvas. Basic mathematical and electromagnetic concepts of the biomagnetic inverse problem. *Physics in Medicine & Biology*, 32(1):11, jan 1987.

[51] J. C. Mosher, P. S. Lewis, and R. M. Leahy. Multiple dipole modeling and localization from spatio-temporal meg data. ieee transactions on bio-medical engineering. *Brain Topography*, 39(6):541–557, 1992.

[52] A Pascarella and A Sorrentino. *Statistical approaches to the inverse problem*. InTech, Rijeka, Croatia, 2011.

[53] Roberta Grech, Tracey Cassar, Joseph Muscat, Kenneth P Camilleri, Simon G Fabri, Michalis Zervakis, Petros Xanthopoulos, and Bart Sakkalis, Vangelis & Vanrumste. Review on solving the inverse problem in eeg source analysis. *Journal of NeuroEngineering and Rehabilitation*, 2008.

[54] Olaf Hauk, Matti Stenroos, and Matthias Treder. *EEG/MEG Source Estimation and Spatial Filtering: The Linear Toolkit*, pages 1–37. Springer International Publishing, Cham, 2019.

[55] Alberto Sorrentino and Michele Piana. Inverse modeling for meg/eeg data. 2017.

[56] L. Soufflet and P Boeijinga. Linear inverse solutions: Simulations from a realistic head model in meg. *Brain Topography*, 18(2):87–99, 2005.

[57] Daniel T. Wehner, Seppo P. Ahlfors, and Maria Mody. Effects of phonological contrast on auditory word discrimination in children with and without reading disability: A magnetoencephalography (meg) study. *Neuropsychologia*, 45(14):3251–3262, 2007.

[58] C. J. Long, P. L. Purdon, S. Temereanca, N. U. Desai, M. S. Hämäläinen, and E. N. Brown. State-space solutions to the dynamic magnetoencephalography inverse problem using high performance computing1. *Institute of Mathematical Statistics*, 5(2):1207–1228, 2011.

[59] A. Sorrentino, L. Parkkonen, A. Pascarella, C. Campi, and M. Piana. Dynamical meg source modeling with multi-target bayesian filtering. *Human brain mapping*, 30(6):1911–1921, 2009.

[60] Arjan Hillebrand and Gareth R. Barnes. Beamformer analysis of meg data. In *Magnetoencephalography*, volume 68 of *International Review of Neurobiology*, pages 149–171. Academic Press, 2005.

[61] B.D. Van Veen and K.M. Buckley. Beamforming: a versatile approach to spatial filtering. *IEEE ASSP Magazine*, 5(2):4–24, 1988.

[62] Kensuke Sekihara. A novel adaptive beamformer for meg source reconstruction effective when large background brain activities exist. *IEEE transactions on bio-medical engineering*, 53(9), 2006.

[63] Maher A. Quraan, Sandra N. Moses, Yuwen Hung, Travis Mills, and Margot J. Taylor. Detection and localization of hippocampal activity using beamformers with meg: A detailed investigation using simulations and empirical data. *Human Brain Mapping*, 32(5), 2011.

[64] B. D. Van Veen, W. Van Drongelen, M. Yuchtman, and A. Suzuki. Localization of brain electrical activity via linearly constrained minimum variance spatial filtering. *Transactions on Biomedical Engineering*, 44(9):867–880, 1997.

[65] MX. Huang, J. Shih, and R Lee. Commonalities and differences among vectorized beamformers in electromagnetic source imaging. *Brain Topogr*, 16:139–158, 2004.

[66] Yvonne Buschermöhle, Malte Höltershinken, Tim Erdbrügger, Jan-Ole Radecke, Andreas Sprenger, Till Schneider, Rebekka Lencer, Joachim Groß, and Carsten H. Wolters. Comparing the performance of beamformer algorithms in estimating orientations of neural sources. *iScience*, 2023.

[67] Amit Jaiswal. Comparison of beamformer implementations for meg source localization. *NeuroImage*, 216, 2020.

[68] Julia Schwarz, Mikel Lizarazu, Marie Lallier, and Anastasia Klimovich-Gray. Phonological deficits in dyslexia impede lexical processing of spoken words: Linking behavioural and meg data. *Cortex*, 171:204–222, 2024.

[69] Karl J. Friston. Functional and effective connectivity: A review. *Brain Connectivity*, 1(1):13–36, 2011. PMID: 22432952.

[70] Tali Bitan, Jimmy Cheon, Dong Lu, Douglas Burman, and James Booth. Developmental increase in top–down and bottom–up processing in a phonological task: An effective connectivity, fmri study. *Journal of cognitive neuroscience*, 21:1135–45, 09 2008.

[71] Véronique Quaglino, Bourdin Béatrice, Gerard Czternasty, Vrignaud Pierre, S Fall, M.E. Meyer, Patrick Berquin, Bernard Devauchelle, and Giovanni de Marco. Differences in effective connectivity between dyslexic children and normal readers during a pseudoword reading task: An fmri study. *Neurophysiologie clinique = Clinical neurophysiology*, 38:73–82, 05 2008.

[72] Victoria Leong and Usha Goswami. Difficulties in auditory organisation as a cause of reading backwardness? an auditory neuroscience perspective. *Developmental Science*, 20, 09 2016.

[73] Erick Ortiz, Krunoslav Stingl, Jana Keune Née Muenssinger, Christoph Braun, Hubert Preissl, and Paolo Belardinelli. Weighted phase lag index and graph analysis: Preliminary investigation of functional connectivity during resting state in children. *Computational and mathematical methods in medicine*, 2012:186353, 09 2012.

[74] Michael Vourkas, Micheloyannis Sifis, Roozbeh Rezaie, Jack Fletcher, Paul Cirino, and Andrew Papanicolaou. Dynamic task-specific brain network connectivity in children with severe reading difficulties. *Neuroscience letters*, 488:123–8, 11 2010.

[75] G. Fraga González, M.J.W. Van der Molen, G. Žarić, M. Bonte, J. Tijms, L. Blomert, C.J. Stam, and M.W. Van der Molen. Graph analysis of eeg resting state functional networks in dyslexic readers. *Clinical Neurophysiology*, 127(9):3165–3175, 2016.

[76] Jean-Philippe Lachaux, Eugenio Rodriguez, Jacques Martinerie, and Francisco J Varela. Measuring phase synchrony in brain signals. *Human brain mapping*, 8(4):194–208, 1999.

[77] Zhongming Liu, Masaki Fukunaga, Jacco A. de Zwart, and Jeff H. Duyn. Large-scale spontaneous fluctuations and correlations in brain electrical activity observed with magnetoencephalography. *NeuroImage*, 51(1):102–111, 2010.

[78] Jarmo A. Hämäläinen, André Rupp, Fruzsina Soltész, Denes Szücs, and Usha Goswami. Reduced phase locking to slow amplitude modulation in adults with dyslexia: An meg study. *NeuroImage*, 59(3):2952–2961, 2012.

[79] Frédéric Roux, Michael Wibral, Wolf Singer, Jaan Aru, and Peter J. Uhlhaas. The phase of thalamic alpha activity modulates cortical gamma-band activity: Evidence from resting-state meg recordings. *Journal of Neuroscience*, 33(45):17827–17835, 2013.

[80] Mattia F. Pagnotta, George Zouridakis, Lianyang Li, Mikel Lizarazu, Marie Lallier, Nicola Molinaro, and Manuel Carreiras. Low frequency overactivation in dyslexia: Evidence from resting state magnetoencephalography. In *2015 37th Annual International Conference of the IEEE Engineering in Medicine and Biology Society (EMBC)*, pages 6959–6962, 2015.

[81] Avniel Singh Ghuman, Jonathan R McDaniel, and Alex Martin. A wavelet-based method for measuring the oscillatory dynamics of resting-state functional connectivity in meg. *Neuroimage*, 56(1):69–77, 2011.

[82] George C O'Neill, Prejaas Tewarie, Diego Vidaurre, Lucrezia Liuzzi, Mark W Woolrich, and Matthew J Brookes. Dynamics of large-scale electrophysiological networks: A technical review. *Neuroimage*, 180:559–576, 2018.

[83] Ilya Zakharov, Timofey Adamovich, Anna Tabueva, Victoria Ismatullina, and Sergey Malykh. The effect of density thresholding on the eeg network construction. *Journal of Physics: Conference Series*, 1727:012009, 01 2021.

[84] C. J. Stam, W. de Haan, A. Daffertshofer, B. F. Jones, I. Manshanden, A. M. van Cappellen van Walsum, T. Montez, J. P. A. Verbunt, J. C. de Munck, B. W. van Dijk, H. W. Berendse, and P. Scheltens. Graph theoretical analysis of magnetoencephalographic functional connectivity in Alzheimer's disease. *Brain*, 132(1):213–224, 10 2008.

[85] Timofey Adamovich, Ilya Zakharov, Anna Tabueva, and Sergey Malykh. The thresholding problem and variability in the EEG graph network parameters. *Scientific Reports*, 12(18659), 11 2022.

[86] Stavros Dimitriadis, Marios Antonakakis, Panagiotis Simos, Jack Fletcher, and Andrew Papanicolaou. Data-driven topological filtering based on orthogonal minimal spanning trees: Application to multi-group meg resting-state connectivity. 09 2017.

[87] Haatef Pourmotabbed, Amy de Jongh Curry, Dave Clarke, Elizabeth Tyler-Kabara, and Abbas Babajani-Feremi. Reproducibility of graph measures derived from resting-state meg functional connectivity metrics in sensor and source spaces. *Human Brain Mapping*, 43, 01 2022.

[88] Stavros Dimitriadis, María López, Fernando Maestú, and Ernesto Pereda. Modeling the switching behavior of functional connectivity microstates (fcμstates) as a novel biomarker for mild cognitive impairment, 04 2019.

[89] R. Abreu, A. Leal, and P. Figueiredo. Identification of epileptic brain states by dynamic functional connectivity analysis of simultaneous eeg-fmri: a dictionary learning approach. *Sci Rep*, 1 2019.

[90] Louis-Emmanuel Martinet, Mark Kramer, W. Viles, L. Perkins, Elizabeth Spencer, Catherine Chu, S. Cash, and E. Kolaczyk. Robust dynamic community detection with applications to human brain functional networks. *Nature Communications*, 11:2785, 06 2020.

[91] Nora Leonardi and Dimitri Van De Ville. On spurious and real fluctuations of dynamic functional connectivity during rest. *NeuroImage*, 104:430–436, 2015.

[92] Matthew J Brookes, Mark Woolrich, Henry Luckhoo, Darren Price, Joanne R Hale, Mary C Stephenson, Gareth R Barnes, Stephen M Smith, and Peter G Morris. Investigating the electrophysiological basis of resting state networks using magnetoencephalography. *Proceedings of the National Academy of Sciences*, 108(40):16783–16788, 2011.

[93] Emma L. Hall, Mark W. Woolrich, Carlos E. Thomaz, Peter G. Morris, and Matthew J. Brookes. Using variance information in magnetoencephalography measures of functional connectivity. *NeuroImage*, 67:203–212, 2013.

[94] Elena A. Allen, Eswar Damaraju, Sergey M. Plis, Erik B. Erhardt, Tom Eichele, and Vince D. Calhoun. Tracking Whole-Brain Connectivity Dynamics in the Resting State. *Cerebral Cortex*, 24(3):663–676, 11 2012.

[95] Zeynep Akalin Acar and Scott Makeig. Neuroelectromagnetic forward modeling toolbox. *Conference proceedings : ... Annual International Conference of the IEEE Engineering in Medicine and Biology Society. IEEE Engineering in Medicine and Biology Society. Conference*, 2008:3991–4, 02 2008.

[96] R.N. Henson, J. Mattout, C. Phillips, and K.J. Friston. Selecting forward models for meg source-reconstruction using model-evidence. *NeuroImage*, 46(1):168–176, 2009.

[97] Federico Chella, Laura Marzetti, Matti Stenroos, Lauri Parkkonen, Risto J. Ilmoniemi, Gian Luca Romani, and Vittorio Pizzella. The impact of improved meg–mri coregistration on meg connectivity analysis. *NeuroImage*, 197:354–367, 2019.

[98] Johannes Vorwerk, Jae-Hyun Cho, Stefan Rampp, Hajo Hamer, Thomas R Knösche, and Carsten H Wolters. A guideline for head volume conductor modeling in eeg and meg. jun 2014.

[99] A Tarkiainen, M Liljeström, M Seppä, and R Salmelin. The 3d topography of meg source localization accuracy: effects of conductor model and noise. *Clinical Neurophysiology*, 114(10):1977–1992, 2003.

[100] M X Huang, J C Mosher, and R M Leahy. A sensor-weighted overlapping-sphere head model and exhaustive head model comparison for meg. 44(2):423, feb 1999.

[101] M Lalancette, M Quraan, and D Cheyne. Evaluation of multiple-sphere head models for meg source localization. *Physics in Medicine & Biology*, 56(17):5621, aug 2011.

[102] Risto Ilmoniemi, Matti Hämäläinen, and Jukka Knuutila. The forward and inverse problems in the spherical model. 01 1985.

[103] Robert Van Uitert, Chris Johnson, and Leonid Zhukov. Influence of head tissue conductivity in forward and inverse magnetoencephalographic simulations using realistic head models. *IEEE transactions on bio-medical engineering*, 51:2129–37, 01 2005.

[104] Christian Schmidt, Sven Wagner, Martin Burger, Ursula van Rienen, and Carsten H Wolters. Impact of uncertain head tissue conductivity in the optimization of transcranial direct current stimulation for an auditory target. *Journal of Neural Engineering*, 12(4), jul 2015.

[105] Aleksandra Kuznetsova, Yulia Nurislamova, and Alexei Ossadtchi. Modified covariance beamformer for solving meg inverse problem in the environment with correlated sources. *NeuroImage*, 228:117677, 2021.

[106] Julia Schwarz, Mikel Lizarazu, Marie Lallier, and Anastasia Klimovich-Gray. Phonological deficits in dyslexia impede lexical processing of spoken words: Linking behavioural and meg data, 10 2023.

[107] Stavros I. Dimitriadis, Christos Salis, Ioannis Tarnanas, and David E. Linden. Topological filtering of dynamic functional brain networks unfolds informative chronnectomics: A novel data-driven thresholding scheme based on orthogonal minimal spanning trees (omsts). *Frontiers in Neuroinformatics*, 11, 2017.

[108] Stavros I. Dimitriadis, Bethany Routley, David E. Linden, and Krish D. Singh. Reliability of static and dynamic network metrics in the resting-state: A meg-beamformed connectivity analysis. *Frontiers in Neuroscience*, 12, 2018.

[109] DB West. *Introduction to Graph Theory*. Prentice Hall, 2000.

[110] Stavros Dimitriadis, Yu Sun, Nitish Thakor, and Anastasios Bezerianos. Mining cross-frequency coupling microstates (cfcμstates) from eeg recordings during resting state and mental arithmetic tasks. volume 2016, 08 2016.

[111] Z. Rezvani, M. Zare, G. Žarić, M. Bonte, J. Tijms, M.W. Van der Molen, and G. Fraga González. Machine learning classification of dyslexic children based on eeg local network features. *bioRxiv*, 2019.

[112] Luke Tait. Meg cortical microstates: Spatiotemporal characteristics, dynamic functional connectivity and stimulus-evoked responses. *NeuroImage*, 251:119006, 2022.

[113] Marios Antonakakis, Stavros I. Dimitriadis, Michalis Zervakis, Andrew C. Papanicolaou, and George Zouridakis. Altered rich-club and frequency-dependent subnetwork organization in mild traumatic brain injury: A meg resting-state study. *Frontiers in Human Neuroscience*, 11, 2017.

[114] Silvia Erla, Luca Faes, Enzo Tranquillini, Daniele Orrico, and Giandomenico Nollo. Multivariate autoregressive model with instantaneous effects to improve brain connectivity estimation. *International Journal of Bioelectromagnetism www.ijbem.org*, 11:74–79, 01 2009.

[115] Nasibeh Talebi, Ali Motie Nasrabadi, and Iman Zadeh. Estimation of effective connectivity using multi-layer perceptron artificial neural network. *Cognitive Neurodynamics*, 12, 02 2018.

[116] Sofia Zahia, Begonya Garcia-Zapirain, Ibone Saralegui, and Begoña Fernandez-Ruanova. Dyslexia detection using 3d convolutional neural networks and functional magnetic resonance imaging. *Computer Methods and Programs in Biomedicine*, 197:105726, 2020.

[117] Priyanka Patel Daria Khanolainen Marja-Kristiina Lerkkanen Anna-Maija Poikkeus Maria Psyridou, Asko Tolvanen and Minna Torppa. Reading difficulties identification: A comparison of neural networks, linear, and mixture models. *Scientific Studies of Reading*, 27(1):39–66, 2023.

[118] T. V. Prasad. Identifying dyslexic students by using artificial neural networks. 2010.